東海大学大学院令和 4 年度博士論文

Experimental and numerical study on propagation of detonation wave in combustible jet train (可燃性噴流列中を伝播する爆轟波に関する実験および数値解析的研究)

指導　　水書稔治　教授

東海大学大学院総合理工学研究科
総合理工学専攻

Faming Wang

Abstract

In the flow field of a rotating detonation engine (RDE), the detonation wave propagates through the reaction with the continuously injected fuel and oxidant mixture. In the previous research using the actual RDE, due to insufficient mixing, combustor shape, centrifugal force, and so forth, the detonation wave velocity generated in RDE is usually significantly lower than the characteristic Chapman-Jouguet(C-J) velocity for the corresponding mixture. In order to elucidate the effect of incomplete fuel mixing on detonation propagation inside RDE, a linear detonation channel was constructed. Use it to perform numerical analysis and experiments on detonation waves propagating in combustible gas jet trains.

Chapter 1 is an introduction. Mainly introduces the research background and previous research.

Chapter 2 mainly introduces the JAXA in-house code Chariot used in this study and explains the numerical analysis methodology. The validation of the code is carried out through the one-dimensional numerical analysis of detonation pressure and velocity.

In chapter 3, the detonation experimental system is established, and whether the experimental system can generate stable detonation waves is confirmed through basic experiments. At the same time, a two-dimensional numerical analysis was carried out to further verify the accuracy of the numerical analysis code, and the most suitable grid size was selected. As a result, it was confirmed that this experimental system could generate a stable detonation wave. The numerical analysis results show that the pressure and velocity of the detonation have a small error with the experimental data, less than 5%. The numerical analysis results of the detonation cellular structure

are also consistent with the experimental data. The 50 μm grid achieves a good balance between numerical analysis results and computational cost.

In chapter 4, the results of experiments and numerical analysis show that the use of premixed fuel can maintain the propagation of detonation waves even at extremely low supply pressures. And the propagation velocity of the detonation wave can reach up to 90% of the C-J velocity, while at low fuel flow rates of non-premixed fuel, it is difficult to maintain detonation propagation without promoting mixing with non-premixed fuel. The detonation propagation velocity of non-premixed fuel after promoting over fuel mixing reached more than 90% of the theoretical C-J velocity. Therefore, it can be expected that the performance can be improved by creating a structure in the RDE that allows the fuel and oxidizer to intersect in advance and be injected in the direction of the detonation wave propagation.

Double injector performs best at a 45-degree angle. The fuel injection velocity at the trailing edge of the detonation in the complete combustion state decreased by about 64%, 33%, and 26% in the opposite, the vertical and same direction as the propagation direction of the detonation wave at a 45-degree angle.

In chapter 5, A two-dimensional numerical analysis of a two-dimensional unwrapped RDE model was performed to verify the effects of various fuel injection methods in Chapter 4.

When using non-premixed fuel, the detonation wave velocity decreases as the number of detonation waves increases. However, when premixed fuel is used, the detonation wave propagation velocity still reaches 90% of the CJ velocity even though there are multiple numbers of detonation waves. Therefore, an imperfect fuel mixture is considered to have a greater effect on the detonation wave velocity than the number of detonation waves.

The detonation propagation velocity with premixed fuel is much higher than with non-premixed fuel, which reduces the detonation velocity loss to C-J velocity from about 30% to 11%.

When using non-premixed fuel, most of the ethylene is consumed in the reaction under all conditions, but about 10% - 20% of oxygen is not consumed and flows out.

In conclusion, Brief conclusions could be drawn as follows:

1. Facilitating the mixing of the fuel can directly increase the propagation speed of the detonation, but it cannot fully reach the C-J velocity.
2. Well-mixed fuel maintains detonation propagation even at very low mass flow rates, and can reach more than 90 % of the C-J velocity. In contrast, non-premixed fuels require a high mass flow rate to maintain detonation propagation, and even if the detonation wave can maintain propagation, the detonation velocity is about 30 % lower than the C-J velocity.
3. The greater the relative inclination angle of the double injector, the more obvious the effect of promoting mixing.
4. During the propagation of rotating detonation, not all the fresh fuel is consumed by the detonation, and a large amount of oxygen will flow out without being consumed.

Contents

List of Figures

List of Tables

Chapter 1

Introduction

in recent years, due to the extremely high pressure and temperature rise of detonation, many countries have actively carried out engineering research on the application of detonation in propulsion system. In fact, according to detonationcycle, higher total temperature and total pressure can be achieved than conventional engines, resulting in higher thermal efficiency and greater thrust. In addition, the detonation engine does not need a compression mechanism and blades in principle, which can make the engine more compact. These reasons promote research and development of detonation burners in the world. There are two representative engines, pulse detonation engine (PDE) and rotating detonation engine (RDE).

The principle of PDE is to generate thrust by repeatedly generating knock in the combustion chamber. The schematic diagram of the PDE operating cycle is shown in Fig. 1.1. The operation cycle of PDE includes the following processes:

1) filling of fuel and oxidant.

2) ignition and deflagration-detonation transition.

3) self-sustained detonation propagation.

4) Purge and cooling

Because PDE can only generate intermittent thrust, researchers pay more attention to RDE. The RDE is usually a double cylindrical combustion chamber as shown in Fig. 1.2, with fuel and oxidizer supplied from the bottom. After ignition by means of predetonators, detonation wave propagates in the double cylinder in the circumferential direction and exhausts the jet flow in the axial direction to generated Thrust.

The basic concept of detonation engine was first proposed by Zeldovich[1]in 1940 and first applied to propulsion institutions in 1957 by a group of Nicholls et al.[2] at the University of Michigan. They initially developed the Pulse Detonation Engine (PDE), which generates thrust in pulses. In the early 1960s, Voitsekhovskii et al.[3][4] subjected to a very short combustion experiment of rotating detonation. They used a stoichiometric mixture ratio of the Acetylene-Oxygen mixture at low pressure to allow the rotating detonation in a double-cylindrical combustion vessel for a considerable long time (The concept of a long time for rotating detonation is less than 1 second) to obtain a stable rotating detonation. Subsequently, in 1966, Nicholls et al.[5] carried out experiments using Hydrogen-Oxygen and Methane-Oxygen mixture gas, and in 1967 Adamson et al.[6],[7] conducted the theoretical analysis. Since then, RDE research has not been actively carried out. As a result, in the more than 30 years since the 1960s experiments, RDE research and development have progressed slowly. In the 2000s, with the advancement of technology, research institutions in various countries resumed research on RDE from experimental and numerical analysis. Russia, Poland, China, the United States and other countries have carried out RDE-related research and made significant progress. In Japan, Japan Aeronautics and Space Administration

(JAXA) also has great interest in the Rotating Detonation Engine (RDE) and has commenced basic research. Currently, RDE has been successfully run at JAXA Kakuda Space Center[8]. Last year, JAXA and Kasahara et al. [9] launched RDE into space by rocket and successfully operated RDE in a space environment. Meanwhile, the research on the clear visualization of the detonation wave propagation inside the RDE by non-traditional methods is also being carried out. J. Burr et al.[10] successfully carried out the visualization experiment by expanding the RDE combustor into a linear combustor. Mizukaki et al.[11] used point-diffraction interferometry to enable interferometric visualization of detonation wave propagation inside RDE.

In 1977, a study by Rolls-Royce's BD. Edwards[12] showed that the continuous propagation of rotating detonation waves was affected by the burned gas in the combustion chamber, so the detonation propagation velocity and pressure could not reach the expected value. Due to the principle of RDE, this problem is difficult to solve fundamentally. Recent studies have also shown the detonation wave propagation in the combustor is not ideal due to the effect of incomplete mixing of fuel, the curvature of the combustion channel, and wall loss, so the detonation velocity in RDE usually only reaches about 70% of Chapman-Jouguet velocity(C-J velocity). Furthermore, the influence of various factors on detonation propagation and their solutions has not been elucidated. Therefore RDE is not yet practical.

Another linearized RDE with optical accesses is used to analyze the spray characteristics of the mixing flow field, and a series of measurement methods such as schlieren[13][14], shadowgraph[15][16], planar laser-induced fluorescence (PLIF)[17][18], Mie scattering[19][20], and phase doppler particle analyzer (PDPA)[21][22] has been applied in this research. Ayers et al. [23] investigated the mixing dynamics by analyzing the refill properties in a linear detonation engine

using 100 kHz acetone PLIF. Duvall et al.[24] employed an optical linear experimental platform to identify the basic flow characteristics of non-reacting mixtures using schlieren and PLIF. In a linear detonation chamber. Bedick et al.[25] analyzed the interaction between the injection process and detonation wave using a three-dimensional printed inlet geometry and completed a quantitative investigation using PLIF. Redial et al. [26] discovered dominant flow structures in linear structures and the effects of reactant distribution on detonation performance.

Although a large number of RDE experiments are being carried out, because the operation of RDE produces a large number of heat and shock waves, it is difficult to carry out clear visualization experiments on RDE. How to accurately understand the detonation wave shape in the combustion chamber has become a topic. Based on the previous research, we also designed a linear combustor that expanded the RDE to a straight line. We named it the linear detonation channel (LDC). For this reason, the double cylinder can become an optical window, increase the range of observation, and reduce the damage of high temperature to the observation part because more than necessary detonation is not generated. So, in theory， It can easily carry out the visual measurement. Although there are premixed gases in previous studies, they are all mixed before injection, not fully mixed premixed gases in the full sense. Therefore, we use a closed linear combustion chamber to complete the visualization of the detonation wave propagation in the fully mixed state, thereby clarifying the effect of mixing on detonation propagation.

This thesis consists of six chapters.

Chapter 1 is the introduction, including the research background, Previous research, Issues, and research objectives.

Chapter 2 is the numerical analysis methodology, introduces the numerical analysis code used

in the numerical analysis of this study, numerical method and code validation.

In chapter 3, to establish a detonation experiment system and validate the numerical analysis methodology, we carried out the basic experiment and two-dimensional numerical analysis. Carried out the experimental and two-dimensional numerical analysis to validate the numerical analysis methodology.

In chapter 4, a linear combustion chamber is designed, through which the influence of shape factors such as curvature on detonation wave propagation can be eliminated. To clarify the effect of fuel mixing on the propagation of detonation waves, carried out the experiment and two-dimensional numerical analysis by using a linear detonation channel.

Chapter 5, based on the fuel injection scheme of chapter 4, carried out a two-dimensional numerical analysis using a two-dimensional unwrapped RDE model to clarify the effect of fuel mixing on the propagation of continuous detonation waves.

Chapter 6 is the conclusion.

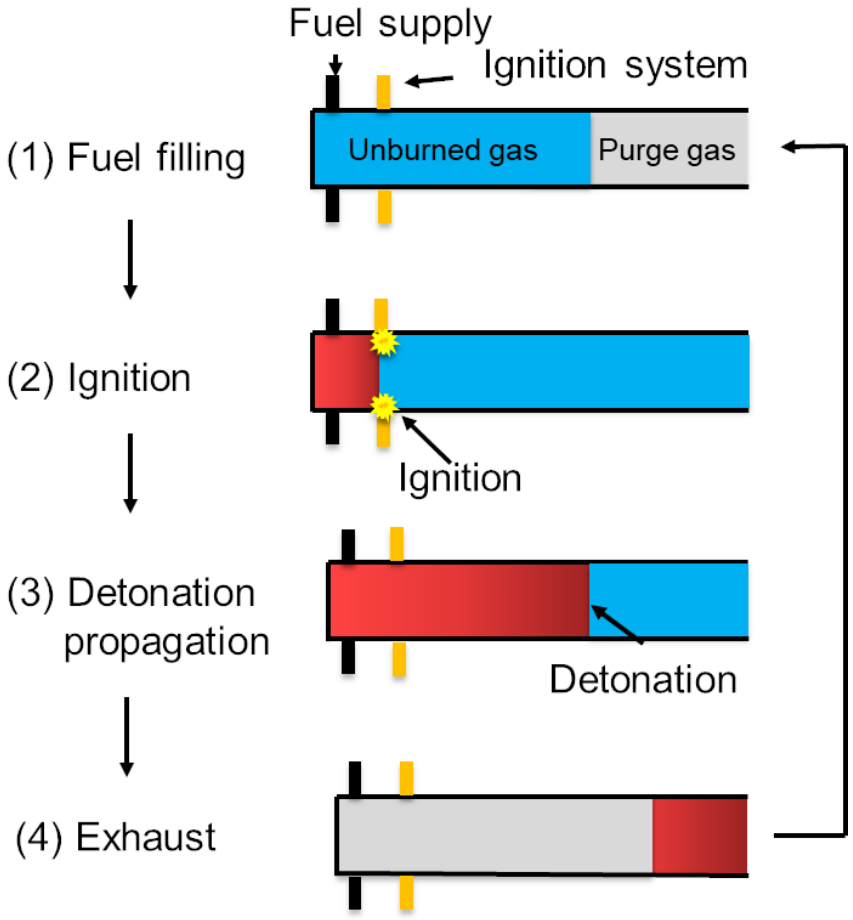

Fig. 1.1 Principle of pulse detonation engine.

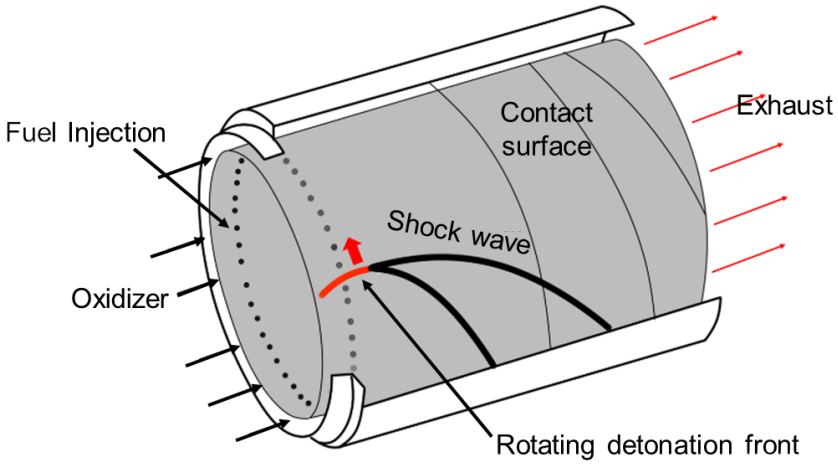

Fig. 1.2 Principle of rotating detonation engine.

Chapter 2

Numerical analysis methodology

2.1 Overview

Numerical analysis is performed by using JAXA’s in-house code CHARIOT (Cost-effective High-order Accurate Reconstruction-scheme Intensively Optimized for Turbulent-combustion).

Turbulent combustion is essential in burners such as gas turbine engines and rocket engines. For a long time, turbulent combustion analysis based on RANS for burners has been widely carried out. Still, with the significant improvement in computer performance in recent years, an unsteady combustion analysis based on LES has also been carried out. In the numerical analysis technology research unit of the Japan Aerospace Exploration Agency (JAXA), to implement LES for burner design performance evaluation and DNS for elucidating turbulent combustion mechanism, turbulent combustion analysis code CHARIOT has been continuously developed and improved since 2010.

2.2 Numerical method

2.2.1 Governing equation

The governing equations of the flow used for the present LES analysis is three-dimensional filtered compressible Navier-Stokes equation.

$$\frac{\partial \bar{\rho}}{\partial t} + \frac{\partial \bar{\rho}\tilde{u}_l}{\partial x_i} = 0 \tag{2.1}$$

$$\frac{\partial \bar{\rho}\tilde{u}_i}{\partial t} + \frac{\partial}{\partial x_j}\left\{\bar{\rho}\tilde{u}_i\tilde{u}_j + \bar{p}\delta_{ij} - \bar{\tau}_{ij} + \bar{\rho}\left(u_l\tilde{u}_j - \tilde{u}_i\tilde{u}_j\right)\right\} = 0 \tag{2.2}$$

$$\frac{\partial \bar{\rho}\tilde{e}}{\partial t} + \frac{\partial}{\partial x_i}\left\{\bar{\rho}\tilde{u}_i\tilde{e} + \bar{p}\tilde{u}_i + \bar{q}_i - \tilde{u}_j\bar{\tau}_{ij} + \bar{\rho}\left(\widetilde{eu_l} - e\tilde{u}_i\right)\right\} = 0 \tag{2.3}$$

$$\frac{\partial \bar{\rho}\tilde{Y}_k}{\partial t} + \frac{\partial}{\partial x_i}\left\{\bar{\rho}\tilde{Y}_k\tilde{u}_i - \bar{\rho}\widetilde{D}_k\frac{\partial \tilde{Y}_k}{\partial x_i} + \bar{\rho}\left(\widetilde{Y}_k u_i - \tilde{Y}_k\tilde{u}_i\right)\right\} = \overline{\dot{\omega}_k} \tag{2.4}$$

where the ρ is density, u is x-axis velocity component, v is y-axis velocity component,, w is z-axis velocity component,, p is pressure, Ys) Although the unclosed SGS terms, $\bar{\rho}\left(\widetilde{u_l\tilde{u}_j} - \tilde{u}_i\tilde{u}_j\right)$, $(\widetilde{eu}_l - e\tilde{u}_i)$, and$\bar{\rho}\left(\widetilde{Y_k u_l} - \overline{Y_k}^{u_i}\right)$, are usually included in the filtered governing equations, LES analysis in this study is performed by implicit LES, in which all SGS terms are set to zero. For the detailed reaction model of ethylene combustion, 31 species and 126 species reactions model are used (Refer to Appendix B.1). In addition, operator-splitting method and a Quasi-Steady-State approximation (QSS)[27] are applied to reduce the stiffness associated with fast chemical reactions.

The CHEMKIN database[28][29] is used to calculate the thermodynamic and transport properties.The governing equations are discretized by the finite volume method. The convective flux is calculated by SLAU2 scheme[30]. The viscous flux is obtained by the central difference method. High-order spatial accuracy is achieved by using several variants of WENO interpolation method, that is realized by interpolating primitive variables (ρ, u, v, w, p, Ys) at the cell interface, this interpolation method considered valid[31]. For the scalar variables (ρ, p, Ys), the second-order MUSCL(Monotone Upwind Scheme for Conservation Laws) method is used, and the velocity components (u, v, w) are interpolated with a fifth order polynomial. The time integration method is employed by the three-stage Runge-Kutta method.

2.2.2 Supercomputer system

Computation was carried out on the JAXA Supercomputer System (JSS3) installed at the Aeronautical Technology Directorate (ATD) of JAXA. Parallel computation was implemented by domain decomposition, with the Message Passing Interface (MPI) library used for inter-processor communication. The performance of JSS3 refers to Appendix B.1.

2.3 1D code validation

For code validation, the one-dimensional detonation propagation problem was analyzed by CHARIOT as a test problem, and the detonation propagation pressure was compared with experimental results. One-dimensional calculation set the Injection conditions as initial pressures are 20 kPa, 48 kPa, and 100 kPa with an equivalence ratio is 1.0. Figure 2.1 shows the computational grid.

Figure 2.2 is a calculation example when the initial pressure is 48 kPa, and the grid size at this time is 50 μm. Figure 2.3 shows the detonation pressure calculation results of different initial pressures for each grid size, and the details are shown in Fig. 2.4-2.6. The comparison of detonation pressure and velocity with C-J value under each mesh size is shown in Fig. 2.7 and Fig. 2.8 respectively.

The numerical analysis results are basically consistent with the C-J value calculated by NASA CEA, and the error is less than 10%.And numerical analysis results tend to be consistent when the grid is smaller than 50 μm.

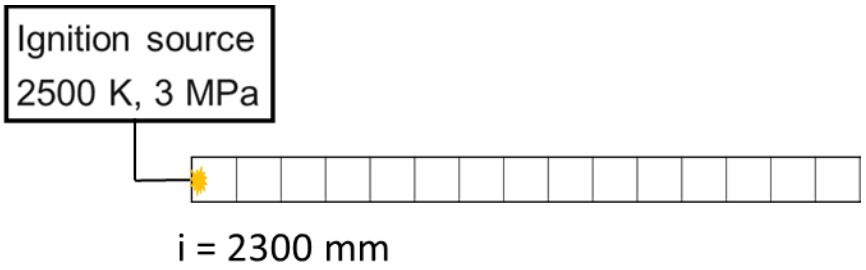

Fig. 2.1 Computational model for 1D code validation.

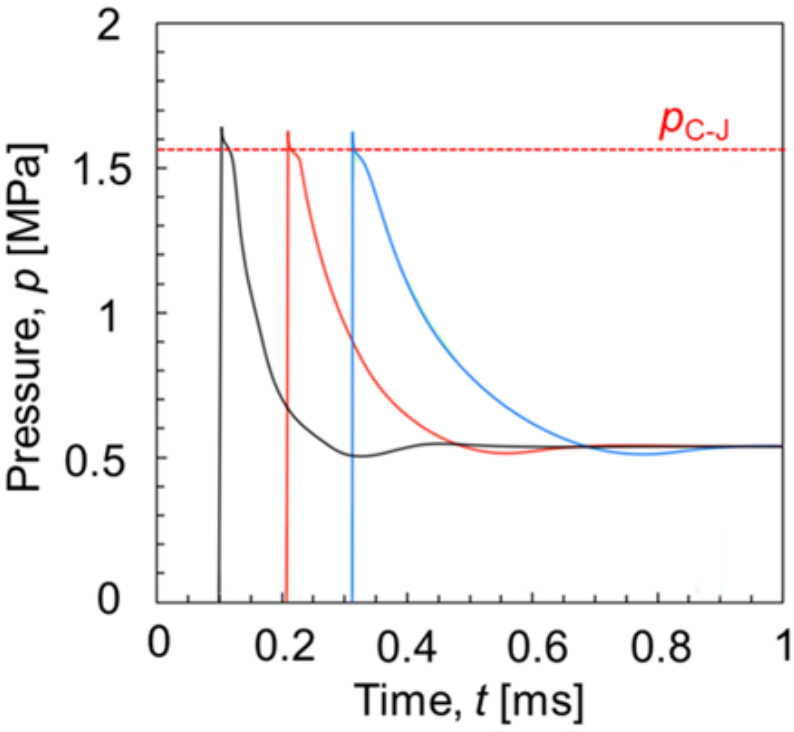

Fig. 2.2 An example of 1D numerical analysis calculation results.

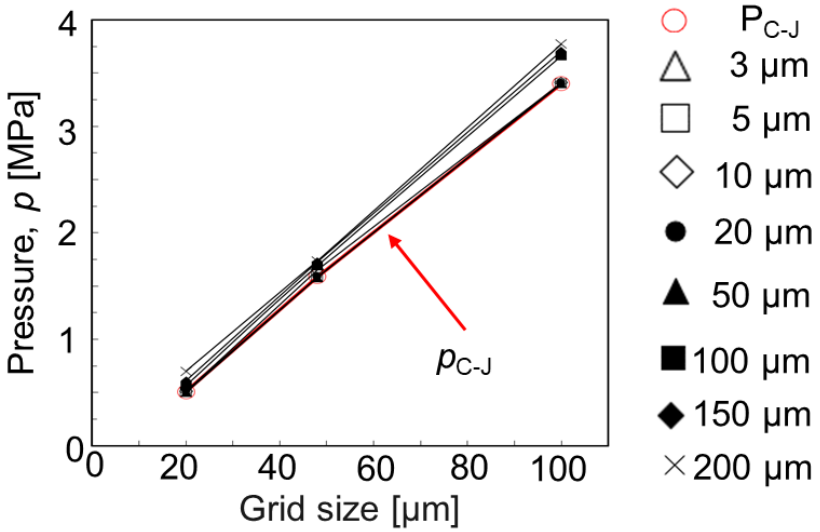

Fig. 2.3 Effect of mesh size on detonation pressure.

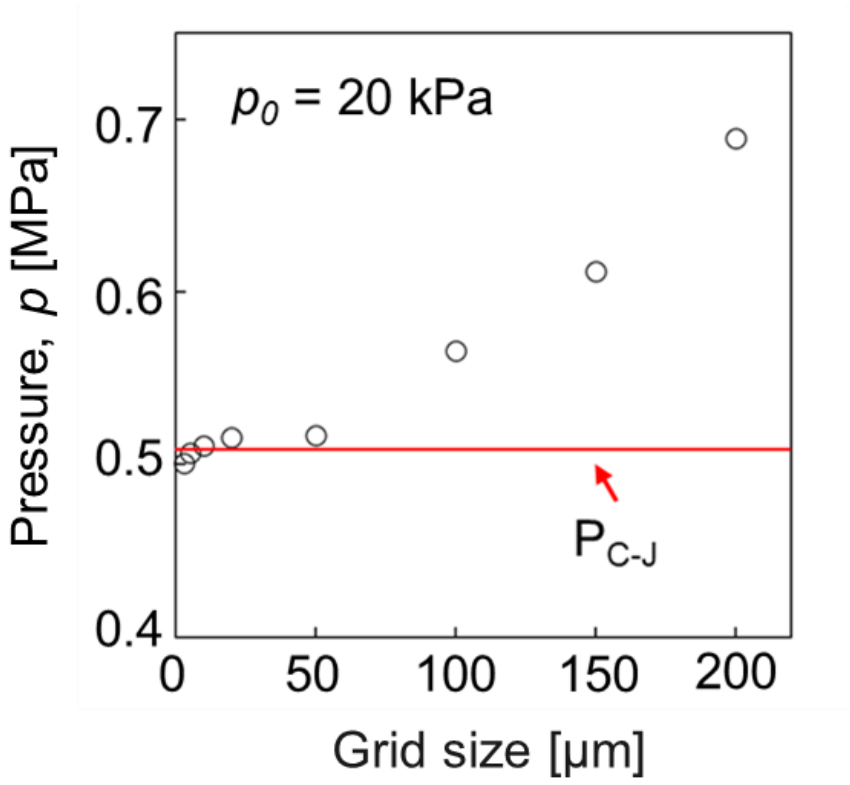

Fig. 2.4 Effect of mesh size on detonation pressure.(p_0 = 20 kPa)

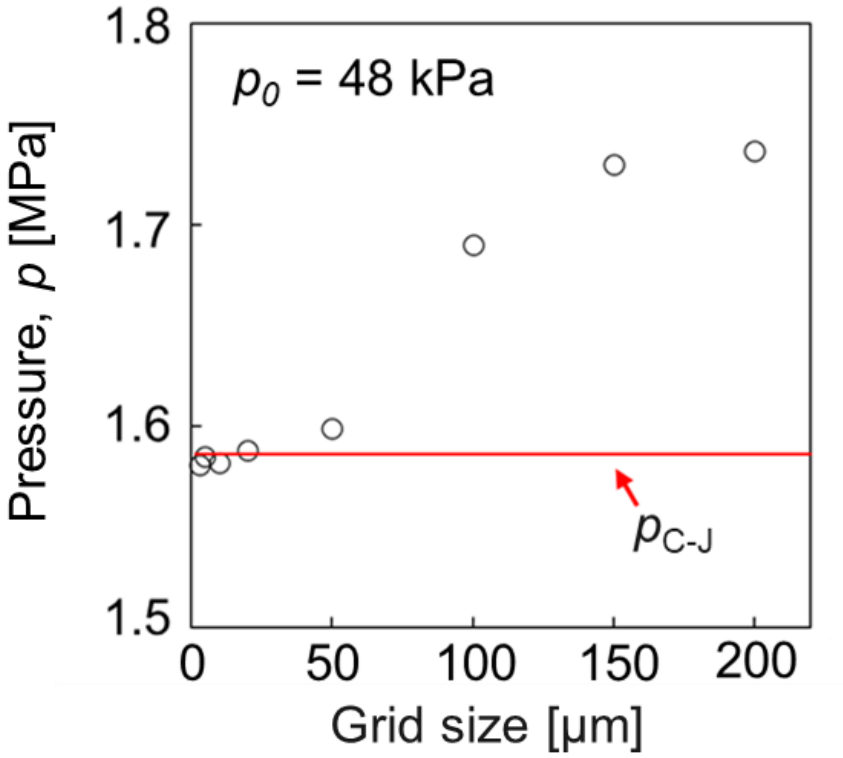

Fig. 2.5 Effect of mesh size on detonation pressure.(p_0 = 48 kPa)

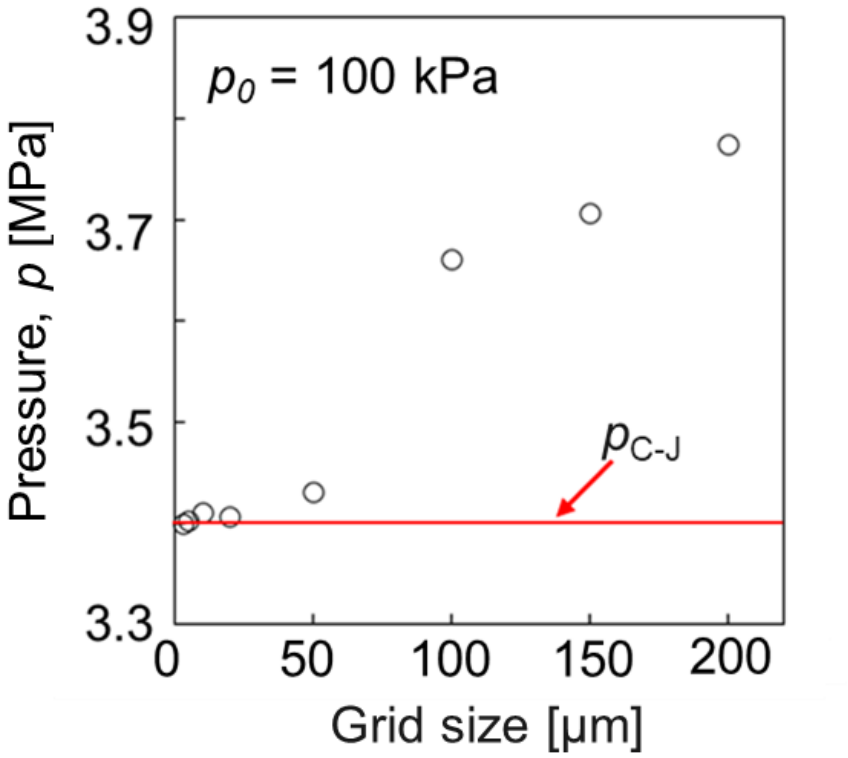

Fig. 2.6 Effect of mesh size on detonation pressure.(p_0 = 100 kPa)

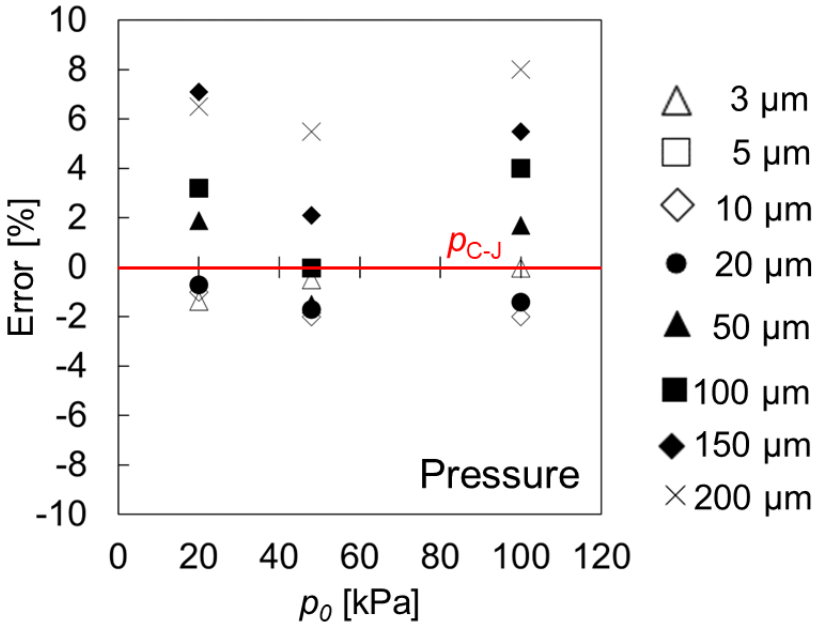

Fig. 2.7 The error of detonation pressure and C-J pressure.

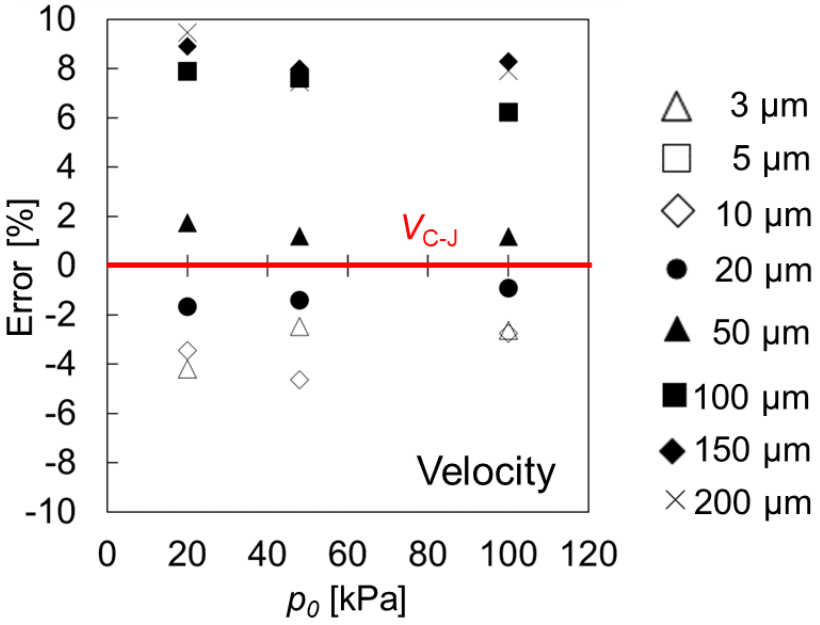

Fig. 2.8 The error of detonation velocity and C-J velocity.

Chapter 3

Validation of velocity and pressure of plane detonation waves and cellular structure in two-dimensional model

3.1 Overview

In this chapter, a detonation experiment system is set up to verify whether a stable detonation wave can be generated through basic experiments. Then, a two-dimensional numerical analysis of detonation velocity and pressure, as well as detonation structure, was carried out to further verify the accuracy of the code. Considering the detonation according to the ZND model in appendix A2, the reactants are heated by a preceding shock wave driven by accompanying reactant generation

and expansion. It is expected to be a planar (one-dimensional) standing wave. However, unlike the predictions of the ZND model, the actual explosion has a complex structure, as shown in Fig. A.5. This basic structure is called a cellular structure and plays an important role in the detonation propagation mechanism. The structure and formation process of the cells is investigated experimentally and numerically, and the experiments usually use a recording method using the soot-foil method.

3.2 Experimental setup

3.2.1 Basic experiment of detonation

The configuration of the experimental system is shown in figure 3.1. The main equipment used comprises a detonation tube (5x5DT) with an inner diameter of 50 mm × 50 mm, a measuring system, a gas supply system, and an ignition system. The full-length 2500 mm of the detonating tube and the distance from the pressure transducer(PCB 113B24) PT1 to PT3 are the same from 250 mm. The detonation tube and the dump tank are separated by a diaphragm made of polyethylene terephthalate (PET) with a thickness of 50 μm. The equipment used in the experiment is shown in Table 3.1.

An oscilloscope(Yokogawa DL750) collects the data. The oscilloscope waveform is shown in Fig. 3.2. By converting the voltage into pressure, the result shown in Fig. 3.3 can be obtained.

3.2.2 soot-foil experiment

To measure the structure of the detonation, the most representative soot foil experiments for measuring the cell size of detonation were carried out. The soot foil experiment is an experimental method to obtain the cell size of the detonation by placing the soot foil inside the detonation tube and letting the detonation wave pass through the soot and leave traces. The manufacturing method of soot foil is shown in Fig. 3.4. The length of the soot film is 500 mm. By making the crease of 15 mm on the soot film, the soot film is sandwiched between the upstream flanges and fixed with double-sided tape. After the experiment, the sootfilm is sprayed with a lacquer to be fixed.

The experimental conditions are shown in Table 3.2. The fuel was premixed with ethylene and oxygen, and the equivalence ratio was 1.0. The soot film used in the experiment is shown in Figure 3.5.

3.3 Computational model and injection Conditions

The computational model is assumed to be a tube 150 mm long and 5 mm wide, as shown in Fig.3.7. Since the calculation model is much smaller than the actual experimental device (Fig. 3.1), the boundary conditions of the calculation model are set as periodic conditions up and down, and the left and right are set as symmetry boundary. The initial conditions for the numerical analysis were a premixed fuel of 20 kPa and 48 kPa ethylene and oxygen with a premixed gas equivalence ratio of 1.0.

Ignition of the internal premixed fuel is achieved by multiple high-temperature and high-pressure sources located on the left. In this numerical analysis, the ignition is to set three

uniformly distributed small high-temperature and high-pressure fields with a temperature of 2500K and a pressure of 3MPa.

3.4 Results of experiment and numerical analysis

The results of detonation pressure and velocity are shown in Fig. 3.8 and Fig. 3.9, respectively, and the errors of the numerical analysis results compared with the experimental results are shown in Fig. 3.10 and Fig. 3.11.

The cellular structure obtained from the soot-foil experiment and numerical analysis are shown in Fig. 3.12, Fig3.13. The scale-like shape outlined by the line in the figure is the detonation cellular structure. The experimental results are summarized in Table 3.3. The results of the experiment and numerical analysis for initial pressures of 20 kPa and 100 kPa with 50% N_2 diluent with a grid size of 50 μ m. The comparison between the experimental and numerical analysis results is shown in Fig. 3.14.

3.5 Summary

In this chapter, experiments and numerical analysis are carried out on the detonation's pressure, velocity, and structure. The experimental results show that the assembled device can generate stable detonation waves.The numerical analysis results show that the pressure and velocity of the detonation have a small error with the experimental data, less than 5%. And numerical analysis results of the detonation cellular structure are also consistent with the experimental data. The 50 μm grid achieves a good balance between numerical analysis results and computational cost.

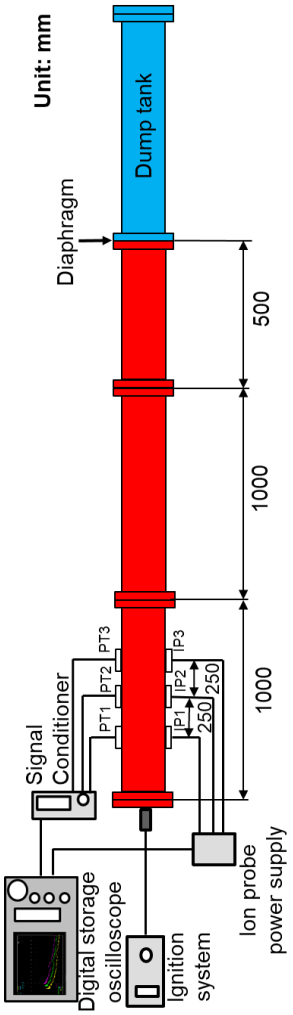

Fig. 3.1 Experimental system for detonation experiments.

Table 3.1 Numerical analysis results of cellular structure.

	20 kPa	48 kPa	100 kPa(with 50% N2 diluent)
3 um	1.0	0.3	2.1
5 um	1.0	0.3	1.9
10 um	0.9	0.3	1.9

Table 3.2 soot-foil experiment conditions.

Initial pressure P_0 [kPa]	20	48	100
N_2 diluent [%]	0	0	50

Table 3.3 soot-foil experiment results.

	Initial pressure P_0 [kPa]	N_2 diluent [%]	Cell width [mm]
1	16	0	1.8
2	20	0	1.6
3	20	0	1.3
4	48	0	0.8
5	100	50	2.8

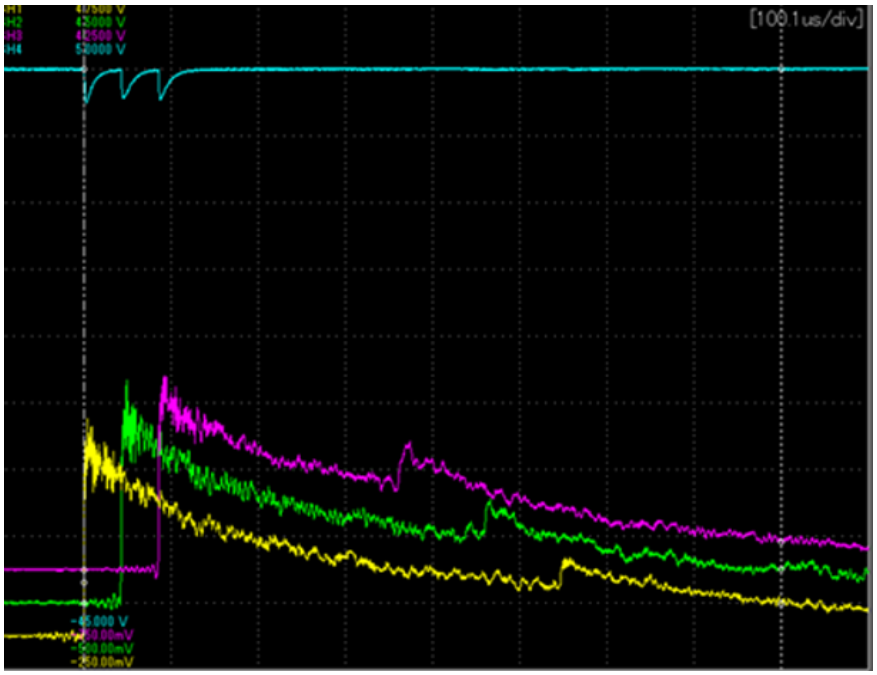

Fig. 3.2 Oscilloscope waveform.(P_0= 48 kPa)

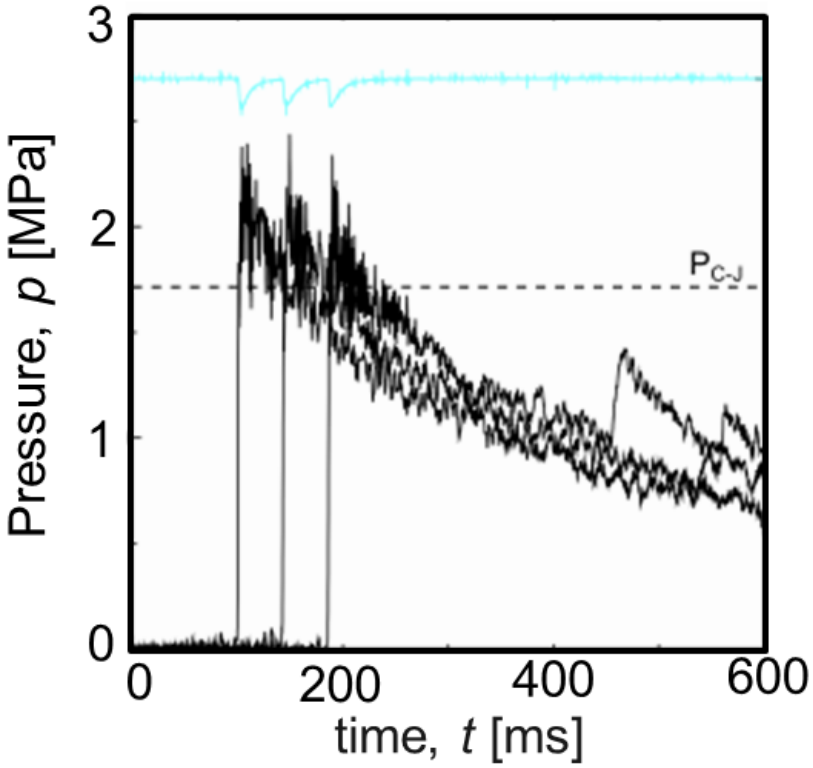

Fig. 3.3 Detonation waveform. (P_0= 48 kPa)

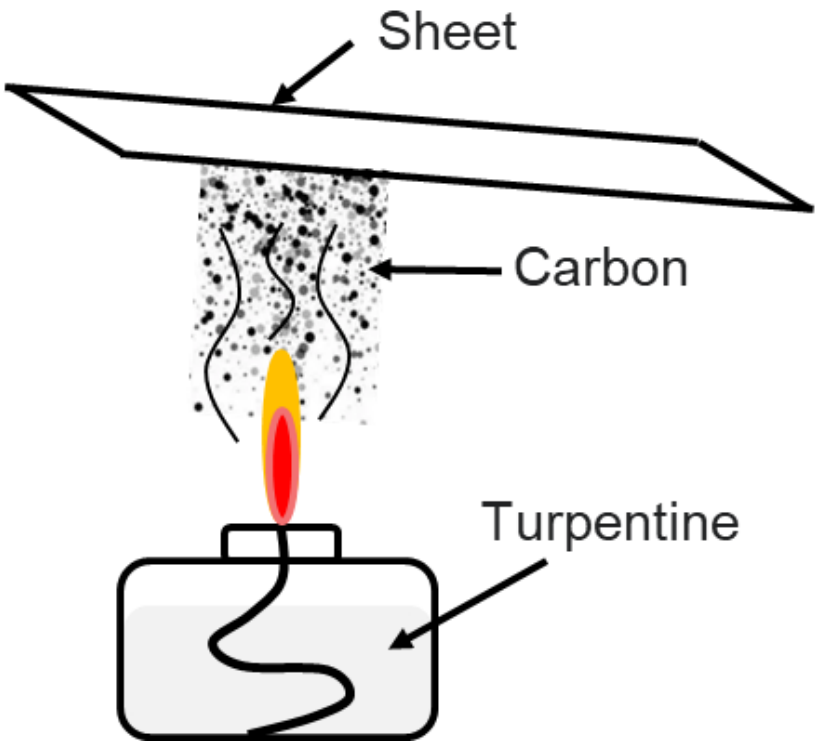

Fig. 3.4 The principle of soot foil.

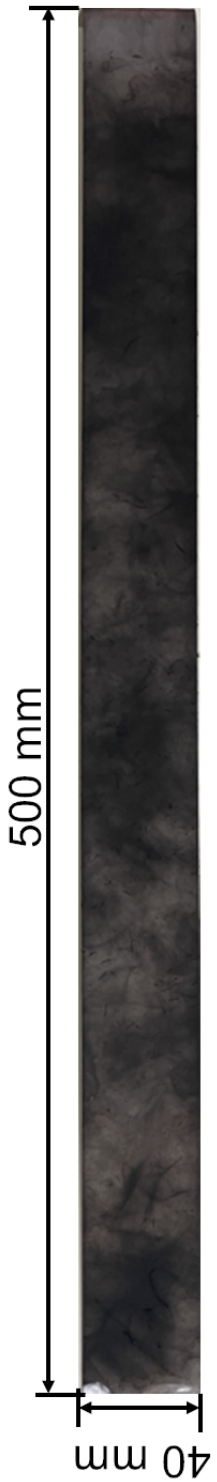

Fig. 3.5 Soot-foil.

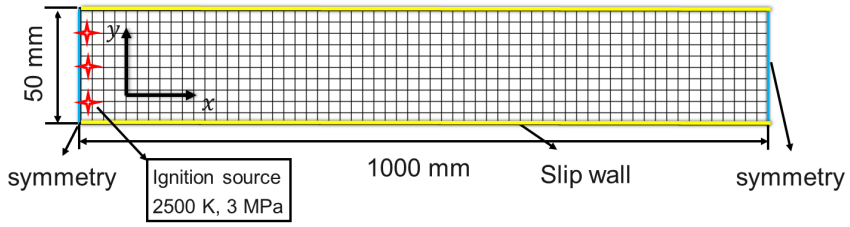

Fig. 3.6 Computational domain for detonation pressure and velocity.

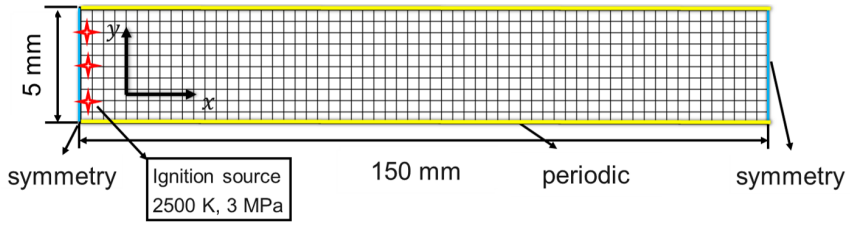

Fig. 3.7 Computational model for cell structure calculation.

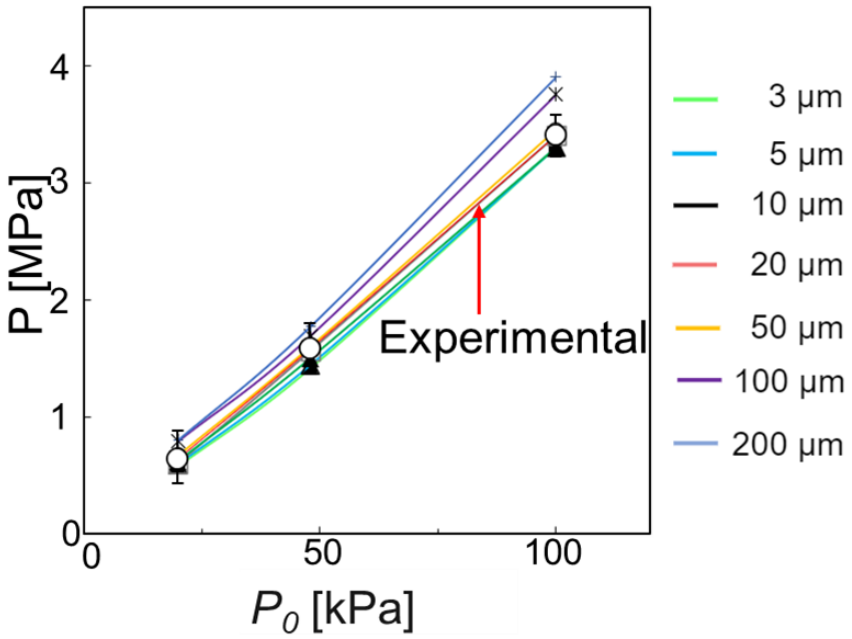

Fig. 3.8 Comparison between the numerical analysis results of the detonation pressure and the experimental results.

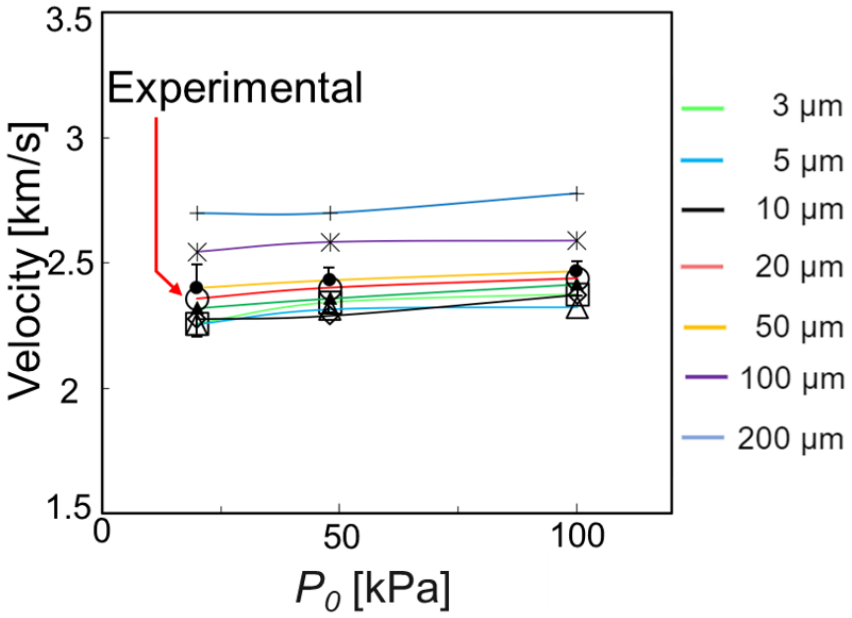

Fig. 3.9 Comparison between the numerical analysis results of the detonation velocity and the experimental results.

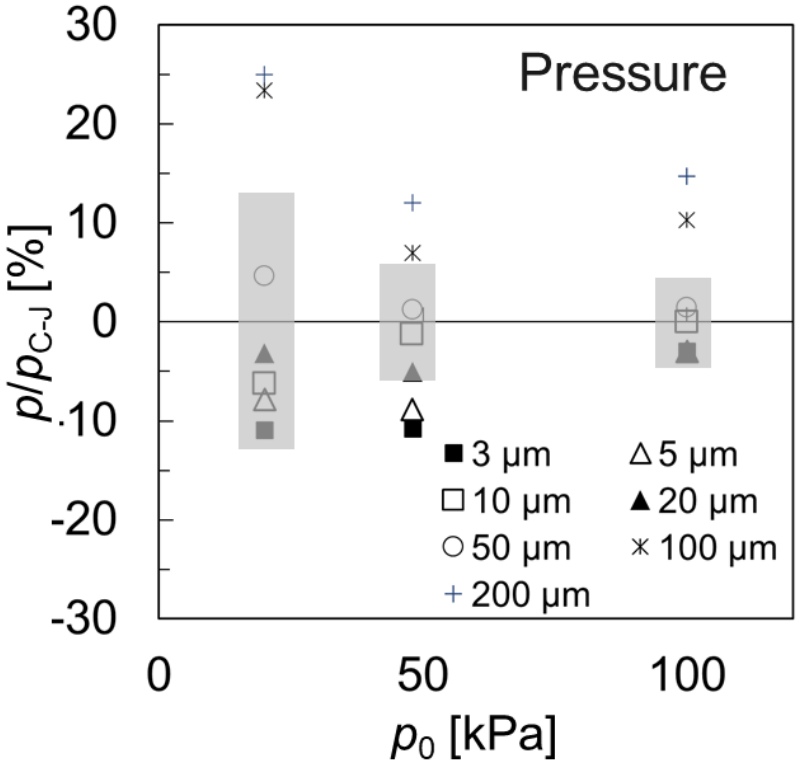

Fig. 3.10 The error between numerical analysis results and experimental results of detonation pressure.

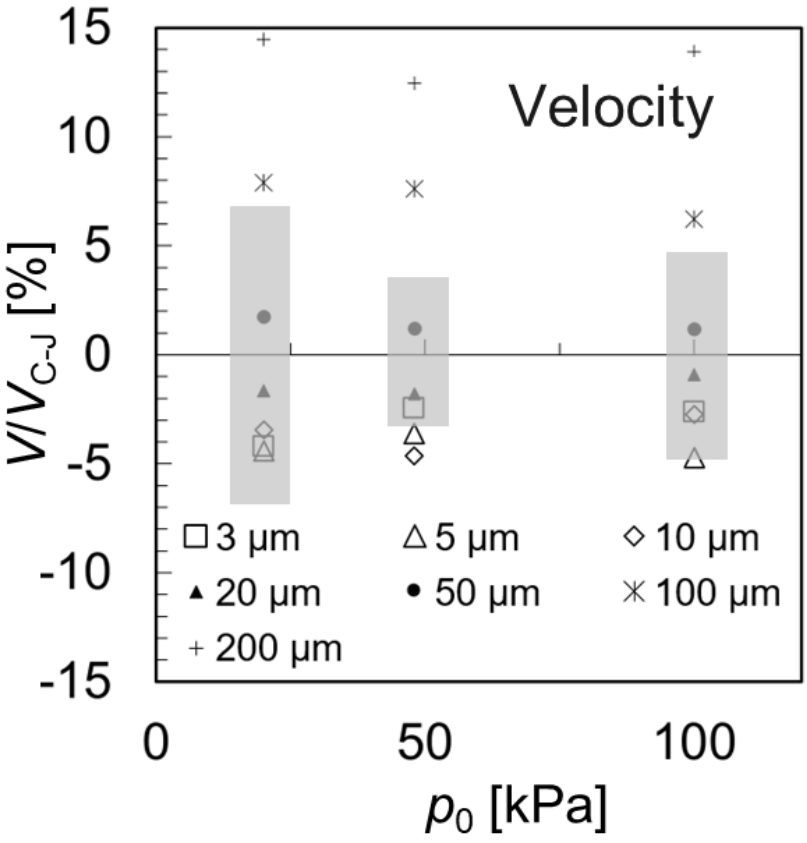

Fig. 3.11 The error between numerical analysis results and experimental results of detonation velocity.

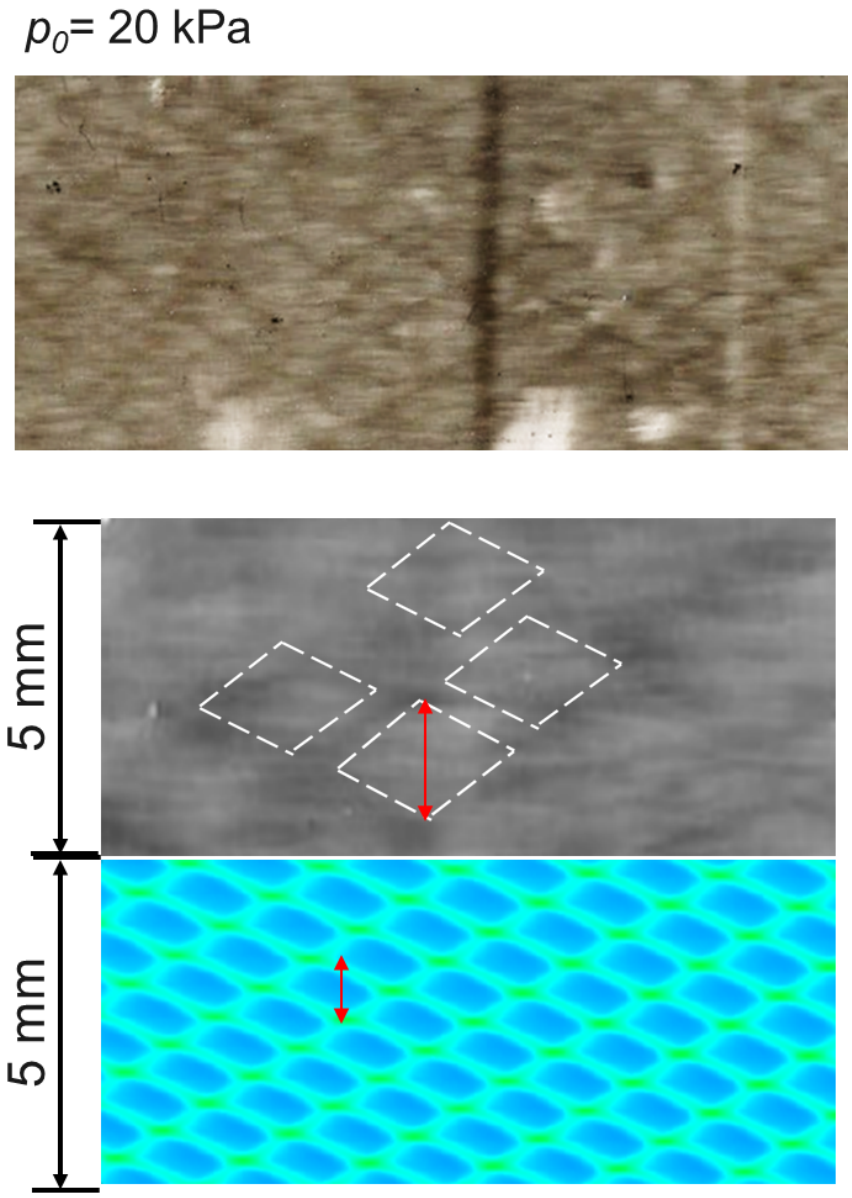

Fig. 3.12 The experimental results and numerical analysis results of the cell size.(P_0= 48 kPa)

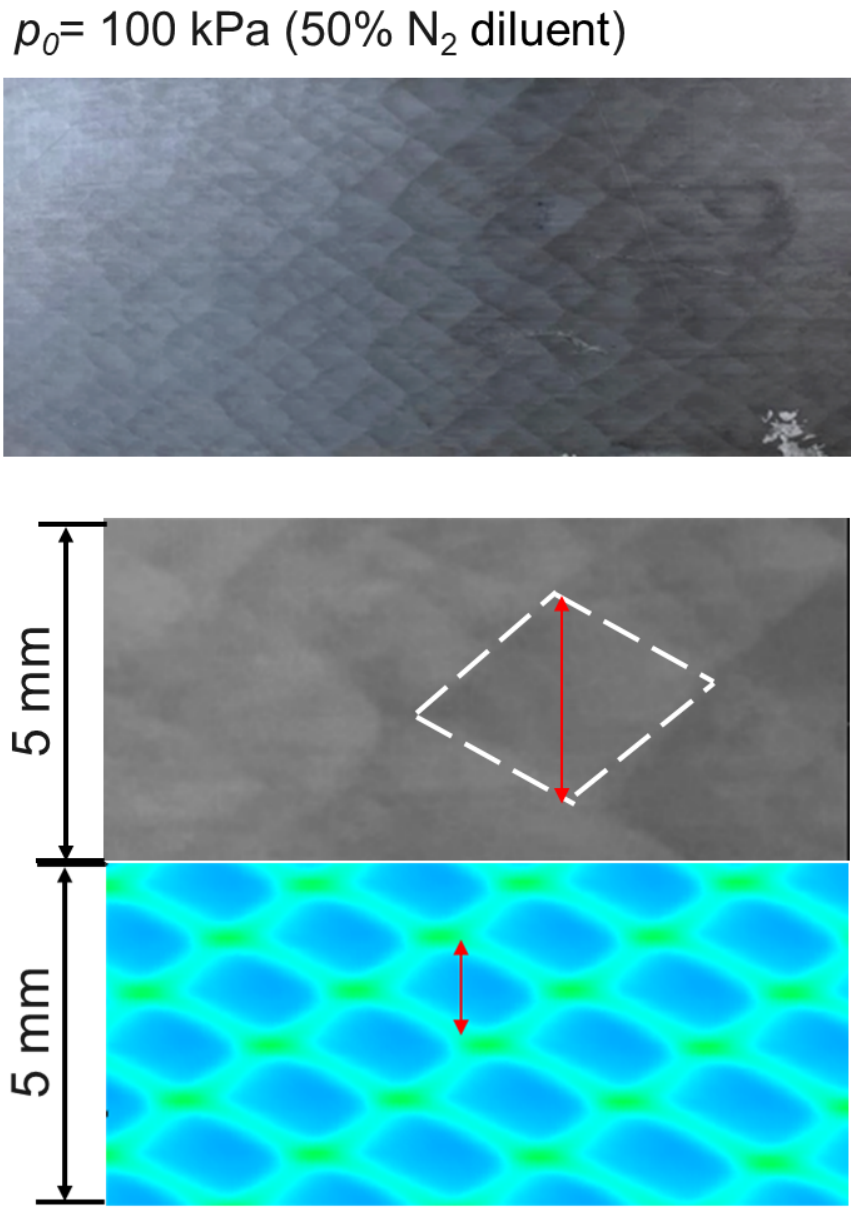

Fig. 3.13 The experimental results and numerical analysis results of the cell size.(P_0= 48 kPa)

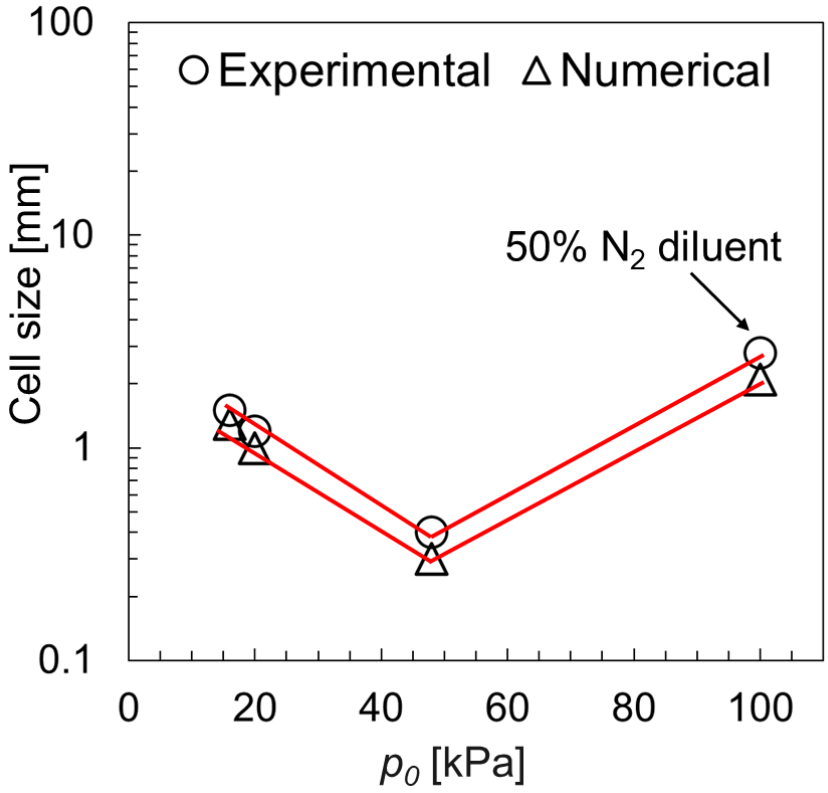

Fig. 3.14 Comparison between the numerical analysis results of the cell size and the experimental results.

Chapter 4

Experiment and numerical analysis of detonation waves propagation inside linear detonation channel

4.1 Overview

In chapter 1, it is mentioned that the main reasons for the poor performance of RDE are the propagation of burned gas at high temperature, insufficient fuel mixing, combustion chamber shape, wall loss, and other factors. Because of the principle of RDE, it is impossible to improve the negative impact of the burned gas in the combustion chamber, so it is more realistic to improve the performance of RDE by improving other factors. It is well known that imperfect fuel mixing directly affects combustion integrity, as is detonation. Therefore, we focus on evaluating the influence of fuel mixing conditions on detonation propagation and the improvement of the fuel

injection scheme on detonation wave propagation.

So we design a linear detonation channel that is different from the usual RDE. By straightening the annular RDE combustion chamber, we can eliminate the influence of the combustion chamber shape on the detonation wave propagation, and the linear detonation channel can get a more extensive range of optical windows and do not have to worry about the impact of unnecessary detonation waves on the device.

4.2 Linear detonation channel

Figure 4.1 shows an overview of the Linear detonation channel(LDC). It' s unfolding a curved RDE combustor into a linear shape. Both sides are equipped with quartz windows for optical visualization. The fuel and oxidant enter the tube through a small hole at the bottom with a controllable flow rate. The diameter of the injectors is 1.4 mm, which is set as d in this chapter as a reference. The LDC has a partially changeable structure, which can change the injection mode of the fuel injection port by changing the injection ports part, the mixing mode by the plenum chamber, and the height of the detonation wave inlet by changing the plate. There are two reasons for this;

1. By limiting the height of the detonation wave, the propagation pattern of the detonation is closer to that of the detonation wave propagating at the fuel nozzles at the bottom of the RDE combustor.
2. The end of the inlet is just at the center of the first injection port, that the fuel can be filled along the inlet, so that there is a fuel field between the diaphragm and the first injection

port, which makes detonation wave enter more stably.

The advantage of the LDC is that the propagation of the detonation wave inside the channel is independent of shape and centrifugal force. The observation windows on both sides of the passage can provide clearer optical visualization.

The device is shown in Fig. 4.2. Normally, in RDE ignition, detonation is generated by a passage where obstacles are installed or a mechanism that generates turbulence. For LDC, a steady detonation wave generates by placing a detonation tube directly on the upper stream of the device. And to be able to compare the changes caused by changes in the configuration of the injection ports, in the early stages of research, the injector is a direct injection without a nozzle.

4.3 Experimental setup and conditions

The experimental setup is shown in Fig. 4.3, the optical system used in this experiment is shown in Fig. 4.4, and the experimental conditions are shown in Table 4.1. As an experimental method, the signal is first sent from the Ignition switch, and the control system that receives the signal will open the solenoid valve so that the premixed gas in the premixed fuel tank will enter the LDC.

After the delay setting, the control system will issue an ignition signal. After ignition through the Ignition plug, the detonation wave will pass through three pressure transducers, and then the signal of the pressure transducer will be used as the trigger to start the high-speed camera.

4.4 Computational model

The LDC and the corresponding calculation model are shown in Fig. 4.5 In the calculation model, the mark on the left is the ignition point. The ignition is to set three uniformly distributed small high-temperature and high-pressure fields with a temperature of 2500K and a pressure of 3 MPa. The black line is the solid wall, the red line is the inflow boundary same as the fuel injection method of the device, and the yellow line is the outflow boundary. The grid size is 50 μm. The injection conditions for numerical analysis are shown in Table 4.2. The fuel injector is set to 90°, 70°, and 45° injection. In calculating the mass flow rate, the setting of the mass flow rate is achieved by setting the fuel flow velocity under 2D numerical analysis. The supply pressure was partially adjusted to increase the mass flow rate.

4.5 Results of Premixed gas injection

4.5.1 Low mass flow rate

Experiments and numerical analysis were carried out under low-pressure conditions. The visualization results and numerical analysis density distribution are shown in Figures 4.7-4.9. The relationship between the distance and velocity of the detonation wave after passing through the Inlet is shown in Figure 4.10. It can be seen that the detonation wave entering the fuel jet first decelerates and then accelerates. The acceleration of the detonation wave is significantly different from the influence of the fuel height. Basically, the higher the fuel height, the faster the detonation wave velocity.

Figure 4.11 illustrates that the detonation wave pressure and temperature also increase as the height of the fuel increases.

4.5.2 High mass flow rate

The numerical analysis results of Different mass flow rates are shown in Table 4.3 and Fig. 4.12 -Fig. 4.14. The detonation was successfully generated and spread. However, what is different from the expectation is that as the mass flow rate increases, the detonation velocity does not increase but decreases. The reason for this result is that when the mass flow rate is different, the volume and height of the injected fuel are completely different (as shown in Fig. 4.15) so that when the detonation ignites the fuel, it consumes more energy and causes the speed to decrease. To verify this idea, a more powerful ignition configuration was used. Increase the initial detonation pressure of ignition to 150 kPa, and the result is shown in Fig. 4.16 under the same condition of $\dot{m}$ = 90 g/s, the detonation velocity is significantly increased.

This shows that simply increasing the mass flow rate is not the best solution for detonation waves propagating in the fuel jet, because igniting the fuel consumes the detonation energy.

4.5.3 Effect of fuel injection angle

The numerical analysis results of Premixed gas injection are shown in Table 4.4 and Fig.4.17 - Fig. 4.19. The injected fuel is ignited, and the detonation wave is maintained and propagated. The shock wave propagating through the inlet and the oblique shock wave generated by the detonation will not reach the bottom through the upper reflection before the detonation wave passes through the fuel injection port, which will affect the propagation of the detonation wave. So the presence

of the ceiling does not affect the propagation of the detonation.

In this calculation, the angle changes of the injectors were not opposite, and the angles of all the injectors were changed in the same direction, as shown in Fig. 4.4(c) and 4.4(d). A total of three conditions are set, vertical injection, 45° injection to the left(45°L), and 45° injection to the right(45°R). A difference was shown in the detonation wave's propagation velocity depending on the fuel's injection angle. The effect of the detonation wave pressure on the combustion injection is the largest when the injector is at an angle opposite to the detonation wave propagation direction, and the propagation velocity is the lowest.

In the premixed fuel injection train, the fuel distribution of the burnt gas behind the detonation wave in each case indicates that the combustion is complete. The detonation velocity in each case reached 93% -98% of the C-J theoretical value.

4.6 Results of Non-premixed gas injection

4.6.1 Effect of grid size on fuel mixing

The mixing of non-premixed fuel adopts double nozzles, and the grid size in the numerical analysis often affects the shape and mixing of the jet flow, so the numerical analysis of the fuel mixing under each grid size is carried out. The jet flow numerical analysis model is shown in Figure 4.20. The flow velocity and fuel distribution information are obtained by setting recording points at the height of 5 mm between adjacent nozzles. The results are shown in Figure 4.22 and Figure 4.23. It can be seen that the fuel flow rate and mixing degree are consistent under the grid within 50 μm.

4.6.2 Effect of fuel injection angle

The numerical analysis results of the non-premixed gas injection are shown in Table 4.5 and Fig.4.24 - Fig.4.26. The injected fuel was successfully ignited. However, the propagation velocity of the wavefront was significantly slowed down, shock wave and combustion wave were separated, and detonation wave propagation could not be maintained. The cause is to avoid the impact of the shock wave generated by the supersonic fuel jet on the propagation of the detonation wave, the flow velocity of the fuel is limited to within the sonic, so it is much smaller than the actual mass flow rate of RDE. After increasing the fuel mass flow rate to the same level as RDE, as shown in Fig. 4.16, Detonation propagation is maintained. However, the detonation wave velocity is not as high as that of the premixed injection, only reaching 80% of the theoretical C-J velocity.

Concurrently, the results also clearly show that the combustion is greatly improved after changing the fuel injection roll angle to improve the fuel's mixing state. In addition, the mixing state of fuel and oxygen in the field between the shock wave and combustion wave is significantly improved compared with the mixing state before the shock wave. The promoting effect of the shock wave on the fuel mixture can be confirmed.

4.6.3 Effect of fuel mass flow rate

By increasing the mass flow rate of the 45° double injector to 60 g/s, the results are shown in Fig. 4.27. By comparing the positions of the shock wave and the combustion wave(Fig. 4.27(a), Fig. 4.27(b)), it can be confirmed that the detonation maintains the propagation. However, it can also be seen that the reason for the supersonic fuel jet is that the flow field inside the combustion chamber

is extremely unstable. Although increasing the mass flow rate maintains the propagation of the detonation, the impact of the shock wave generated by the supersonic jet has to be considered.

4.7 Results of Non-premixed gas injection promoted mixing

The numerical analysis results are shown in Table 4.6 and Fig. 4.28 - Fig. 4.30. The injection conditions are the same as for non-premixed gas injection, and a partially mixed state is created by filling the entire pipe with 20 kPa of Ethylene-Oxygen premixed gas. The injected fuel is successfully ignited, and the detonation wave is maintained and propagated. The detonation wave propagation velocity tends to increase as the facing angle of the fuel injection increases, and the improvement in the fuel consumption rate is also clear.

4.8 Summary

Premixed fuel maintains detonation propagation even at very low mass flow rates. Numerical results of premixed fuel all achieve more than 90% of the C-J velocity, while at low fuel flow rates, it is difficult to maintain detonation propagation without promoting mixing with non-premixed fuel. The detonation propagation velocity of non-premixed fuel after promoting over fuel mixing reached more than 90% of the theoretical C-J velocity. Therefore, it can be expected that the performance can be improved by creating a structure in the RDE that allows the fuel and oxidizer to intersect in advance and be injected in the direction of the detonation wave propagation.

Double injector performs best at a 45-degree angle. The fuel injection velocity at the trailing edge of the detonation in the complete combustion state decreased by about 64%, 33%, and 26%

in the opposite, the vertical and same direction as the propagation direction of the detonation wave at a 45-degree angle.

Table 4.1 Optical visualization experimental conditions.

Experiment condition	
Camera	High Speed camera (Shimadzu:HPV-1)
Lens	f = 600
Light source	CAVILUX Smart UHS
Frame interval	50 ns
Exposure time	1 μm
Number of pixels	312 x 260

Table 4.2 Injection conditions.

Number of gird	8001 x 1001
Grid width	50 μm
Fuel-Oxid.	Ethylene-Oxygen
Equivalent ratio	1
Filling pressure (Detonation tube)	0.1 MPa
P_0 (Linear detonation channel)	1 atm.

Table 4.3 Detonation velocity results of premixed gas injection.(mass flow rate change)

Mass flow rate	30 g/s	60 g/s	90g/s
Detonation velocity	2107 m/s	1976 m/s	1833 m/s
C-J velocity		2439 m/s	

Table 4.4 Detonation velocity results of premixed gas injection.(angle change)

Injector angle	45°L	45°	45°R
Detonation velocity	2277 m/s	2348 m/s	2425 m/s
C-J velocity		2439 m/s	

Table 4.5 Detonation velocity of non-premixed gas injection.

Injector angle	90°	70°	45°
Detonation velocity	1478 m/s	1482 m/s	1497 m/s
C-J velocity		2439 m/s	

Table 4.6 Detonation velocity of promote mixed non-premixed fuel.

Injector angle	90°	70°	45°
Detonation velocity	1935 m/s	2238 m/s	2290 m/s
C-J velocity		2439 m/s	

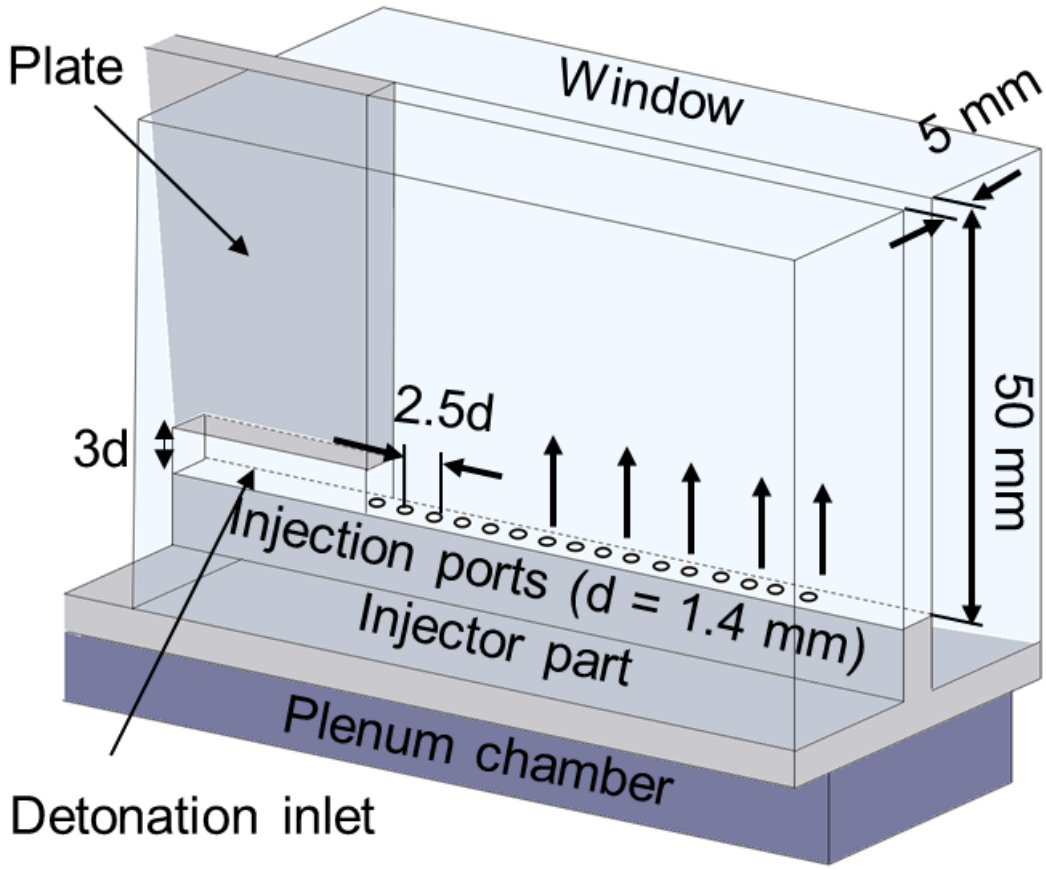

Fig. 4.1 Overview of closed linear detonation channel.

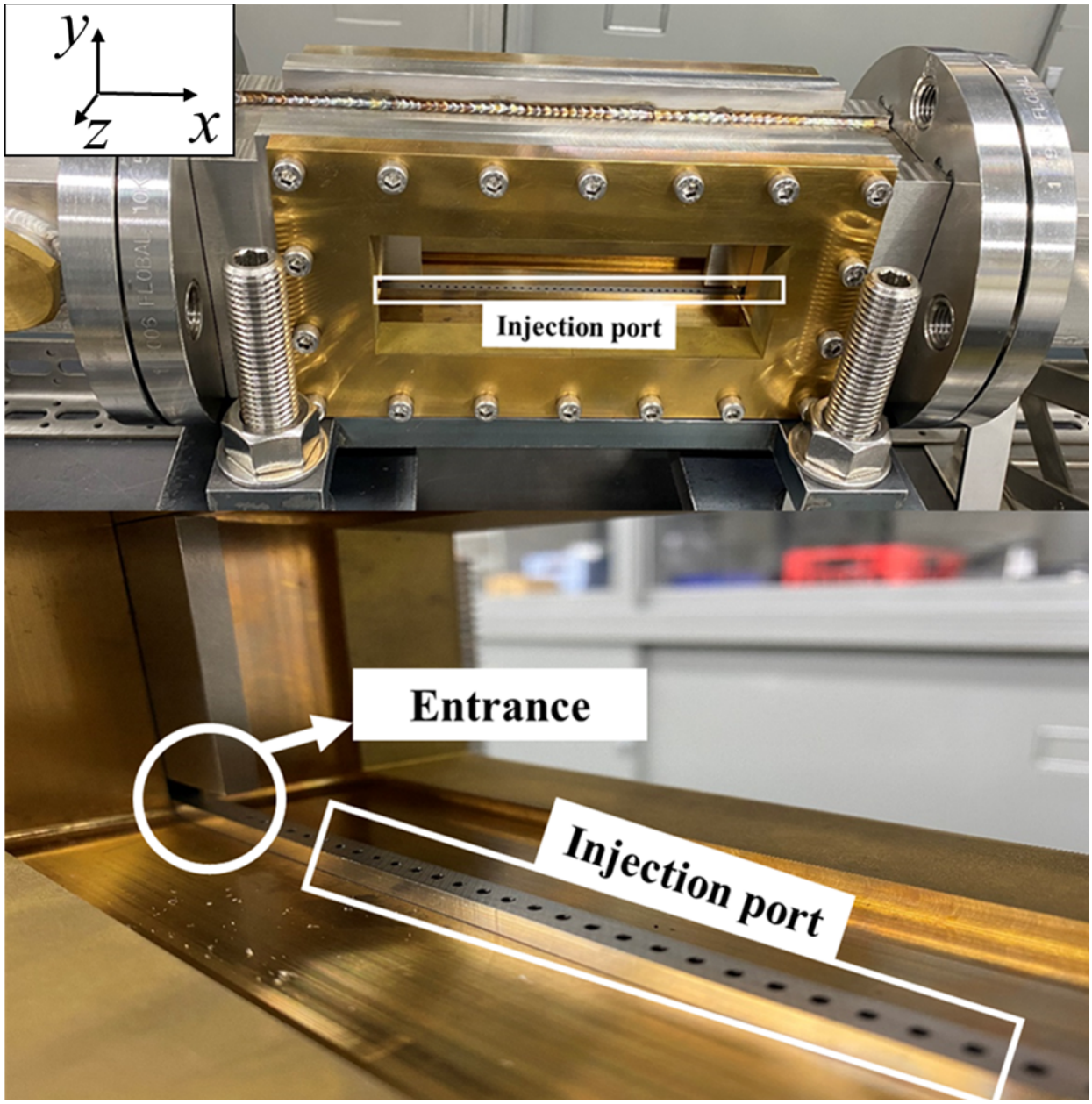

Fig. 4.2 LDC and injector.

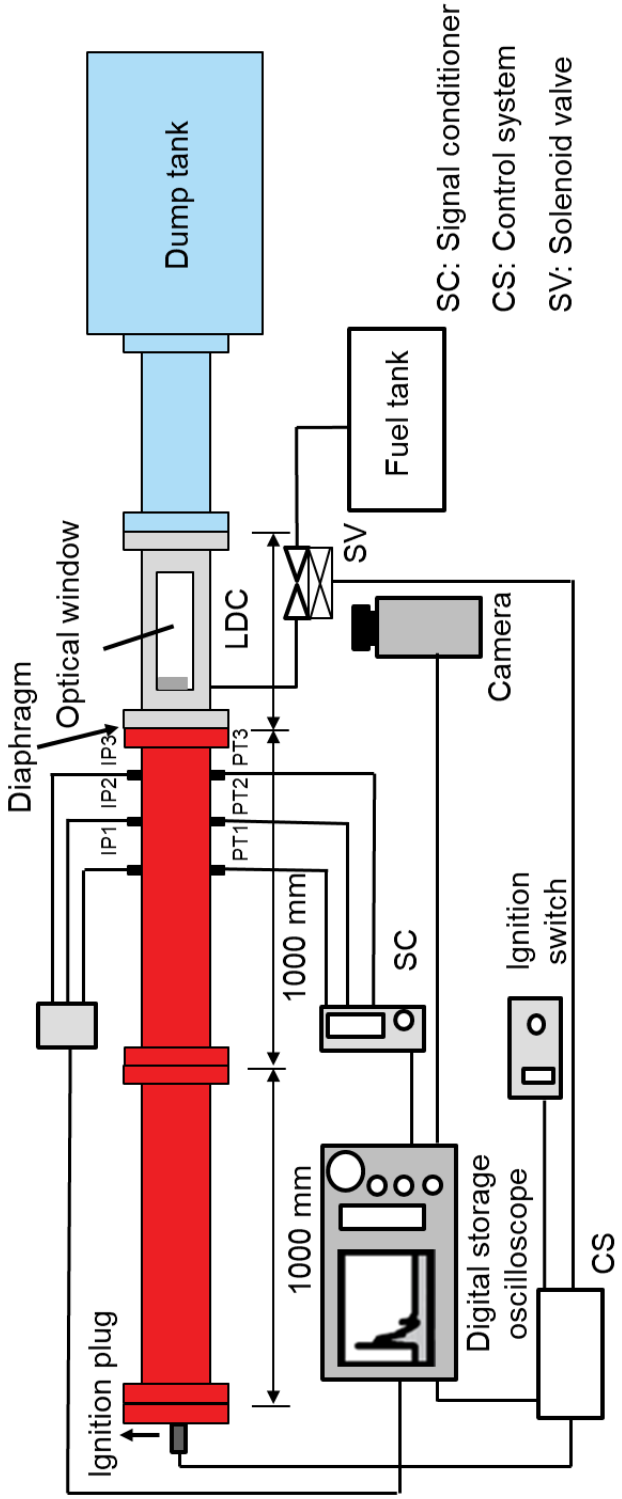

Fig. 4.3 Visualization experimental setup.

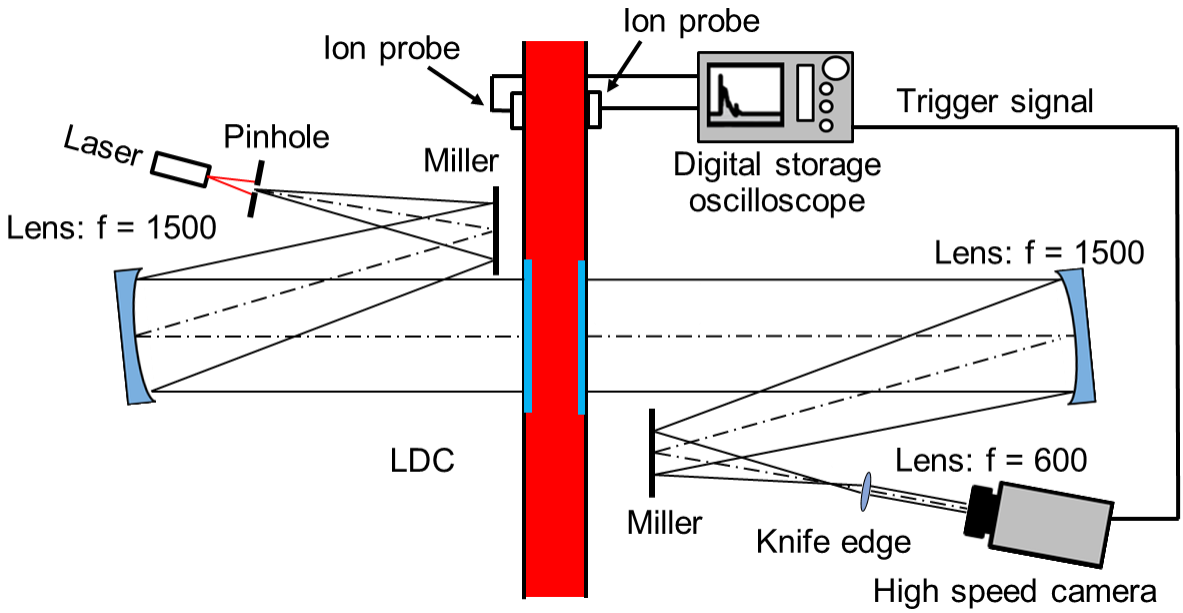

Fig. 4.4 Schematic diagram of the Schlieren setup.

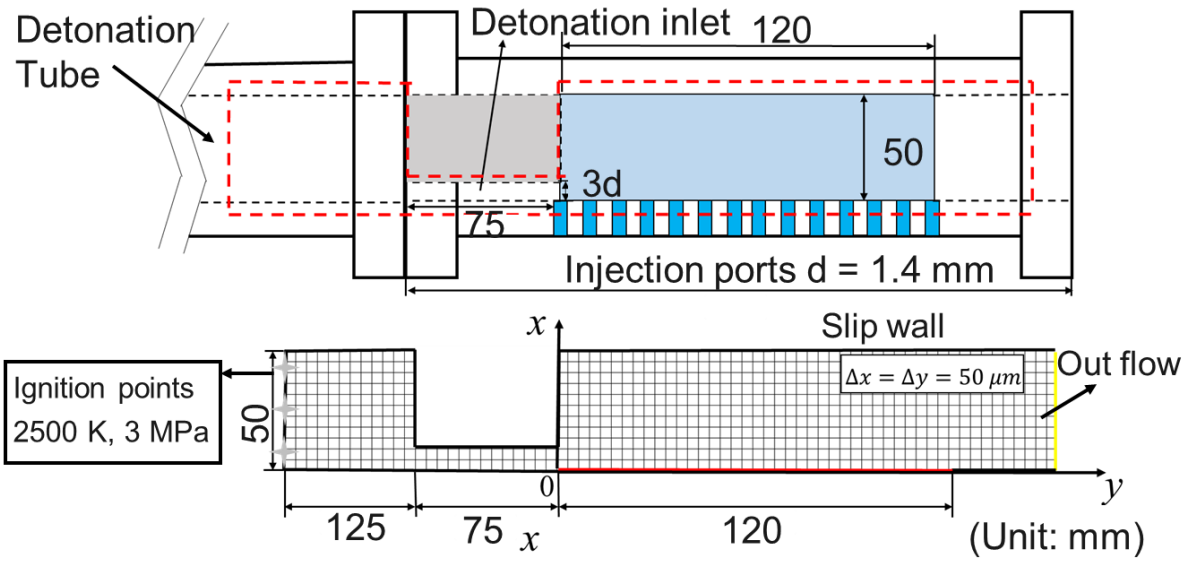

Fig. 4.5 Computational domain.

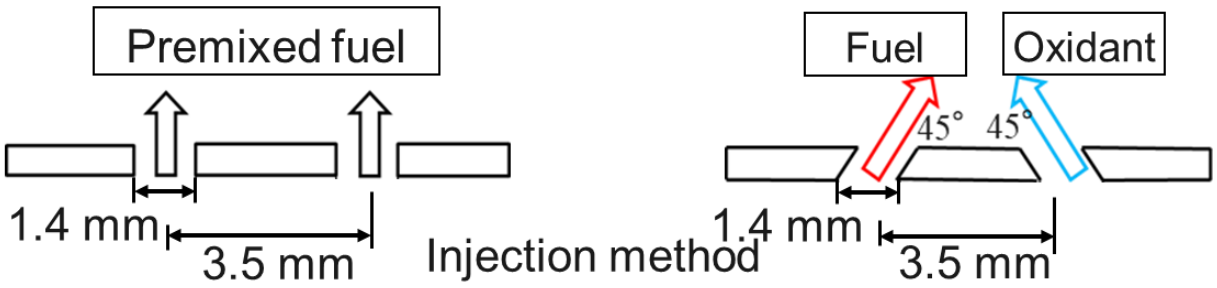

Fig. 4.6 Injection method.

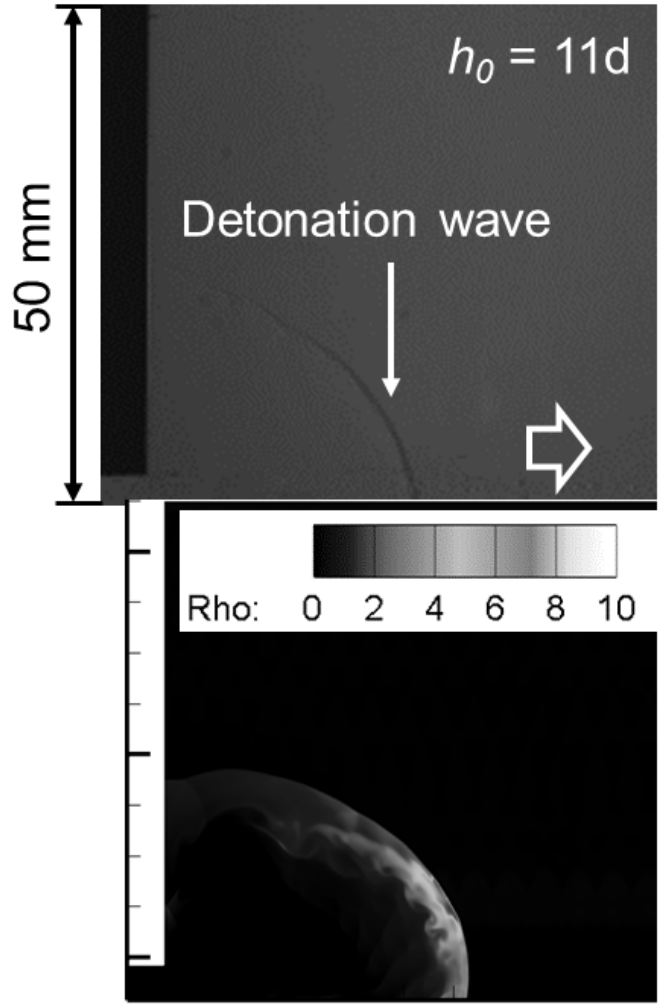

Fig. 4.7 Visualization result of h_0= 11d.

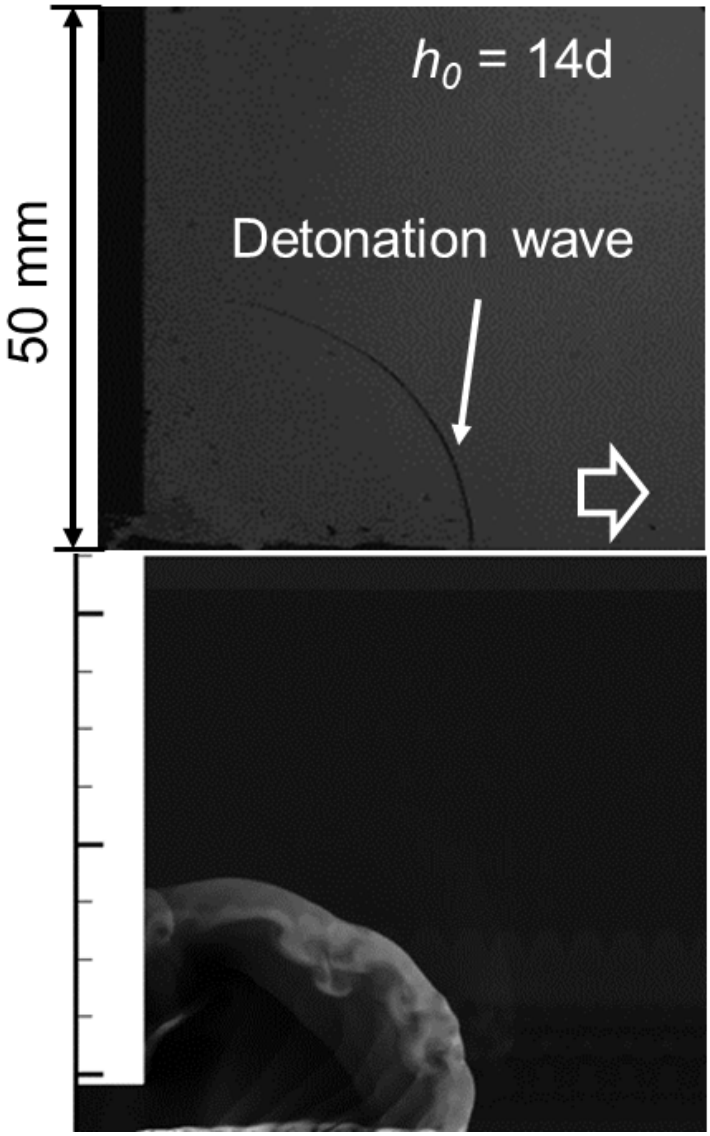

Fig. 4.8 Visualization result of h_0= 14d.

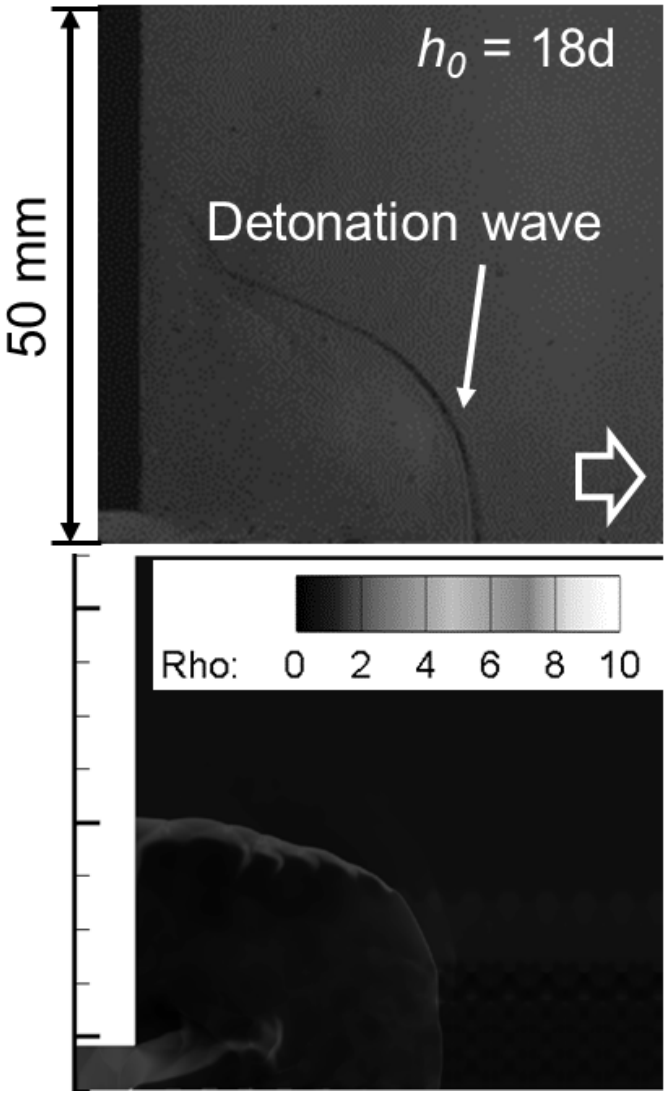

Fig. 4.9 Visualization result of h_0= 18d.

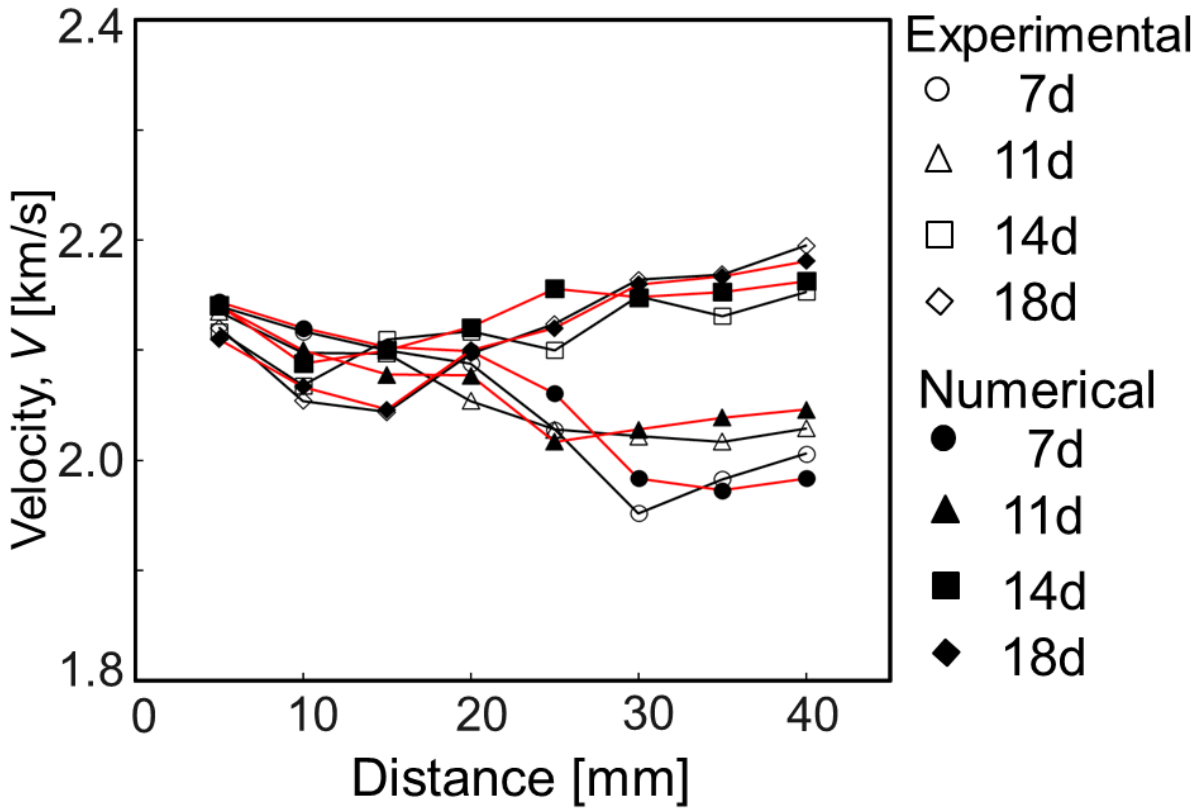

Fig. 4.10 Detonation velocity changes entering the LDC.

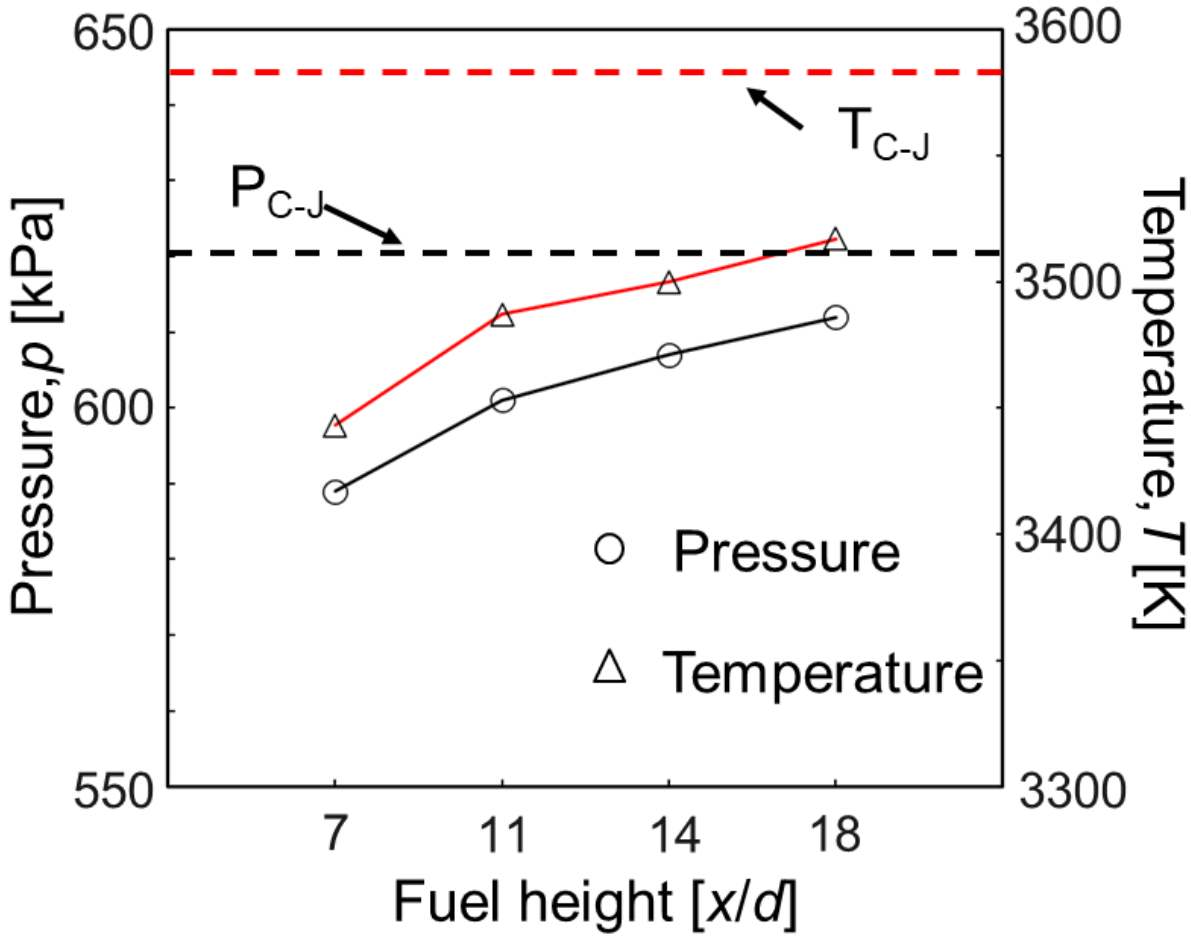

Fig. 4.11 Detonation pressure and temperature at different fuel heights.

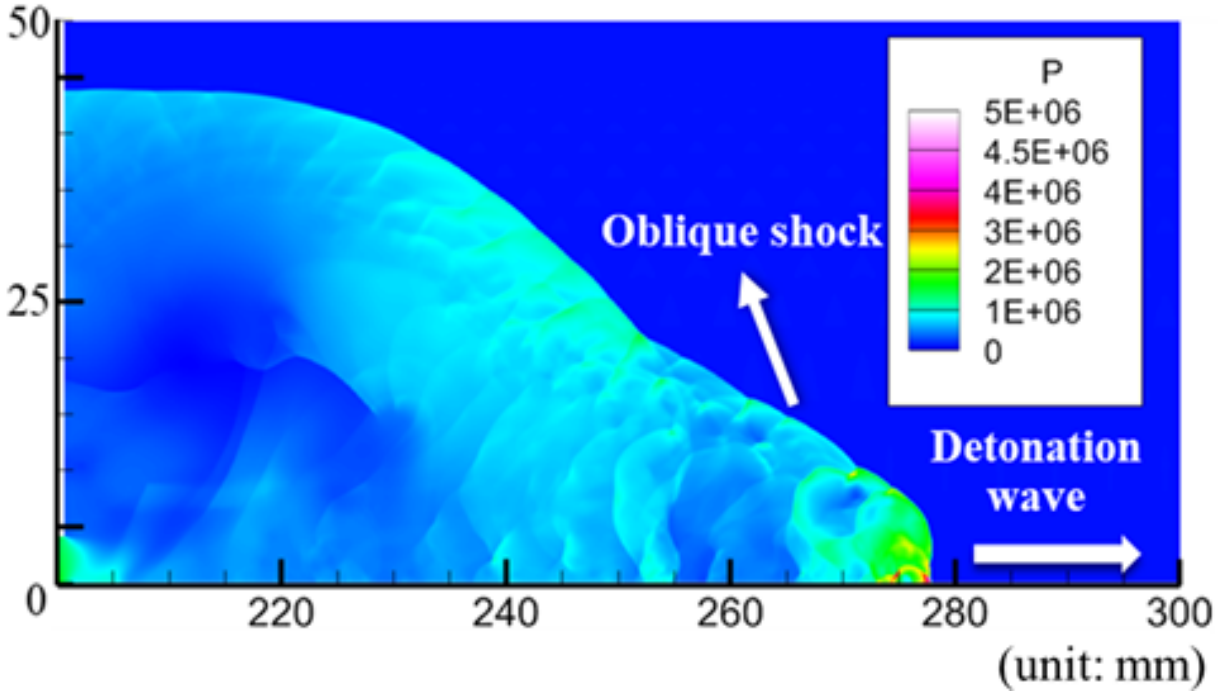

Fig. 4.12 Pressure distribution of $\dot{m}$ = 30 g/s.

Source: F. Wang, T. Mizukaki, and S. Matsuyama, S Proc. Schl. Eng. Tokai Univ., Ser. E., 47, pp.31-35 (2022).

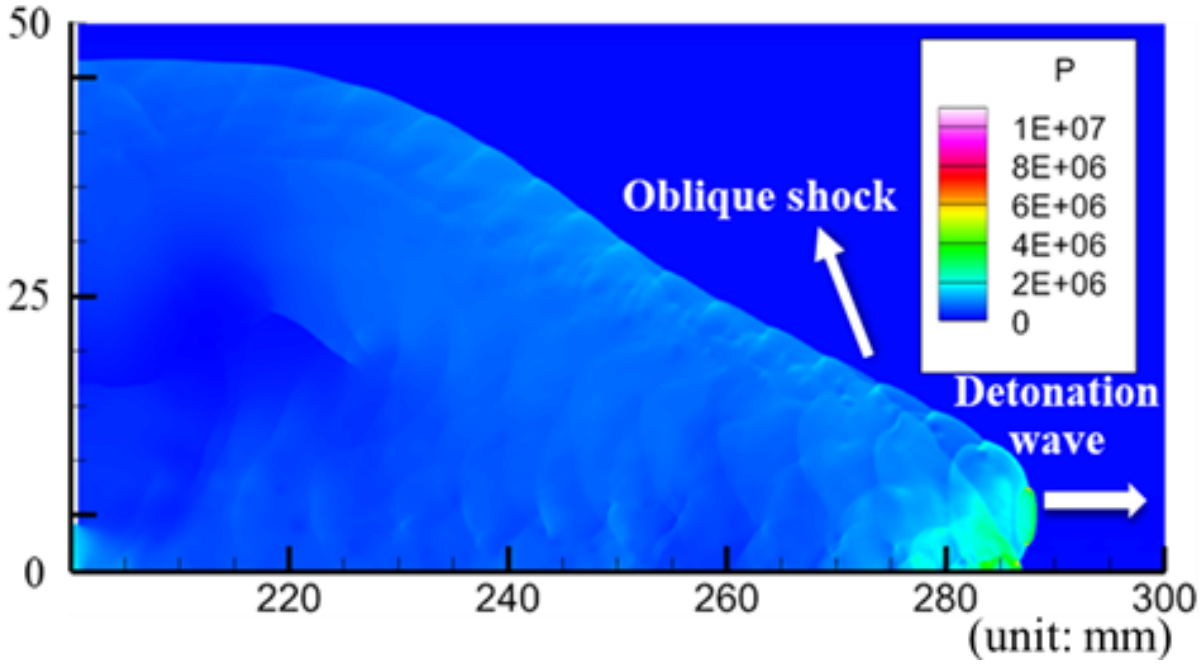

Fig. 4.13 Pressure distribution of $\dot{m}$ = 60 g/s.

Source: F. Wang, T. Mizukaki, and S. Matsuyama, S Proc. Schl. Eng. Tokai Univ., Ser. E., 47, pp.31-35 (2022).

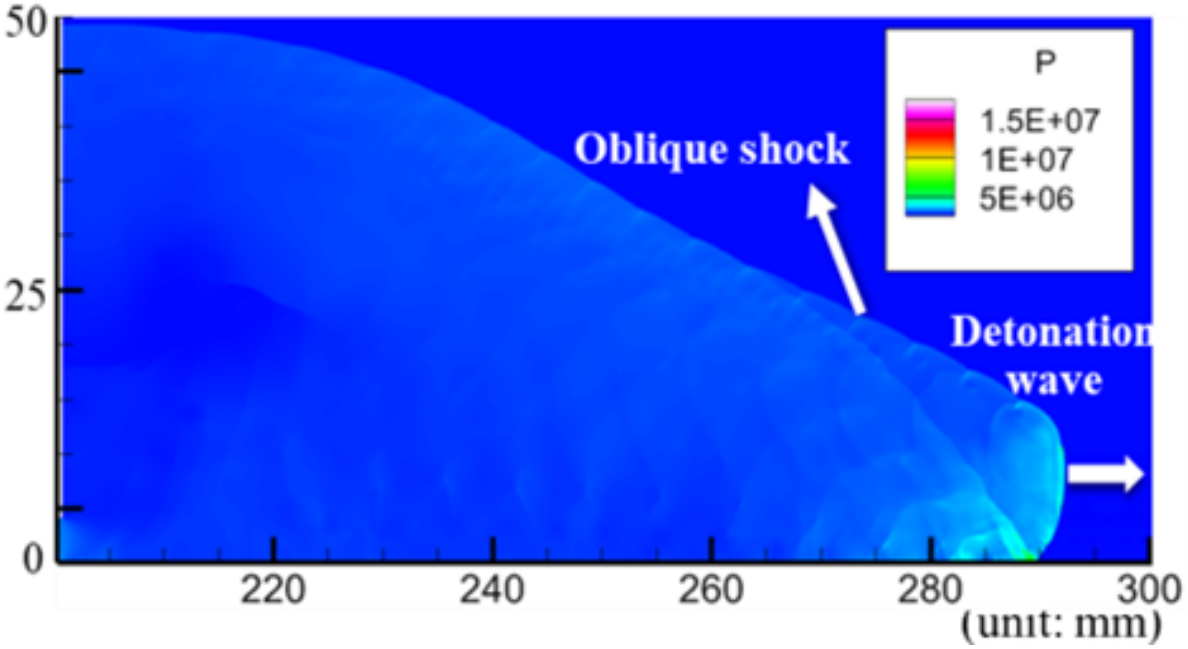

Fig. 4.14 Pressure distribution of $\dot{m}$ = 90 g/s.

Source: F. Wang, T. Mizukaki, and S. Matsuyama, S Proc. Schl. Eng. Tokai Univ., Ser. E., 47, pp.31-35 (2022).

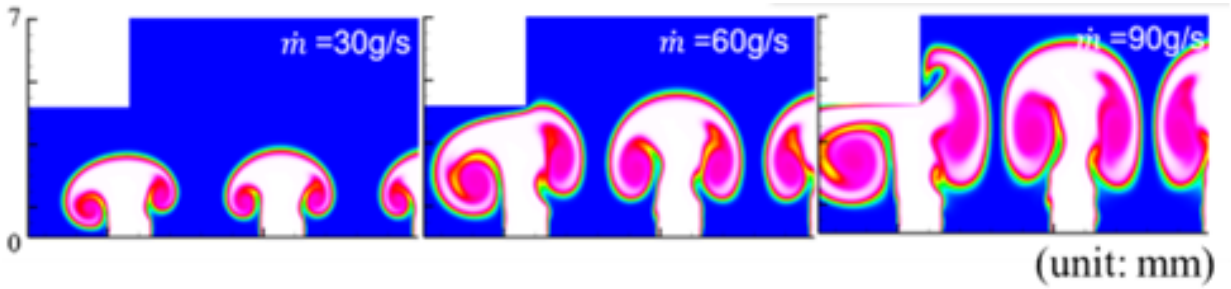

Fig. 4.15 Fuel injection height comparison at the same time.

Source: F. Wang, T. Mizukaki, and S. Matsuyama, S Proc. Schl. Eng. Tokai Univ., Ser. E., 47, pp.31-35 (2022).

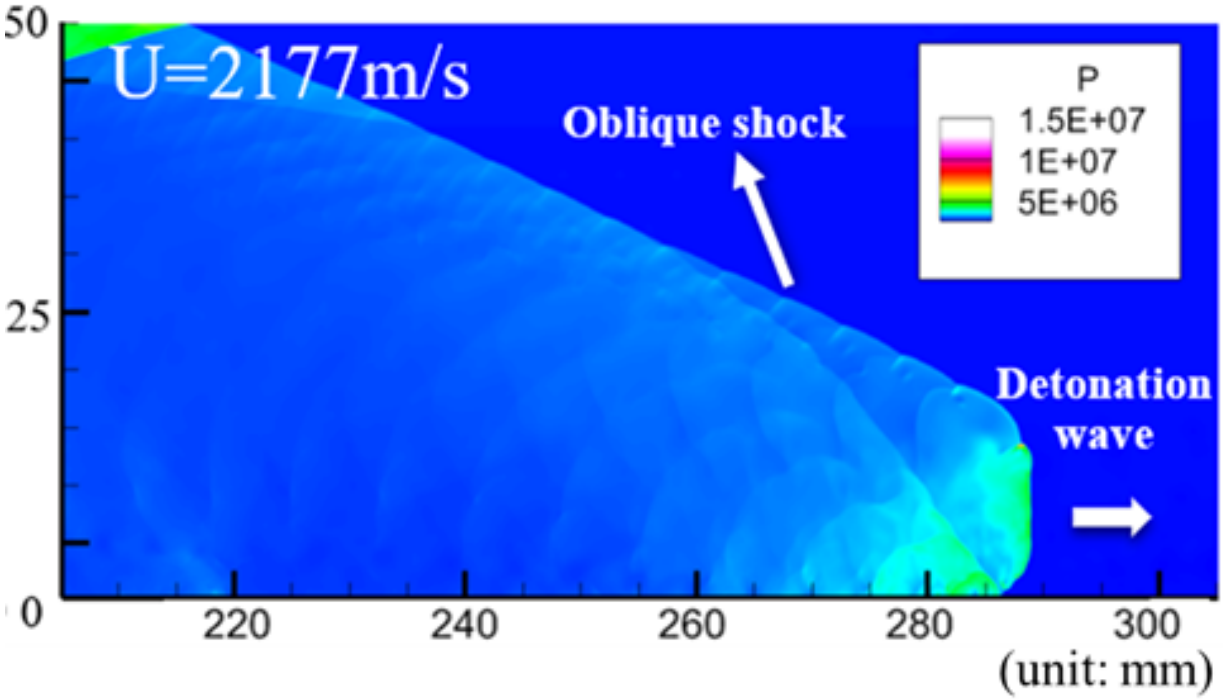

Fig. 4.16 Pressure distribution of $\dot{m}$ = 90 g/s of ignition pressure 150 kPa.

Source: F. Wang, T. Mizukaki, and S. Matsuyama, S Proc. Schl. Eng. Tokai Univ., Ser. E., 47, pp.31-35 (2022).

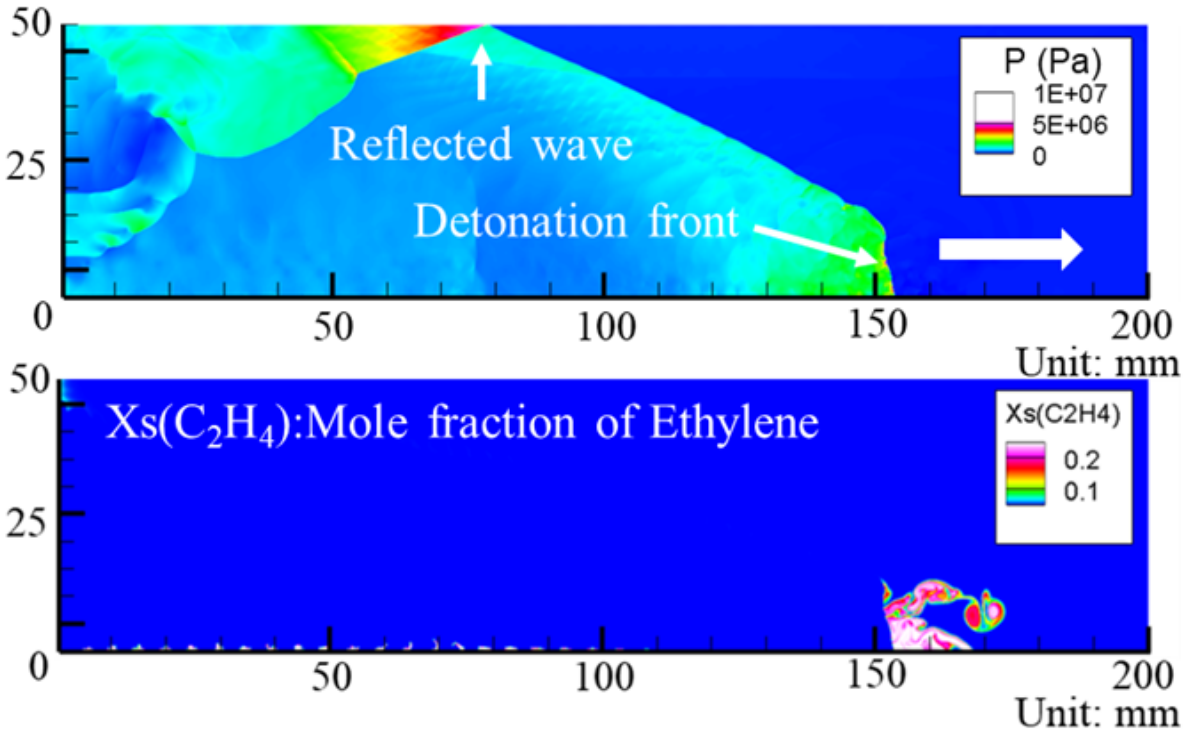

Fig. 4.17 Pressure distribution and fuel distribution of 45°L.

Source: F. Wang, and T. Mizukaki, Sci. Technol. Energ. Mater. Vol. 83, No.5, pp.125-131 (2022).

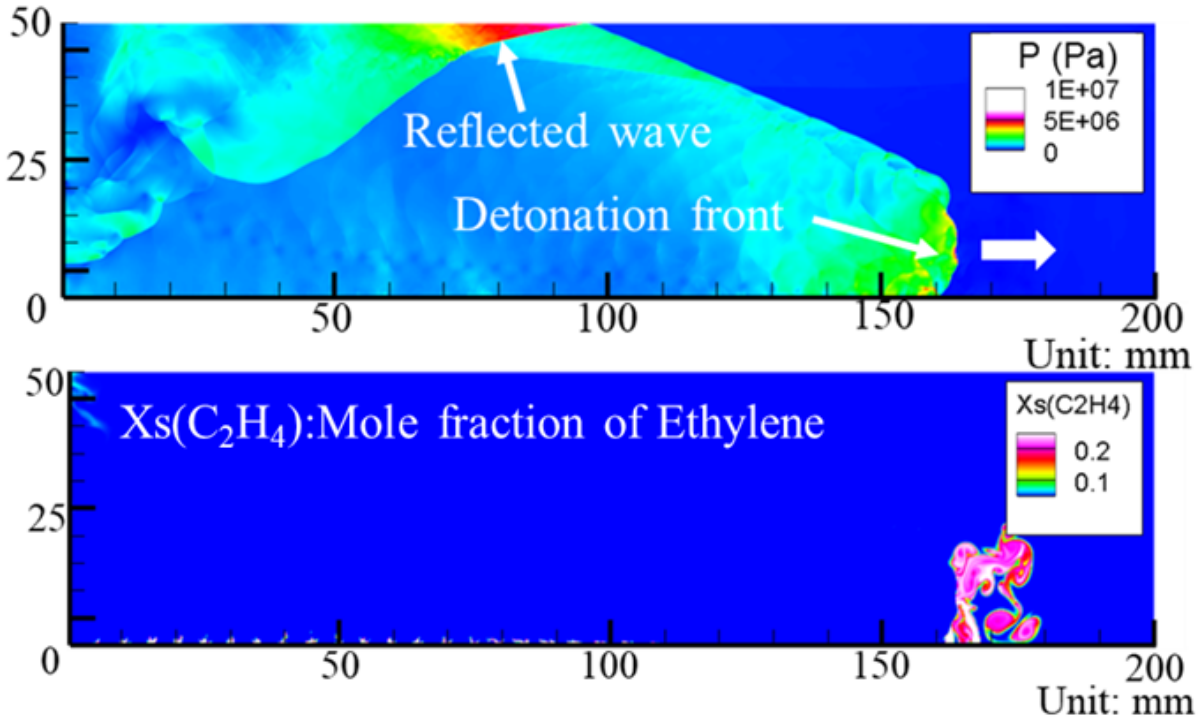

Fig. 4.18 Pressure distribution and fuel distribution of 90°.

Source: F. Wang, and T. Mizukaki, Sci. Technol. Energ. Mater. Vol. 83, No.5, pp.125-131 (2022).

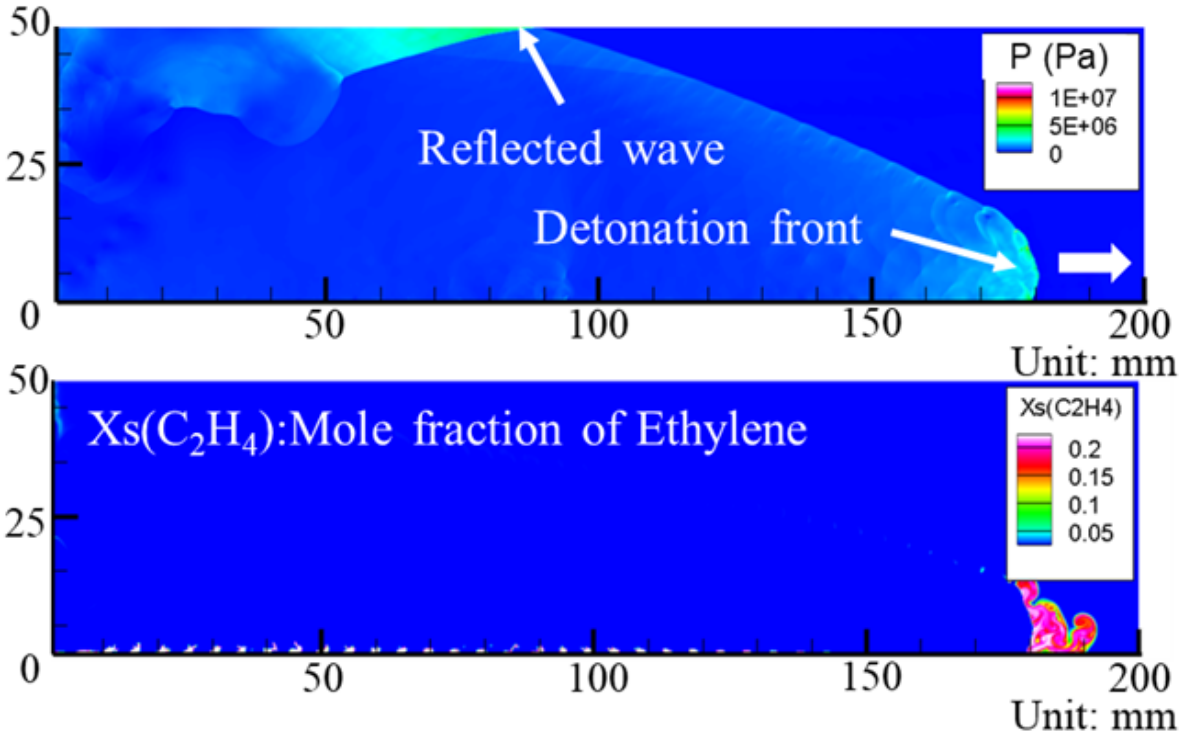

Fig. 4.19 Pressure distribution and fuel distribution of 45°R.

Source: F. Wang, and T. Mizukaki, Sci. Technol. Energ. Mater. Vol. 83, No.5, pp.125-131 (2022).

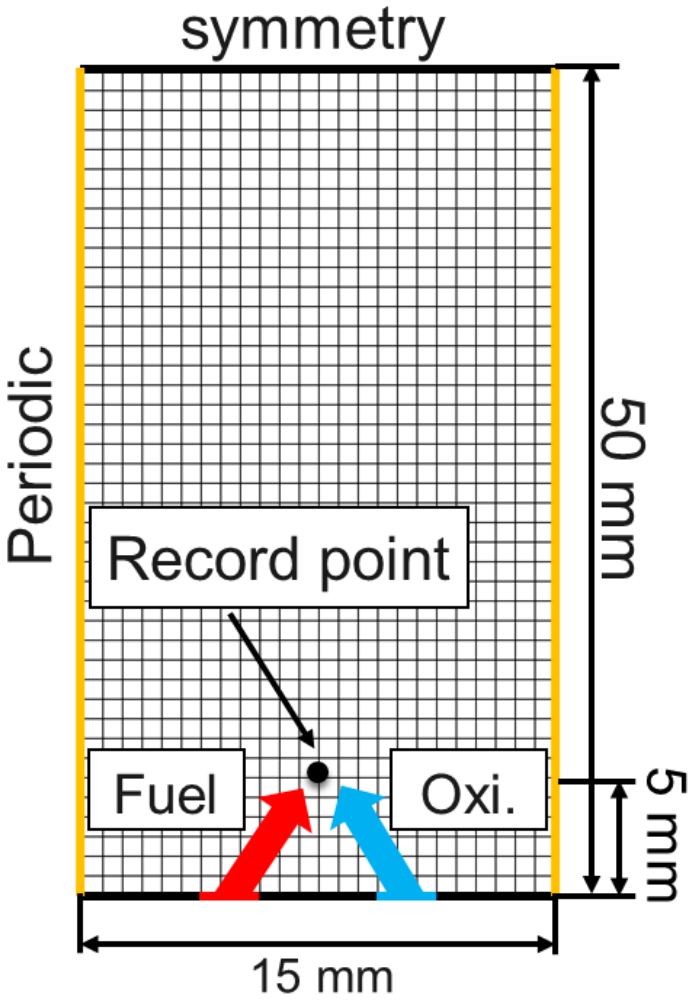

Fig. 4.20 Computational domain of fuel mixing.

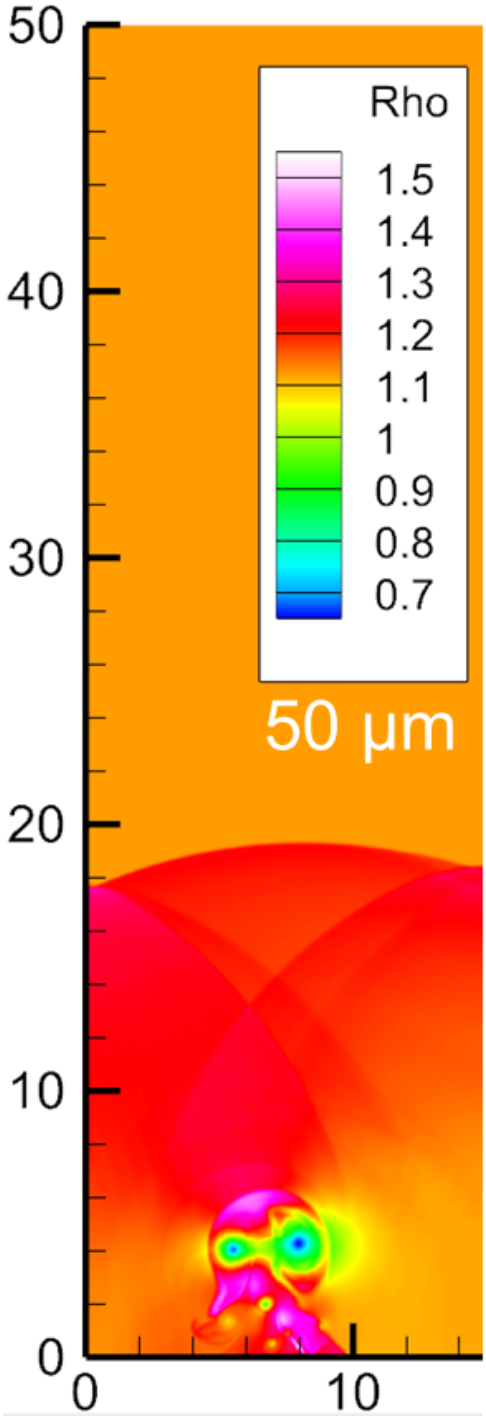

Fig. 4.21 Calculation example of fuel mixing (50 μm).

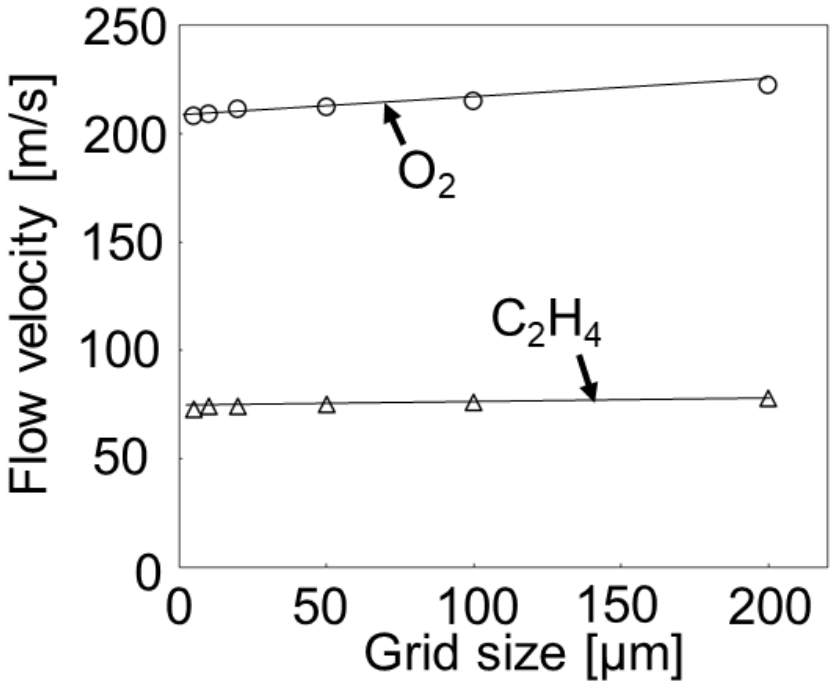

Fig. 4.22 Effect of mesh size on fuel flow rate.

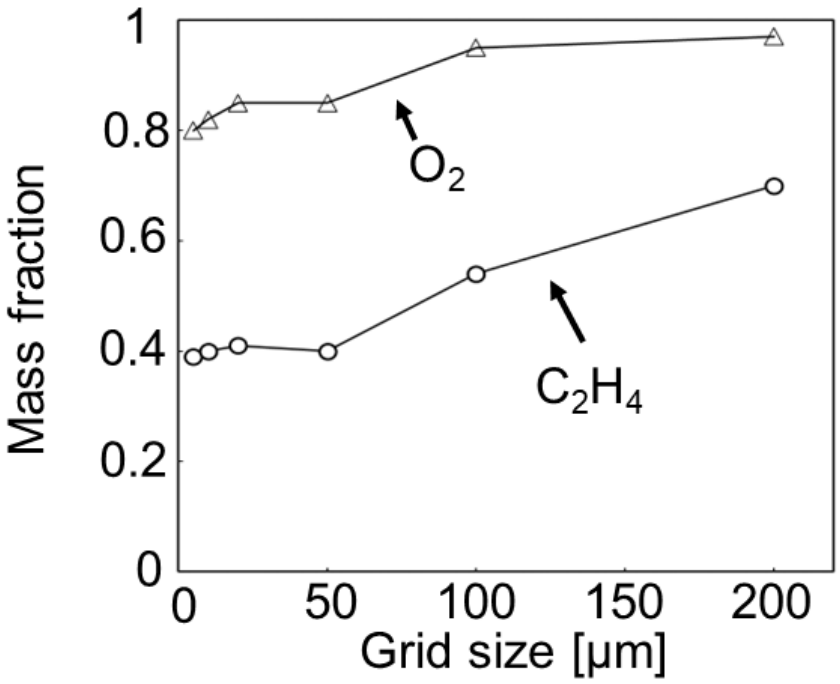

Fig. 4.23 Effect of mesh size on fuel mixing.

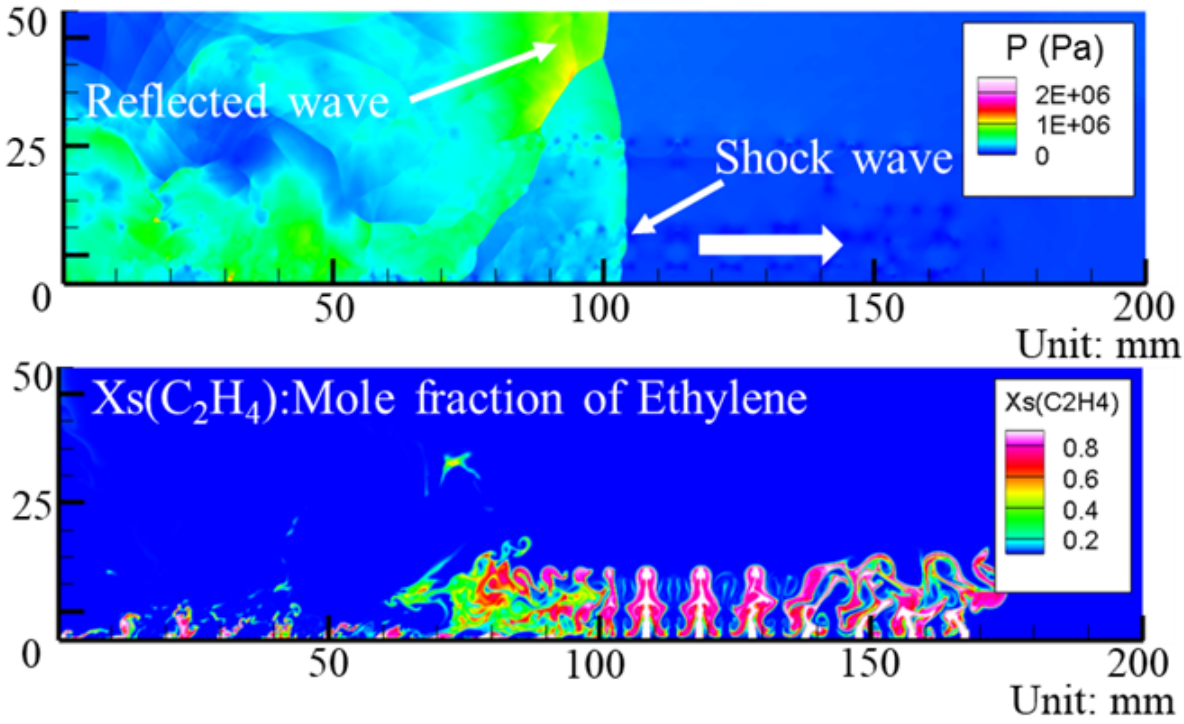

Fig. 4.24 Pressure distribution and fuel distribution of 90°.

Source: F. Wang, and T. Mizukaki, Sci. Technol. Energ. Mater. Vol. 83, No.5, pp.125-131 (2022).

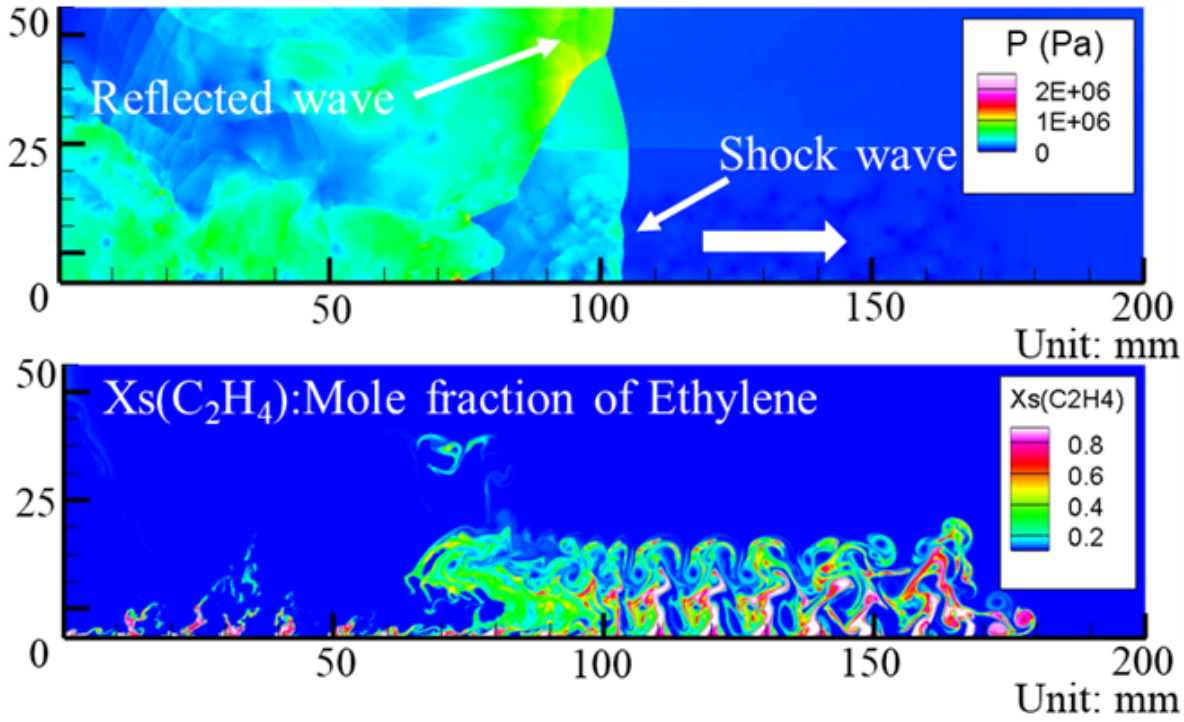

Fig. 4.25 Pressure distribution and fuel distribution of 70°.

Source: F. Wang, and T. Mizukaki, Sci. Technol. Energ. Mater. Vol. 83, No.5, pp.125-131 (2022).

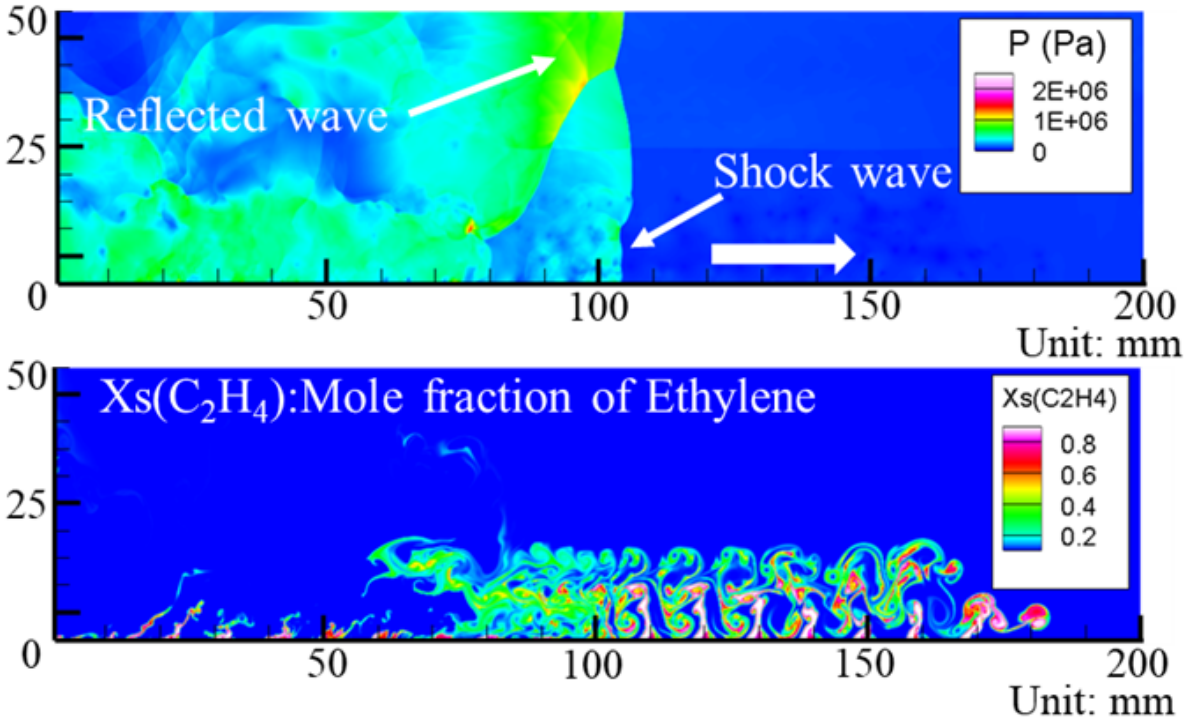

Fig. 4.26 Pressure distribution and fuel distribution of 45°.

Source: F. Wang, and T. Mizukaki, Sci. Technol. Energ. Mater. Vol. 83, No.5, pp.125-131 (2022).

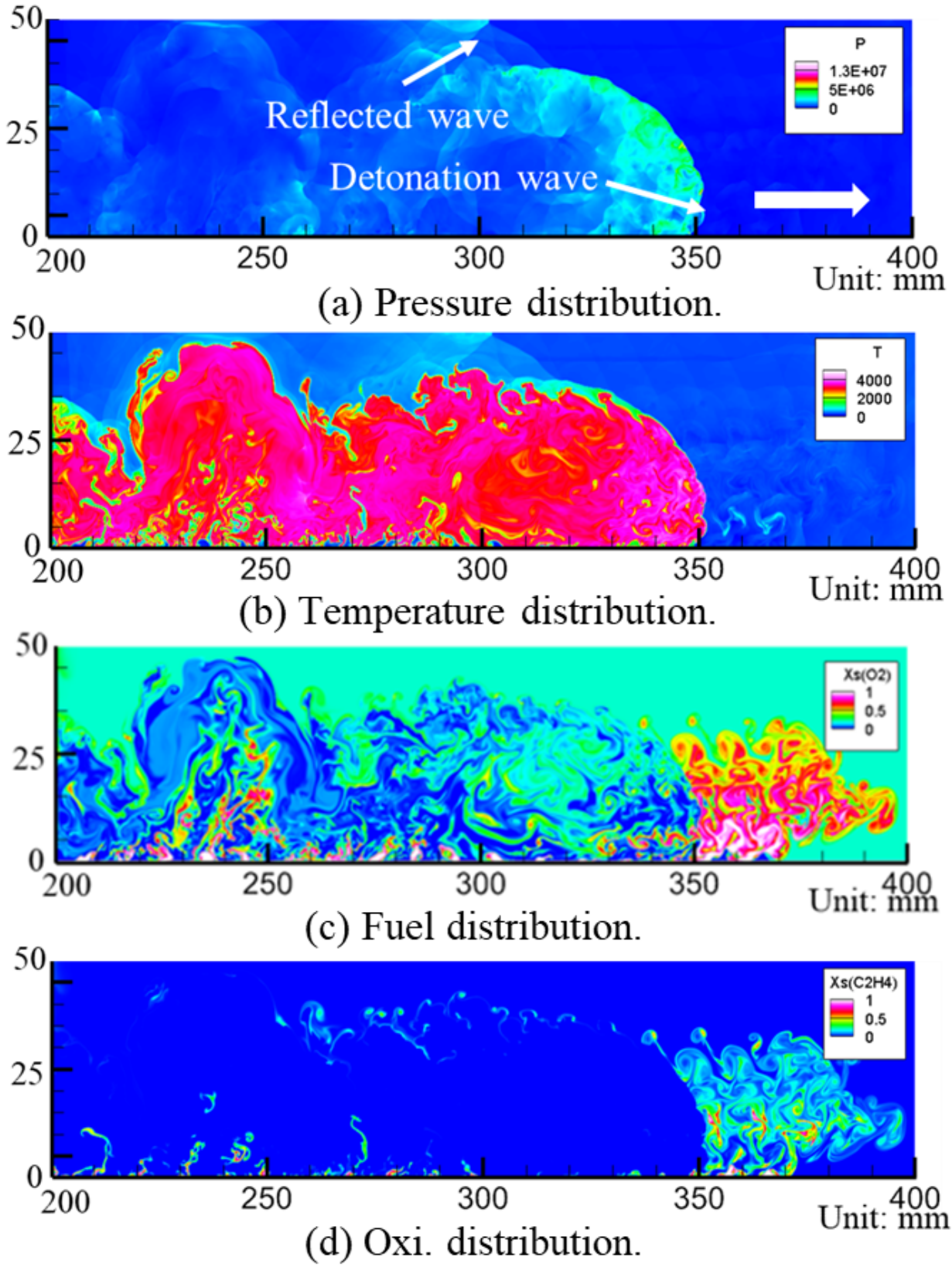

Fig. 4.27 Pressure distribution and fuel distribution of 45° with high mass flow rate.

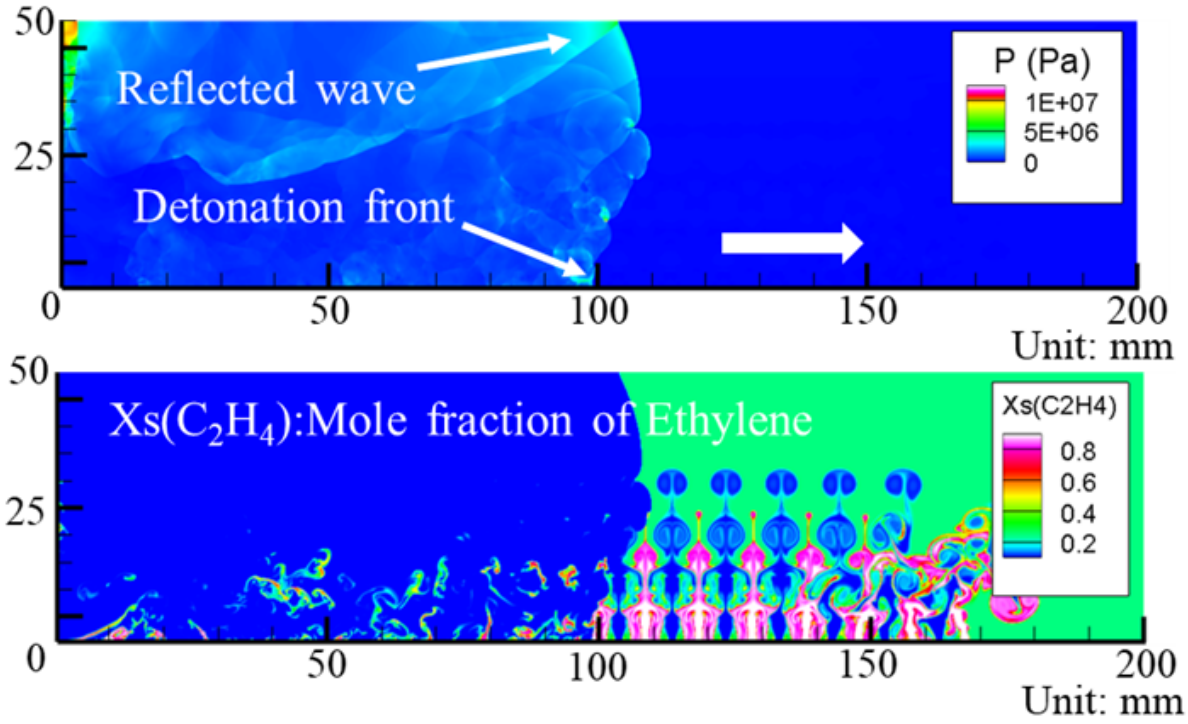

Fig. 4.28 Pressure distribution and fuel distribution of 90°.

Source: F. Wang, and T. Mizukaki, Sci. Technol. Energ. Mater. Vol. 83, No.5, pp.125-131 (2022).

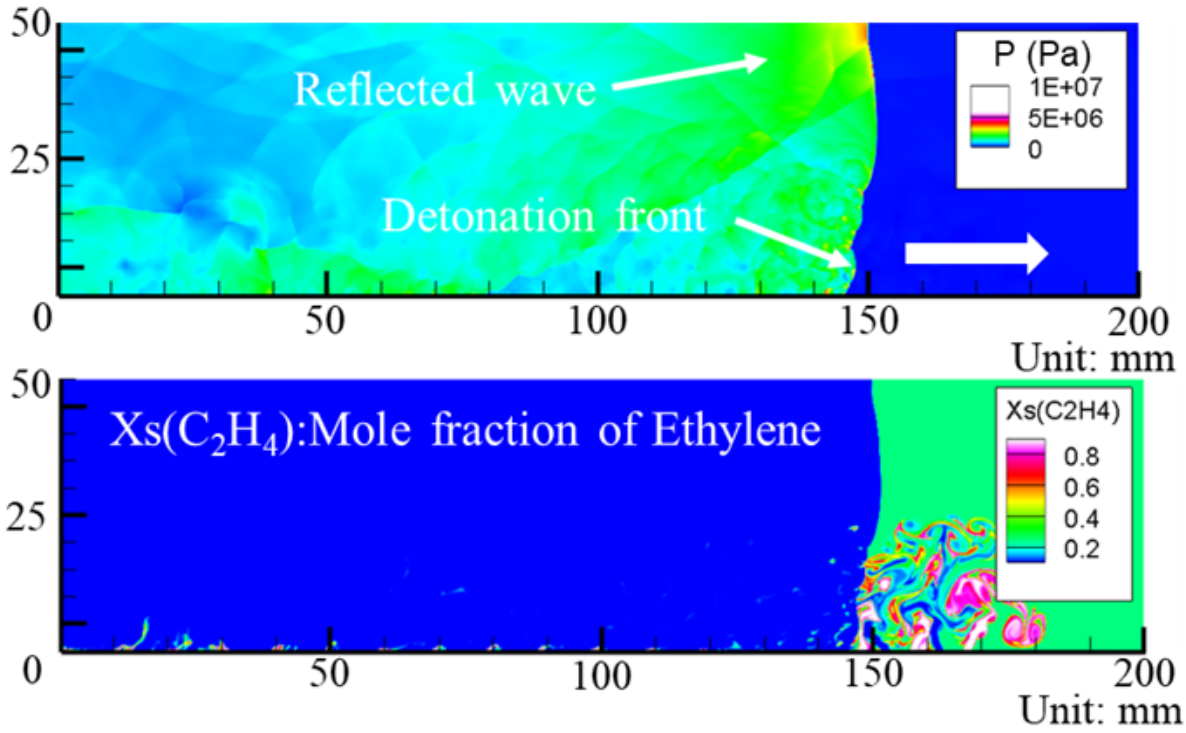

Fig. 4.29 Pressure distribution and fuel distribution of 70°.

Source: F. Wang, and T. Mizukaki, Sci. Technol. Energ. Mater. Vol. 83, No.5, pp.125-131 (2022).

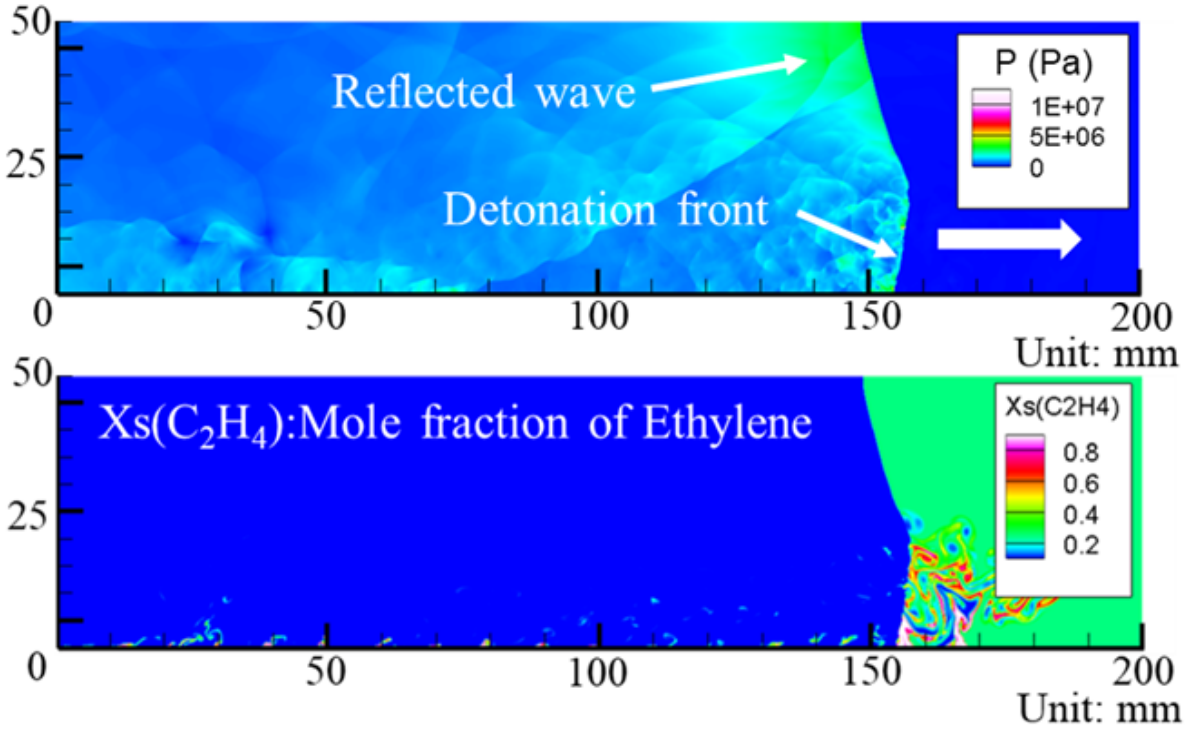

Fig. 4.30 Pressure distribution and fuel distribution of 45°.

Source: F. Wang, and T. Mizukaki, Sci. Technol. Energ. Mater. Vol. 83, No.5, pp.125-131 (2022).

Chapter 5

Effect of mixture on propagation of detonation waves inside two-dimensional unwrapped RDE

5.1 Overview

Following the content of the previous chapter, the numerical analysis of the detonation wave propagation inside a two-dimensional unwrapped RDE is carried out, and the different propagation states of the rotating detonation wave in the combustible fuel injection train are analyzed. The RDE prototypes that were analyzed were derived from small experimental RDE held by our laboratory.

5.2 Computational model

This analysis is performed for a two-dimensional RDE combustor expanded in the circumferential direction. Each dimension of the computational domain was determined with reference to the small RDE shown in Fig. 5.1. Figure 5.2 shows the computational grid and initial conditions. The grids are all 50 μm square grids, and the total number of grids is 18,377,361. A boundary condition is applied that simulates opposing fuel and oxygen injectors with a diameter of 1 mm, which are installed equidistantly on the bottom surface, and set as d in this chapter as a reference. The walls between the injectors are non-slip walls. In addition, the angle of the injector can be changed from a vertical 90° injection to an opposing 45° injection. The upper edge of the computational grid is a constant pressure outflow boundary of 0.1 MPa.

5.3 Initial Conditions

The initial conditions consist of two regions, the source, and still air. The ignition source is a high-temperature and high-pressure region with a pressure of 3 MPa and a temperature of 3000 K. The set values of temperature and pressure refer to the detonation pressure and temperature under standard air pressure. The position and width of the ignition region were set to match the position and diameter of the small RDE predetonator. Fuel is injected for 0.1 ms before ignition. The initial airflow conditions for the entire calculation region are 100 kPa pressure and 300 K still air temperature. As a result, the fuel and oxidizer are ignited from the detonation source after 0.1 ms has passed since the start of injection, and a detonation wave propagating to the right is obtained.

5.4 Numerical analysis Results

5.4.1 Mode of propagation of detonation waves

The instantaneous pressure field after the steady propagation of the detonation wave is shown in Fig. 5.3 -Fig 5.5. In all calculations, the typical detonation wave state accompanied by the inclined shock wave propagating near the bottom of the combustion chamber is obtained. And produced more detonation waves, some of which propagated in the opposite direction to the ignition setting.

When premixed fuel is used, the wavefront height of the detonation wave is low, and the angle of the oblique shock wave is large. Calculations using non-premixed fuel show that the direction of propagation is more stable in the cross injection than in the vertical injection.

Figure 5.6 shows a comparison of detonation wave propagation velocities. To compare the relationship with the equivalence ratio, calculations were performed for three cases of equivalence ratios of 0.8, 1.0, and 1.2.

The propagation velocity is the instantaneous velocity of the detonation wave 5 ms after ignition. Only the fastest propagating detonation wave is recorded when there are multiple detonation waves.

When using premixed fuel, the detonation wave propagation velocity reaches more than 90% of the C-J velocity. In contrast, when using non-premixed fuel, the detonation wave velocity is about 70% - 88% of the C-J velocity. Compared to non-premixed fuel, the premixed fuel injection improved the speed loss rate from the C-J speed from about 30% to 11%. This is thought to be related to the number of detonation waves and the non-uniformity of the mixed state of the mixture

in front of the detonation wave.

The number of detonation waves and the direction of propagation is shown in Figure 5.7. All case multiple detonation waves were generated in all calculation cases. Still, the number of detonation waves was smaller in the cross injection than in the vertical injection, and the direction of propagation tended to be stable.

5.4.2 Fuel and oxidant consumption

Figure 5.8 - Fig. 5.10 shows the fuel distributions in the RDE when the equivalence ratio is 1.0. It can be seen that when premixed fuel is used, unconsumed fuel only exists before the detonation wave, while non-premixed fuel still has a large amount of unconsumed fuel even after the detonation wave passes. Compared with vertical injection, there is less unconsumed fuel in the angled injection mode, and a significantly higher pressure rise can be obtained.

5.5 Summary

Continuing the content of the previous chapter, the numerical analysis of the influence of two fuel injection modes on the internal flow of RDE is carried out by using a two-dimensional unwrapped RDE. The state of the detonation wave propagating in the combustible fuel injection train in the RDE burner is analyzed, and the following results are obtained.

When using non-premixed fuel, the detonation wave velocity decreases as the number of detonation waves increases. However, when premixed fuel is used, the detonation wave propagation velocity still reaches 90% of the CJ velocity even though there are multiple numbers of detonation waves. Therefore, an imperfect fuel mixture is considered to have a greater effect on the deto-

nation wave velocity than the number of detonation waves. The detonation propagation velocity with premixed fuel is much higher than with non-premixed fuel, which reduces the detonation velocity loss to C-J velocity from about 30% to 11%. And double injector for fuel mixing and improved detonation propagation are reconfirmed.

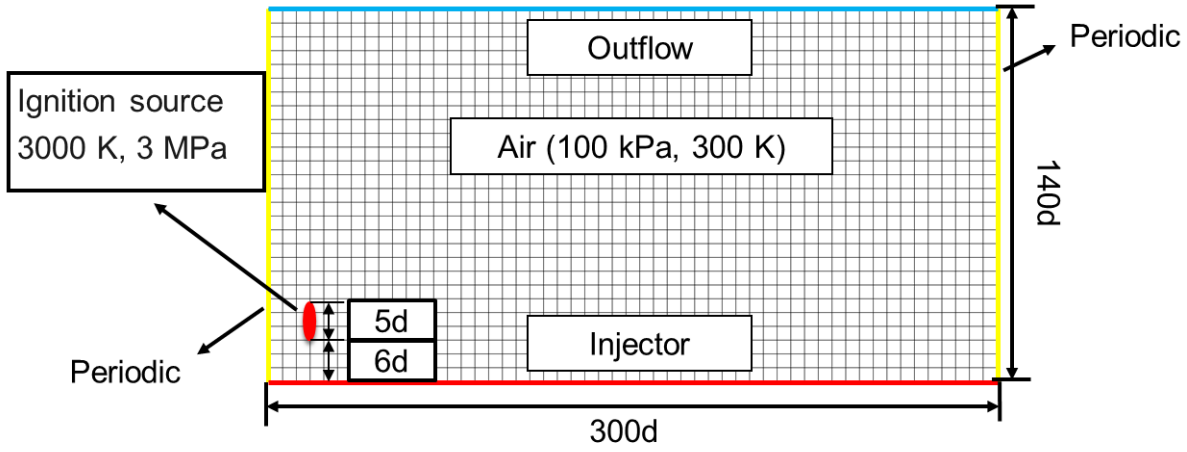

Fig. 5.1 Calculation domain.

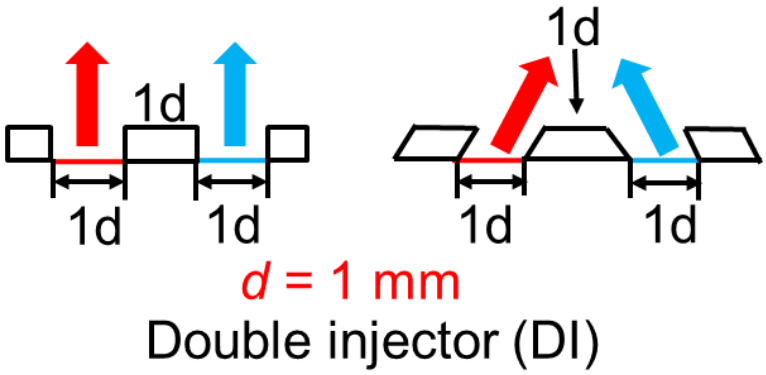

Fig. 5.2 Injection method.

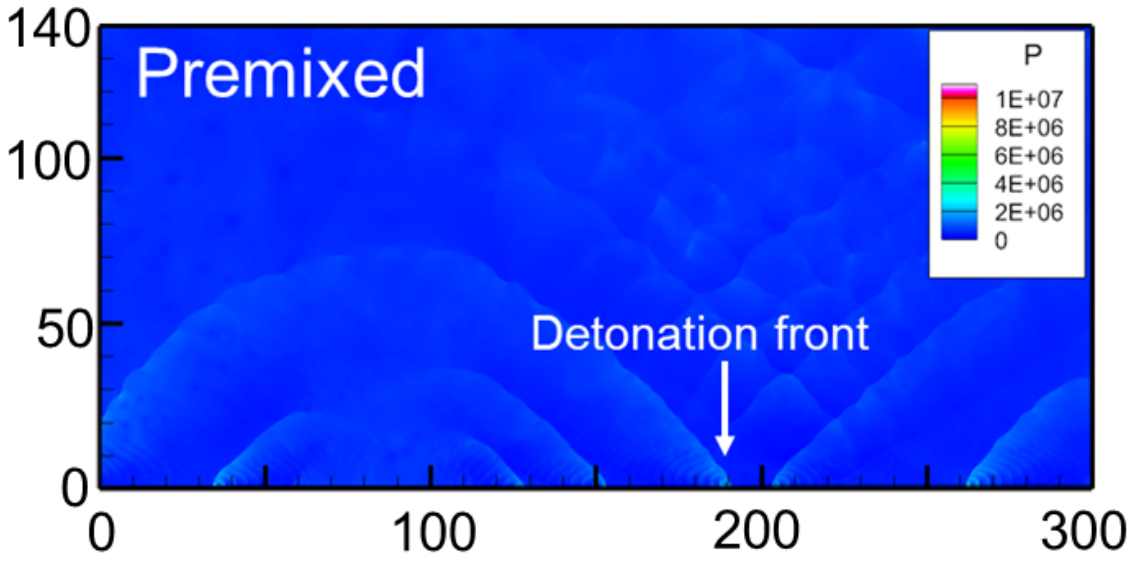

Fig. 5.3 Propagation mode of vertical injection of premixed fuel.

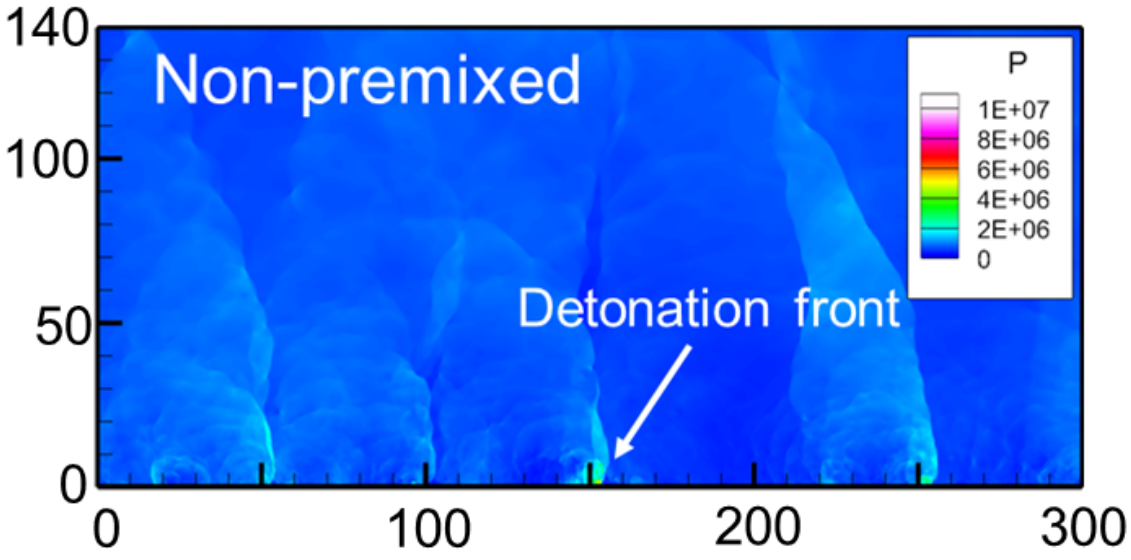

Fig. 5.4 Propagation mode of vertical injection of non-premixed fuel.

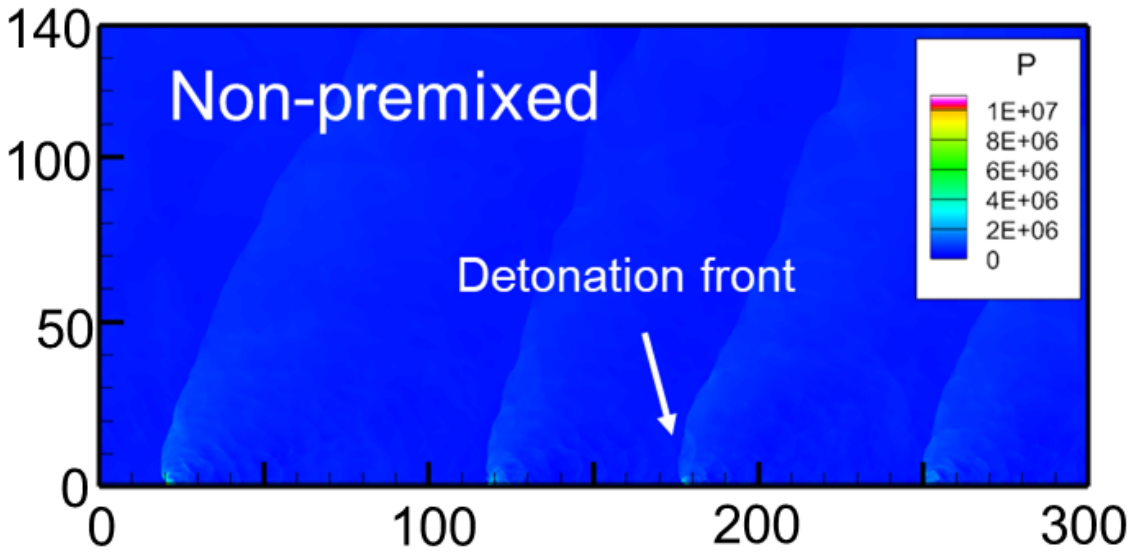

Fig. 5.5 Propagation mode of opposed injection of non-premixed fuel.

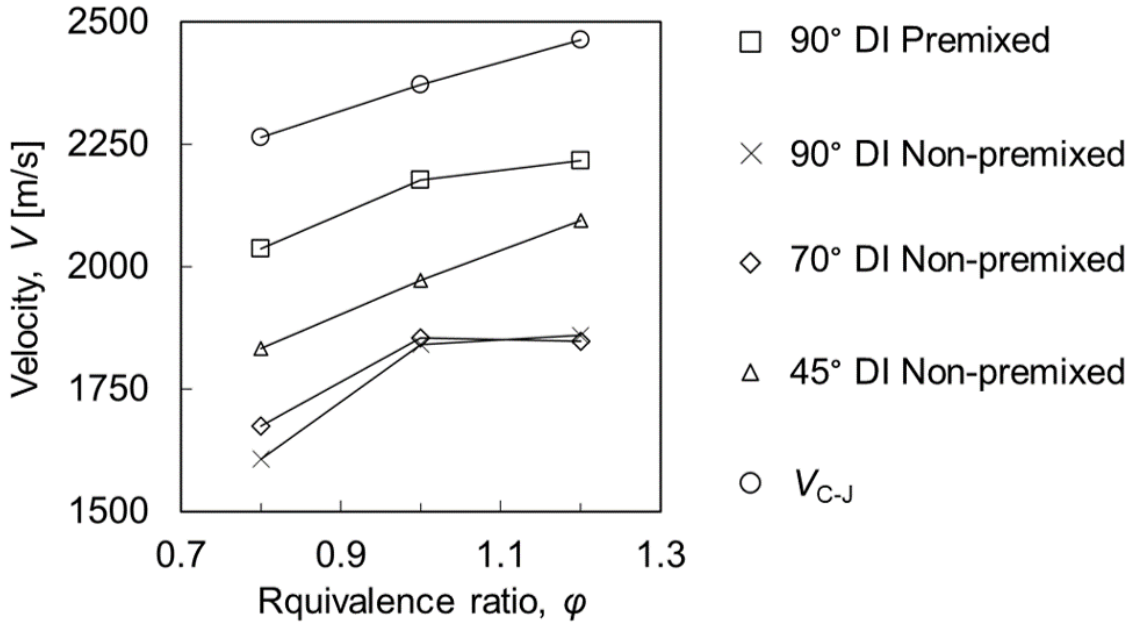

Fig. 5.6 Detonation velocity under different injection modes.

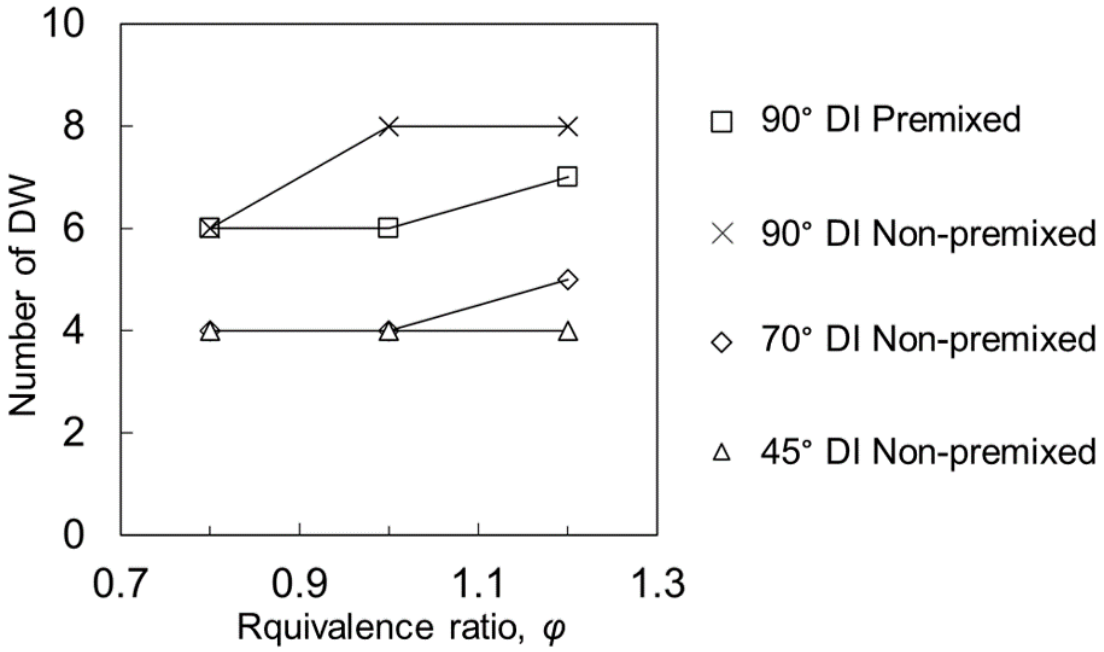

Fig. 5.7 The number of detonations with different injection modes.

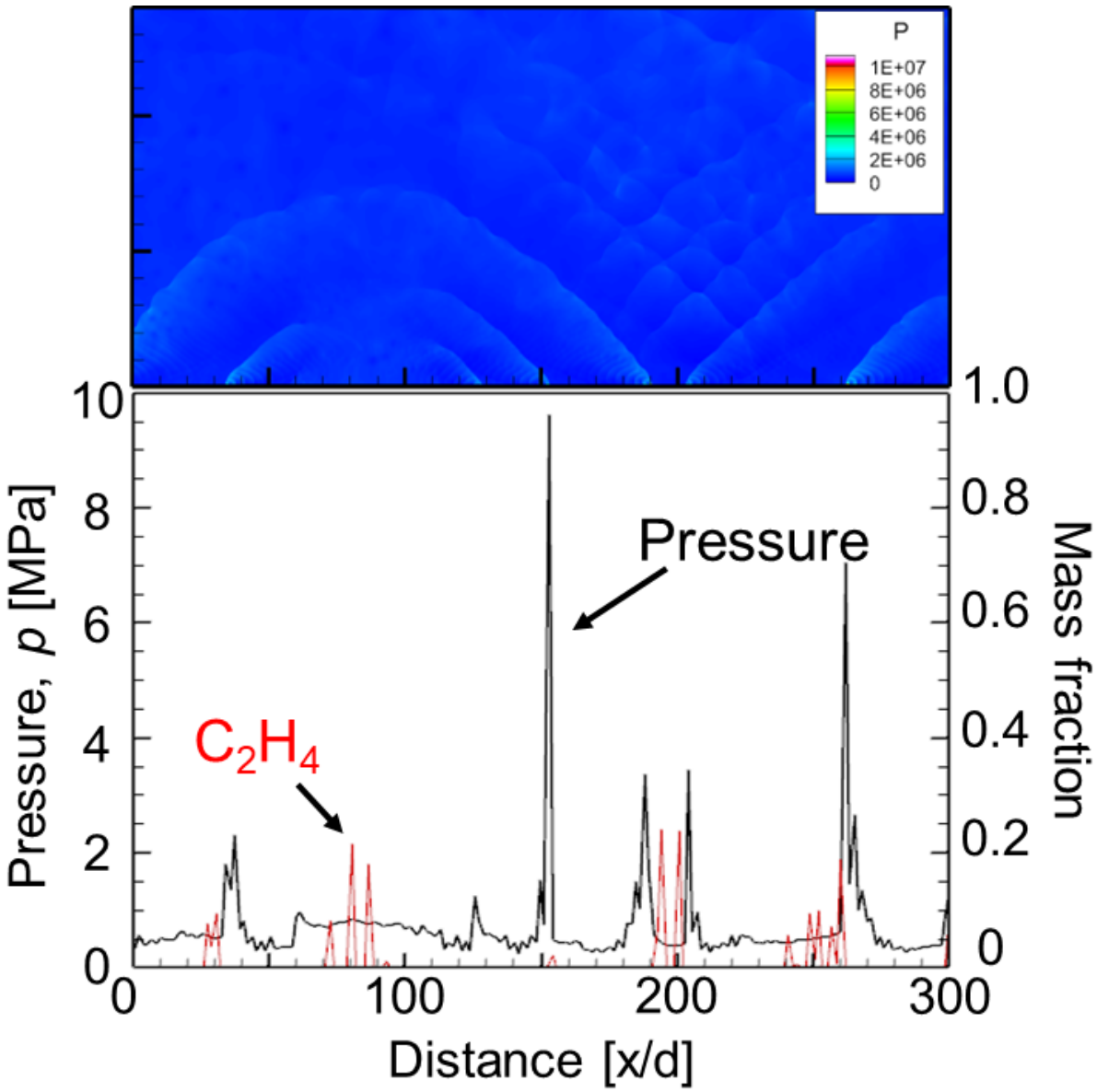

Fig. 5.8 Fuel distribution under vertical injection of premixed fuel.

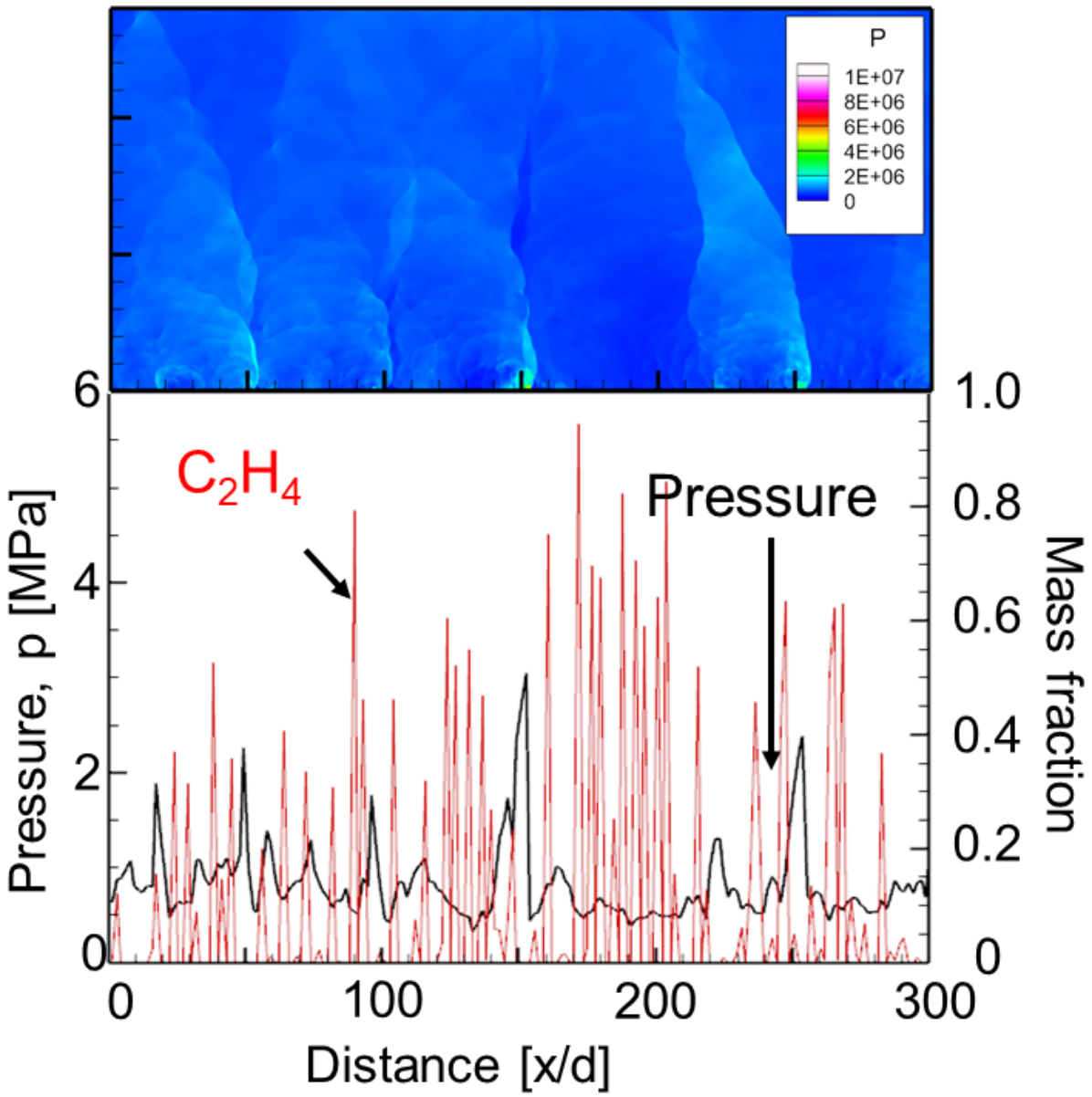

Fig. 5.9 Fuel distribution under vertical injection of non-premixed fuel.

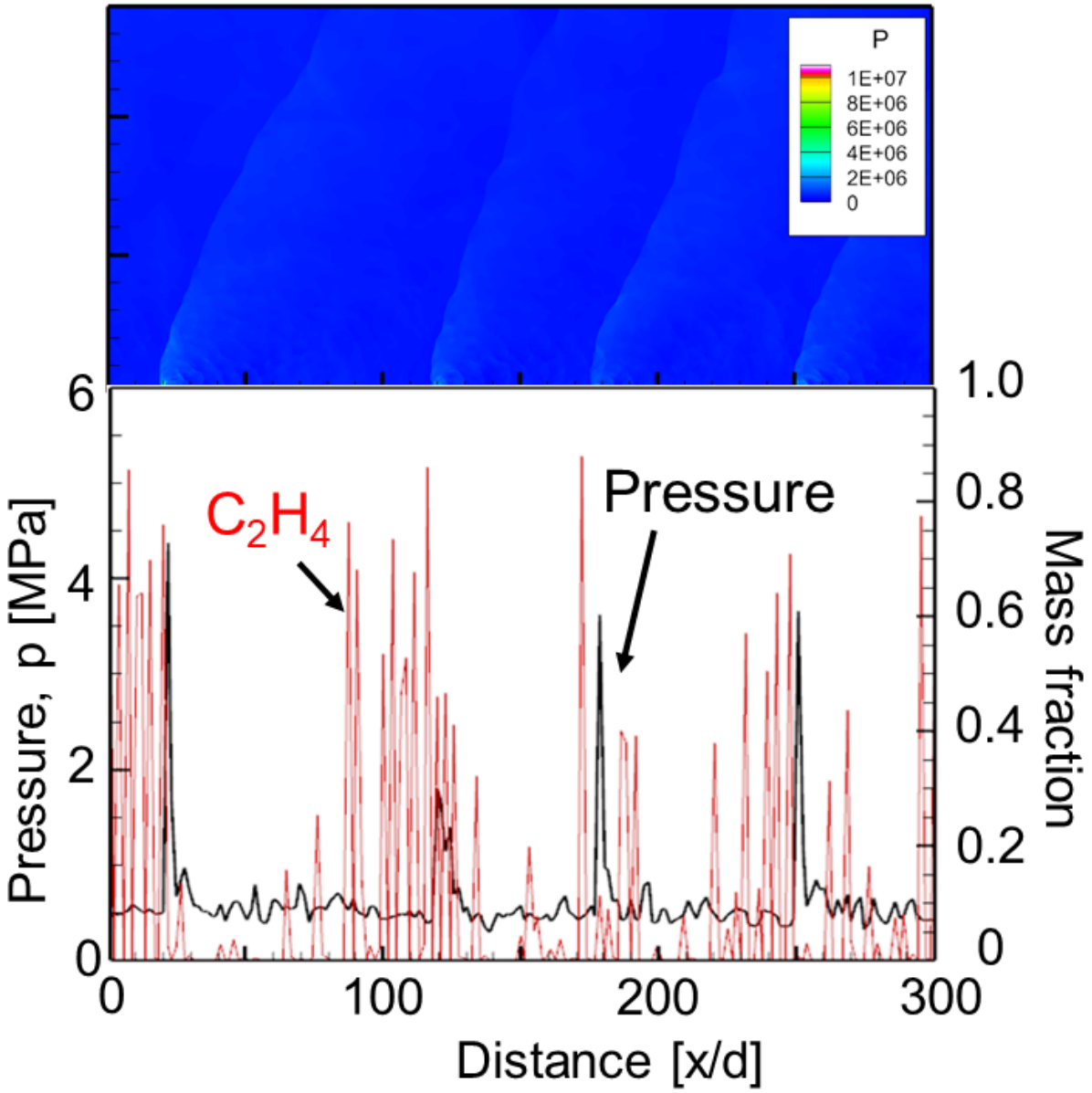

Fig. 5.10 Fuel distribution under opposed injection of premixed fuel.

Chapter 6

Conclusions

Experiment and 2D numerical analysis was conducted to clarify effect of the propagation state of the detonation wave propagation in combustible jet train, conclusions are showed as follows;

1. A numerical analysis method for detonation was established.

   (Chater 2)

2. A experimental system was established. Numerical analysis can well restore the velocity and pressure of detonation through the comparison with experimental results.

   (Chater 3)

3. Premixed fuel maintains detonation propagation at meager mass flow rates and can reach more than 90% of the C-J velocity.The more significant the relative inclination angle of the double injector, the more pronounced the effect of promoting mixing.

   (Chater 4)

4. The propagation velocity of continuous detonation in premixed fuel can reach more than 90% of C-J velocity, which reduces the detonation velocity loss to C-J velocity from about

30% to 11%. The promotion of mixing also greatly improves the propagation of rotating detonation.

(Chater 5)

Bibliography

[1] Ya.B. Zel’dovich, Journal of Technical Physics., 10 1453–1461 (1940).

[2] J. A.Nicholls, H. R.Wilkinson, and R. B.Morriso, Jet Propul. 27 (5), 534-541 (1957).

[3] B. V. Voitsekhovskii, J. Appl. Mech. Technol. Phys.3 157–164 (1960).

[4] B. V. Voitsekhovskii, V. V. Mitrofanov, and M. E. Topchiyan, Structure of Detonation Front in Gases, Siberian Branch USSR Academy Science, Novosibirsk (1963).

[5] J. A. Nicholls, R. E. Cullen, and K. W. Ragland, Journal of Spacecraft and Rockets., 3 (6) 893-898 (1966).

[6] T. C. Adamson Jr, and G. R. Olsson, Astronaut. Acta., 13,405-415 (1967).

[7] P. I. -W. Shen,and T. C. Adamson Jr, Acta Astronautica., 17, 715-728 (1972).

[8] M. Kojima, Experimental Study of Rotating Detonation Rocket Engine at JAXA, Proc. The32nd International Symposium on Shock Waves, OR-04-0120, The Combustion Institute, Singapore (2019).

[9] K. Goto, K. Matsuoka, K. Matsuyama, A. Kawasaki, H. Watanabe, N. Itouyama, K. Ishihara, V. Buyakofu, T. Noda, J. Kasahara, A. Matsuo, I. Funaki, D. Nakata, M. Uchiumi, H. Habu, S. Takeuchi, S. Arakawa, J. Masuda, K. Maehara, T. Nakao and K. Yamada, Flight Demonstration of Detonation Engine System Using Sounding Rocket S-520-31: System Design, AIAA

2022-0229 (2021).

[10] J. R. Burr, and K. H. Yu, Mixing in linear detonation channel with discrete injectors and side relief, AIAA 2019-1014 (2019).

[11] T. Mizukaki, F. Wang, M. Kojima, H. Kawashima, S. Matsuyama, Y. Nunome, and H. Tanno, Visualization of detonation waves inside a rotating-detonation rocket engine by using point-diffraction interferometry, AIAA 2022-1115 (2021).

[12] B D.Edwards, Maintained detonation waves in an annular channel: A hypothesis which provides the link between classical acoustic combustion instability and detonation waves, Symposium on Combustion, 16, 1, 1611-1618 (1977).

[13] W. Qi, Y. Zhou, Y. Zhang An optical diagnostic technique based on ultraviolet absorption and schlieren for components stratification in a binary-component fuel–air mixture, Exp Fluids, 61, 11, 1-12 (2020).

[14] H. Yang, F. Li, B. Sun, Trajectory analysis of fuel injection into supersonic cross flow based on schlieren method, Chin J Aeronaut, 25, 1, 42-50 (2012).

[15] D.R. Emberson, B. Ihracska, S. Imran, A. Diez, Optical characterization of Diesel and water emulsion fuel injection sprays using shadowgraphy, Fuel, 172, 253-262 (2016).

[16] R.J.H. Klein-Douwel, P.J.M. Frijters, L.M.T. Somers, W.A. De Boer, R.S.G. Baert, Macroscopic diesel fuel spray shadowgraphy using high speed digital imaging in a high pressure cell, Fuel, 86, 12–13, 1994-2007 (2007).

[17] J. Austin, F. Pintgen, J. Shepherd January, Lead shock oscillation and decoupling in propagating detonations, 43rd AIAA aerospace sciences meeting and exhibit, 1170 (2005).

[18] V. Athmanathan, J. Braun, Z.M. Ayers, C.A. Fugger, A.M. Webb, M.N. Slipchenko, et al.

On the effects of reactant stratification and wall curvature in non-premixed rotating detonation combustors,Combust Flame, 240, 112013 (2022).

[19] K. Sun, Q.i. Zhang Effect of nitroethane on explosion parameters of multi-component mixed fuel aerosol, Fuel, 320, 123897(2022).

[20] S. Huang, Y. Wu, K. Zhang, D.i. Jin, Z. Zhang, Y. Li Experimental investigation of spray characteristics of gliding arc plasma airblast fuel injector, Fuel, 293, 120382 (2021).

[21] R.G. Johnson, Design, characterization, and performance of a valveless pulse detonation engine, Naval Postgraduate School Monterey CA (2000).

[22] X. Song, B. Li, L. Xie, Experimental investigation on the properties of liquid film breakup induced by shock waves Chin Phys B, 29, 8, 086201 (2020).

[23] Z. Ayers, A.I. Lemcherfi, E. Plaehn, C.D. Slabaugh, T.R. Meyer, C.A. Fugger, S. Roy, Application of 100 kHz acetone-PLIF for the investigation of mixing dynamics in a self-excited linear detonation channel, AIAA Scitech 2021 Forum, 0554 (2021).

[24] J. Duvall, M. Gamba, Characterization of reactant mixing in a rotating detonation engine using schlieren imaging and planar laser induced fluorescence, 2018 joint propulsion conference, 4690 (2018).

[25] C. Bedick, D. Ferguson, P. Strakey, Characterization of rotating detonation engine injector response using laser-induced fluorescence, J Propul Power, 35, 4, 827-838 (2019).

[26] S.C. Redhal, J.R. Burr, K. Yu, Propellants breakup and mixing characteristics in model rotating detonation engine, 22nd AIAA international space planes and hypersonics systems and technologies conference, 5200 (2018).

[27] Y. Morii, H. Terashima, K. Mitsuo, S. Taro, and S. Eiji, Journal of Computational Physics.,

322, 547-558 (2016).

[28] R. J. Kee, F. M. Rupley, and J. A. Miller, The Chemkin thermodynamic data base, Sandia National Laboratories Report SAND87-8215B, (1994).

[29] R. J. Kee, G. Dixon-Lewis, J. Warnatz, M. E. Coltrin, and J. A. Miller, A Fortran Computer Code Package for the Evaluation of Gas Phase, Multicomponent Transport Properties, SAND86-8246B (1986).

[30] K. Kitamura, and E. Shima, Journal of Computational Physics., 245, 62-83 (2013).

[31] S. Matsuyama, Computers and Fluids., 91, 130–143 (2014).

[32] Gordon, S., and McBride, B. J., "Computer Program for Calculation of Complex Chemical Equilibrium Compositions and Applications I. Analysis," NASA RP-1311, 1994.

[33] A.Briand B.Veyssiere, B.A.Khasainov. Investigation of detonation initiation in aluminium suspensions. Shock Waves, Vol. 18, No. 4, pp. 307–315, (2008).

[34] J.E. Shepherd M. Kaneshige. Detonation database. Explosion Dynamics Laboratory Report FM97-8, (1999).

[35] B. Thornber, A. Mosedale, D. Drikakis, D. Youngs, and R. J. R. Williams, Journal of Computational Physics., 227, 4873–4894 (2008).

[36] R. N. Smartt, W. H. Steel ：Theory and Application of Point-Diffraction Interferometer, Japan journal of applied, (1974).

[37] M. S. Chandrasekhara：Interferometric Investigations of Compressible Dynamic Stall over a Transiently Pitching Airfoil, AIAA journal Vol. 32, No. 3, (1994).

[38] N. J. Brock：A Real time Interferometry System for Unsteady Flow Measurements, ICIAS ' 91 RECORD, IEEE Publication 91CH3028-8, 423-430, (1991).

[39] Soma Nakagami, Ken Matsuoka, Jiro Kasahara, Akiko Matsuo, Ikkoh Funaki : Visualization of Rotating Detonation Waves in a Plane Combustor with a Cylindrical Wall Injector, 53rd AIAA Aerospace Sciences Meeting, (2015).

[40] Akira Kawasaki, Tomoya Inakawa, Jiro Kasahara, Keisuke Goto, Ken Matsuoka, Akiko Matsuo, Ikkoh Funaki : Critical condition of inner cylinder radius for sustaining rotating detonation waves in rotating detonation engine thruster, Proceedings of the Combustion Institute Vol. 37, No. 3, pp. 3461-3469, (2019).

[41] G. Ciccarelli, S. Dorofeev : Flame acceleration and transition to detonation in ducts, Progress in Energy and Combustion Science, (2008).

[42] Y. Morii, H. Terashima, K. Mitsuo, S. Taro, and S. Eiji, Journal of Computational Physics., 322, 547-558 (2016).

[43] R. J. Kee, F. M. Rupley, and J. A. Miller, The Chemkin thermodynamic data base, Sandia National Laboratories Report SAND87-8215B, (1994).

[44] R. J. Kee, G. Dixon-Lewis, J. Warnatz, M. E. Coltrin, and J. A. Miller, A Fortran Computer Code Package for the Evaluation of Gas Phase, Multicomponent Transport Properties, SAND86-8246B (1986).

[45] K. Kitamura, and E. Shima, Journal of Computational Physics., 245, 62-83 (2013).

[46] S. Matsuyama, Computers and Fluids., 91, 130–143 (2014).

[47] B. Thornber, A. Mosedale, D. Drikakis, D. Youngs, and R. J. R. Williams, Journal of Computational Physics., 227, 4873–4894 (2008).

[48] T. Araki, K. Yoshida, Y. Morii, N. Tsuboi, and K. A. Hayashi, Combustion Science and Technology., 188, 346-369 (2016).

[49] T. Sato, S. Voelkel, and V, Raman, Detailed Chemical Kinetics based Simulation of Detonation-Containing Flows, Proceedings of ASME Turbo Expo 2018 Turbomachinery Technical Conference and Exposition, GT2018-75878 (2018).

[50] J.A. Nicholls, R.E.Cullen, and K.W.Ragland, Journal of Spacecraft and Rockets., 3(6), 893-898 (1966).

[51] S. A. Zhdan, A. M. Mardashev, and V. V. Mitro-fanov, Combustion, Explosion and Shock Waves., 26, 210-214 (1990).

[52] F. Wang, T. Mizukaki, and S. Matsuyama, Visualization and CFD of the influence of mixing on detonation wave propagation inside a rotating-detonation engine by using linear detonation channel, AIAA 2022-1456 (2021).

[53] S. Matsuyama, K. Iwata, Y. Nunome, H. Tanno, T. Mizukaki, M. Kojima, and H. Kawashima, Large-Eddy Simulation of Rotating Detonation with a Non-premixed CH4/O2 Injection, AIAA 2020-1174 (2020).

Acknowledgement

First of all, I would like to express my sincere gratitude to my thesis advisor, Professor Toshiharu Mizukaki, for his invaluable help and constant encouragement throughout my doctoral education.

I am very grateful to Prof. Hideyuki Horisawa, Prof. Yoshinobu Inada, Associate Prof. Kota Fukuda, Associate Prof. Shun Takahashi, Lecturer Daiju Numata from School of Engineering, Tokai University. And Prof. Akiko Matsuo from Faculty of Science and Technology, Keio University. Reviewed this thesis and provided many valuable comments.

I would also like to express my gratitude extended to Dr. Shingo Matsuyama from JAXA for his help and advice on the numerical analysis of this study.

I would also like to thank all the research staffs of Tokai University for their valuable guidance throughout my experiment for using each equipment. They provided me with tools that I needed to find the right direction and successfully complete my dissertation.

Many thanks everyone in Mizukaki's laboratory for their help throughout my study process. With their assistants, I was able to successfully complete my research.

I sincerely thank my parents for their support in all aspects and their trust and understanding all the time. Because of them, I can finish my studies without burden.

This research we used JAXA Supercomputer System generation 3 (JSS3) for numerical analysis. The experiment was sponsored by Acquisition, Technology & Logistics Agency, Japan.

A

Appendix A

A.1 Detonation theory

According to the situation of unburned mixture, combustion can be divided into two types, premixed combustion and non-premixed combustion. In premixed combustion, fuel and oxidizer are fully mixed before ignition and can spread unburned gas mixtures. On the other hand, non-premixed combustion is supported by diffusion between separately supplied fuel and oxidizer and does not achieve self-propagation. Premixed combustion can be further divided into deflagration and detonation, and their combustion mechanism and combustion characteristics are completely different. Table 1.1 shows the difference between detonation and deflagration. First of all, the propagation velocity of detonation wave is supersonic and subsonic during deflagration. The combustion wave is a compression wave for knock and an expansion wave for deflagration. In addition, the ignition mechanisms of the two combustion waves are also different. In the process of combustion, the propagation of the mixture is affected by the heat and mass transfer, thus igniting the mixture. On the other hand, the adiabatic compression of the leading shock wave

ignites the mixture in detonation. The explosion phenomenon is concerned and studied in this paper. Detonation is a self-sustaining supersonic premixed combustion wave, which is formed by the coupling of an advanced shock wave and a reaction zone.

A.1.1 Chapman-Jouguet theory

A quantitative theory that predicts the detonation velocity of an explosive mixture was formulated by Chapman (1889) and Jouguet (1904, 1905) shortly after discovering the phenomenon.

Both Chapman and Jouguet based their theory on the works of Rankine (1870) and Hugoniot (1887, 1889), who analyzed the conservation equations across a shock wave. For a detonating wave, the conversion of reactants into products across the wave results in the release of chemical energy. Assuming equilibrium downstream of the wave, it is possible to determine the chemical composition of the products in terms of the thermodynamic state. Thus the chemical energy released across the detonation can be determined. Unlike a non-reacting shock wave, two possible solutions exist for a given detonation wave speed: the strong and weak detonation solutions. The pressure and density of the strong detonation solution are larger than those of the weak detonation solution. The flow downstream of a strong detonation is subsonic (relative to the wave), whereas it is supersonic for a weak detonation. Both solutions converge when the detonation velocity is minimized. No solution exists for detonation velocities below this minimum. Since a continuous spectrum of detonation velocities above the minimum is possible for a given explosive mixture, the task of a detonation theory is to provide a criterion for the proper choice of detonation velocity for an explosive mixture given initial conditions.

Chapman's criterion is essential to choose the minimum velocity solution. The argument he

provides is that for a given explosive mixture. Experiments show that different detonation velocities are observed. It follows that the minimum velocity solution must be the correct one. Jouguet, on the other hand, investigated the locus of the thermodynamic states for various detonation velocities (i.e., the Hugoniot curve). He determined the entropy variation along the Hugoniot curve and found a minimum. He also noted that the lowest entropy solution corresponds to the sonic condition downstream of the detonation. Jouguet then postulated that the minimum-entropy solution (the sonic solution) is the appropriate one to choose. His collaborator, Crussard (1907), later showed that the minimum-velocity solution corresponds to the minimum-entropy solution and gives sonic flow downstream of the wave. Thus, both Chapman and Jouguet provided a criterion (i.e., minimum velocity or minimum entropy) for choosing the appropriate detonation velocity for a given explosive mixture, which is now referred to as the C-J theory. Neither Chapman nor Jouguet provided physical or mathematical justification for their postulates.

Through this theory, the velocity of detonation wave propagating in one-dimensional stability and the characteristic values of detonation such as pressure, temperature and density behind detonation wave can be predicted. The predicted detonation velocity based on C-J theory is often in good agreement with the experimental value in gas detonation.

The C-J state will be described below using the Rayleigh line and the Hugonio curve.

A.1.2 Basic equations

The basic conservation equations of mass, momentum, and energy for onedimensional steady flow across a combustion wave with respect to a co-ordinate system fixed to the wave are given by

$$\rho_1 u_1 = \rho_2 u_2 \tag{A.1}$$

$$p_1 + \rho_1 u_1^2 = p_2 + \rho_2 u_2^2 \tag{A.2}$$

$$h_1 + \frac{u_1^2}{2} = h_2 + \frac{u_2^2}{2} \tag{A.3}$$

where the ρ, u, p, h and q are density, velocity, pressure, enthalpy and the difference between the enthalpies of formation of reactants and products, respectively. And the subscripts 0 and 1 denote reactant and product states from the detonation as in the Fig. A.1.

From the mass and momentum conservation equation, the Rayleigh line which defines the thermodynamic path across the combustion wave can be obtained under the assumption that the gas is the calorically perfect gas.

$$\frac{p_2}{p_1} = \left(1 + \gamma_1 M_1^2\right) - \left(\gamma_1 M_1^2\right) \frac{v_2}{v_1} \tag{A.4}$$

where the v, γ and M are specific volume, specific heat ratio and Mach number, respectively. The slope of the Rayleigh line is proportional to the wave speed. Also, the Hugoniot curve can be derived from Eqs. (A.1)-(A.3) as the following equation.

$$\frac{p_2}{p_1} = \left(\frac{\gamma_1 + 1}{\gamma_1 - 1} - \frac{v_2}{v_1} + \frac{2q}{p_1 v_1}\right) / \left(\frac{\gamma_1 + 1}{\gamma_1 - 1}\frac{v_2}{v_1} - 1\right) \tag{A.5}$$

All thermodynamic states across the shock wave from the initial condition are given by the

Hugoniot curve. Especially, the Hugoniot curve for the case that q = 0, namely, no heat release during the shock wave, is called adiabatic Hugoniot curve. By differential Eq. (A.5), the slope and curvature of the Hugoniot curve are

$$\left(\frac{\mathrm{d}\left(p_2/p_1\right)}{\mathrm{d}\left(v_2/v_1\right)}\right)_{\mathrm{H}} = -\frac{\frac{p_2}{p_1}+\frac{\gamma_1+1}{\gamma_1-1}}{\frac{v_2}{v_1}-\frac{\gamma_1+1}{\gamma_1-1}} \tag{A.6}$$

$$\left(\frac{\mathrm{d}^2\left(p_2/p_1\right)}{\mathrm{d}\left(v_2/v_1\right)^2}\right)_{\mathrm{H}} = 2\frac{\frac{p_2}{p_1}+\frac{\gamma_1+1}{\gamma_1-1}}{\left(\frac{v_2}{v_1}-\frac{\gamma_1+1}{\gamma_1-1}\right)^2} \tag{A.7}$$

Where the subscript *H* denotes the state by the Hugoniot curve, from Eq. (A.7), the curvature of the Hugoniot curve is always positive as the specific heat ratio is positive, and the Hugoniot curve is the concave curve. The schematic of the relation between the Hugoniot curve and Rayleigh line in the p-v diagram is shown in Fig. A.2 and Fig. A.3. The conservation value across the front is the same, and the state downstream the detonation front is signified as the intersection point of the Rayleigh line and Hugoniot curve. The solution in the upper branch is for the detonation, and those for the lower branch denote the deflagration. The upper side of the detonation solution is called strong detonation, whose velocity is supersonic upstream and subsonic downstream. The Mach number for the strong detonation on the downstream side is subsonic so that the disturbance can catch up with the front, and no steady solution is possible. On the other hand, the lower side of the detonation solution is the weak detonation solution. In the weak detonation, the Mach number on both the downstream and upstream sides is supersonic.

Generally, the steady weak detonation does not appear in the entropy consideration. However, the recent studies by Mi et al. (2017) confirmed that steady weak detonation exists for a

highly discretized source mixture due to the non-equilibrium state of mechanical fluctuation. The detonation solution where the Rayleigh line is tangent to the Hugoniot curve has the minimum detonation velocity, and the 7 Mach number downstream is unity. This detonation is called C-J detonation, and the C-J velocity predicts the experimental value well when the mixture is within the detonability limit and free from the boundary effects. The relation for the C-J solution can be obtained by equaling Eqs. (A.4)(A.5).

$$(p_2/p_1)^* = \frac{-(v_2/v_1)^*}{\gamma_1 - (\gamma_1 + 1)(v_2/v_1)^*} \tag{A.8}$$

From Eqs. (1.4)(1.6)(1.8), the slope of Rayleigh line and Hugoniot curve is the same as below formula.

$$\left(\frac{\mathrm{d}(p_2/p_1)}{\mathrm{d}(v_2/v_1)}\right)_{\mathrm{H}} = \left(\frac{\mathrm{d}(p_2/p_1)}{\mathrm{d}(v_2/v_1)}\right)_{Ray} = \frac{-\gamma_1 (p_2/p_1)^*}{(v_2/v_1)^*} \tag{A.9}$$

where the subscript *Ray* is the state by Rayleigh line. The isentropic relation can be written as /2//1 /2//1 ,1 = const. and the derivative of the isentropic is

$$\left(\frac{\mathrm{d}(p_2/p_1)}{\mathrm{d}(v_2/v_1)}\right)_{\mathrm{S}} = \frac{-\gamma_1 (p_2/p_1)^*}{(v_2/v_1)^*} \tag{A.10}$$

where the subscript S is the state under isentropic relation. From Eqs. (A.9)(A.10). the flow is the isentropic at the C-J state.

A.2 Detonation wave structure

A.2.1 ZND model

As the C-J velocity is derived only from the control volume which encompasses the shock front to the sonic plane, the structure of detonation is kept unknown. Zeldovich, von Neumann and Doring established the model for the structure of the detonation waves (ZND model). They considered the detonation wave to be a steady one-dimensional structure consisting of the leading shock wave, induction zone, reaction zone and sonic plane. The unburned mixture ignites by the adiabatic compression and endothermic reaction occurs after a pool of intermediate species proliferate. The flow is accelerated by the heat addition from the chemical reaction and choked at the downstream. The sonic plane is established at the end of the reaction zone (C-J state) and detonation wave is independent of the disturbance downstream of the C-J state. Then, the leading shock is supported by the expansion of the burned gas and the detonation wave keeps propagating stably. The schematic of the ZND model is shown in Fig. A.4. The ZND model clarified the laminar structure of detonation and the propagation mechanism.

A.2.2 Detonation cellular structure

The structure for detonation in the ZND model is the steady, laminar and onedimensional structure. However, detonations are intrinsically unstable and are prone to develop multidimensional cellular structures, of which regularity depends on the reactivity of the mixture. The schematic of the cellular structure is shown in Fig. A.5. The cellular structures are formed by the interaction

of incident shock, Mach stem and transverse waves. After the local explosion, the strong Mach stem propagates in the first half of the cell and gradually decay to the weak incident shock wave. The speed of the leading shock wave normalized by C-J velocity fluctuates around 1.7 to 0.7 for unstable mixture and 1.25 to 0.9 for stable mixture (Gamezo, Desbordes and Oran 1999). The transverse waves propagate vertical to the propagation direction and collide with each other or reflect on the wall. The width between the cell apex is called the cell width and often used as the one of the dynamic parameter for the detonation phenomena such as the critical tube diameter and critical initiation energy. The shear layer appears from the cell boundaries into the reaction zone behind the shock wave. The interaction between the shock-shock, shock-vortex and shock-density layer causes the complicated flow field behind the detonation. Also, the unburned gas pocket is generated for unstable mixture by detaching it from the shock front. These instabilities delay the mean sonic line, propagating as the same speed as the shock and which isolates the detonation front from the rear. The shape of this cell depends on the shape of the tube that propagates detonation and the type of air-fuel mixture, but the cell width is determined only by thermodynamic properties such as the type of air-fuel mixture, initial pressure ratio, and initial temperature. , is known to affect the chemical reaction rate of the mixture. A highly reactive (fast-reacting) mixture has a small cell size, while a low-reactivity mixture has a large cell size. Therefore, the lower the reactivity of the air-fuel mixture, the stronger the three-dimensionality of the wavefront.

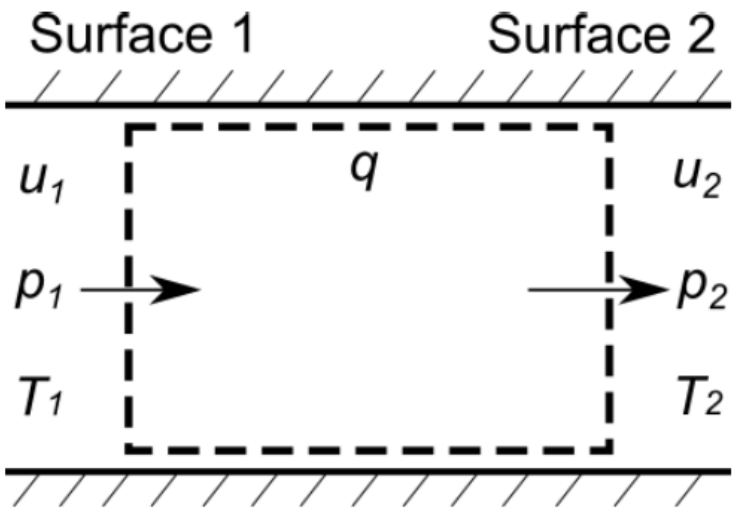

Fig. A.1 one-dimensional steady flow across a combustion wave with respect to a co-ordinate system .

Table A.1 Comparison of detonation and deflagration.

	Deflagration	Detonation
M_c	0.0001 - 0.03	5 - 10
u_2/u_1	4 - 6	0.4 - 0.7
p_2/p_1	0.98	13 -55
T_2/T_1	4 - 16	8 - 21
ρ_2/ρ_1	0.06 - 0.25	1.7 - 2.6

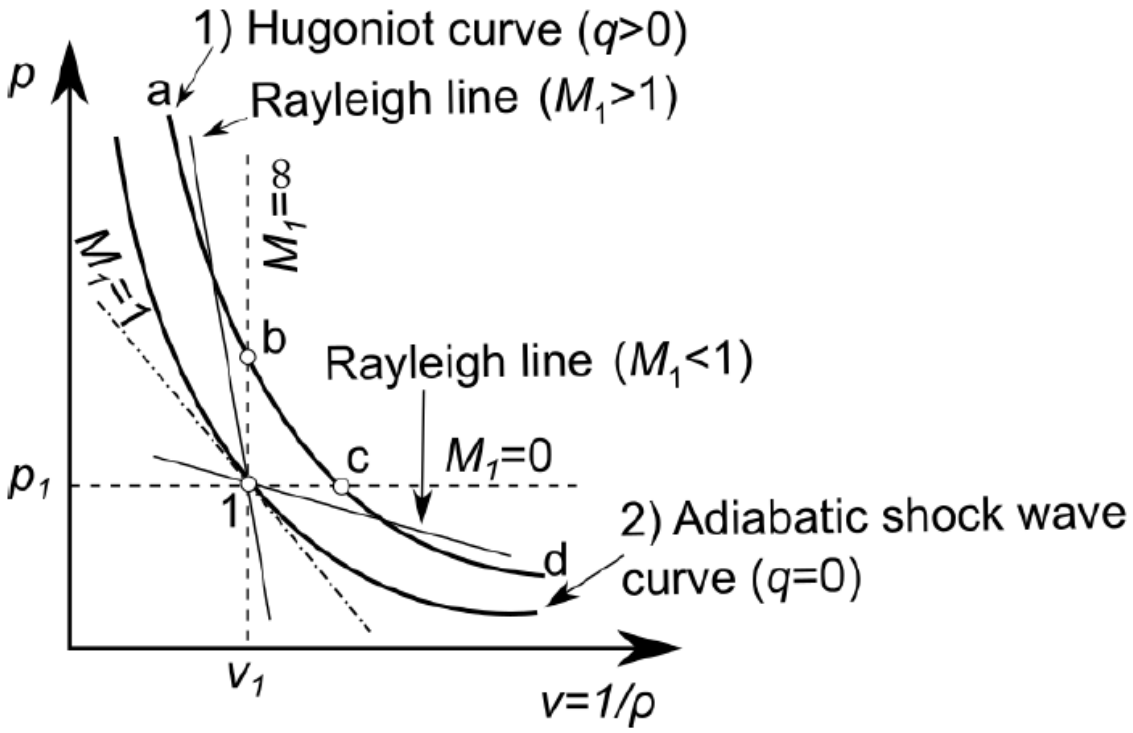

Fig. A.2 Hugoniot curve and Rayleigh line.

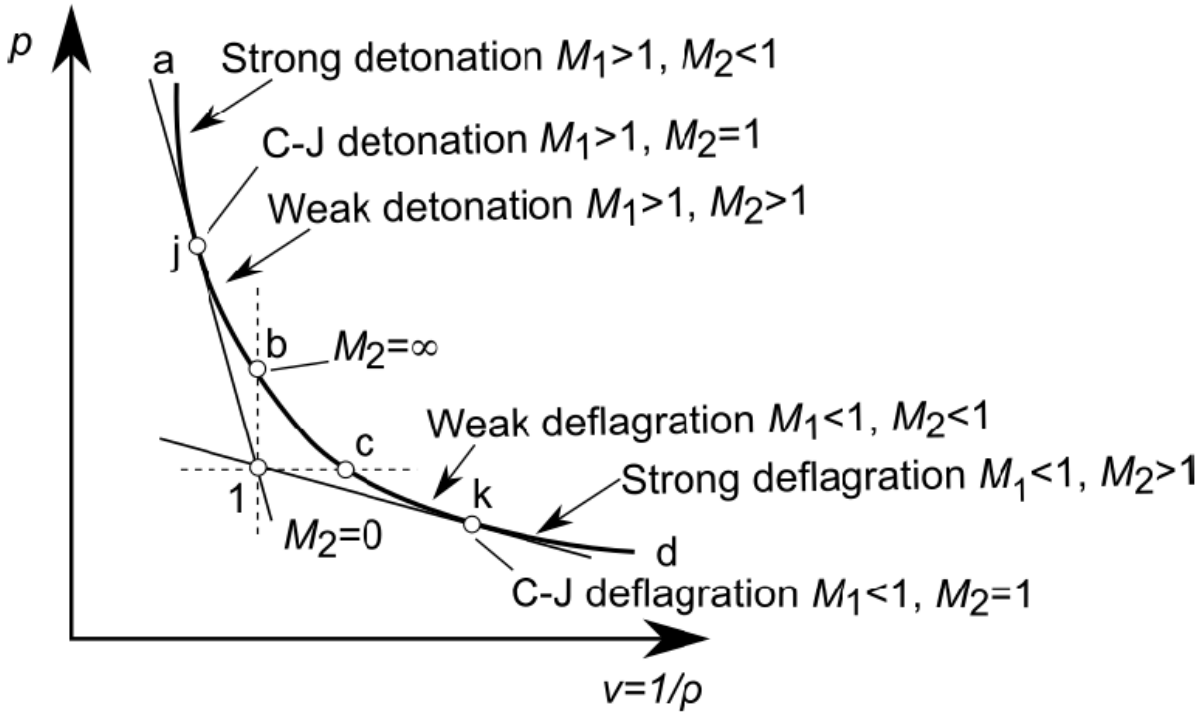

Fig. A.3 Various combustion waves.

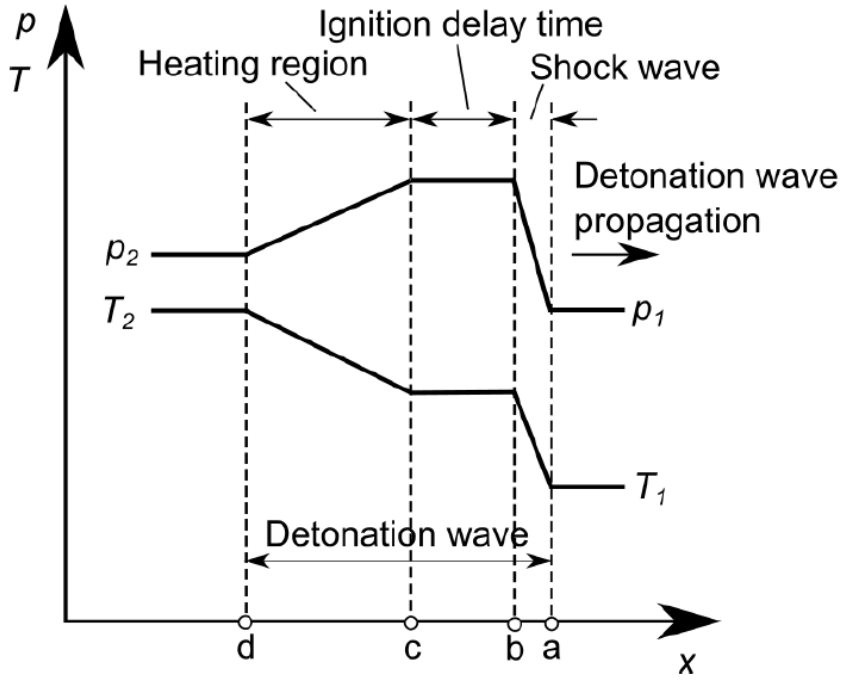

Fig. A.4 Schematic of ZND model.

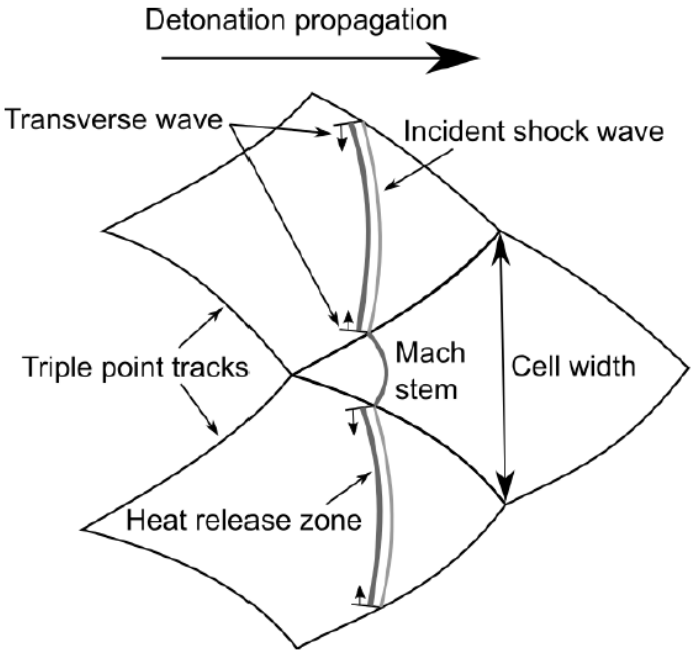

Fig. A.5 Schematic of cellular structure.

B

Appendix B

B.1 Supercomputer system JSS3

In 2020, JAXA started operation of new supercomputer system called JSS3, JSS3 consists of TOKI as the computing infrastructure, and J-SPACE, the archiving infrastructure.

The name TOKI comes from the name of Japanese bird toki (crested ibis (Nipponia nippon)), Japanese expression of “time and space” and “solution”. TOKI also expresses “TOkyo and ibaraKI”, where JSS3 is located. Major components of TOKI are, TOKI-SORA, TOKI-RURI and TOKI-FS.

The performance of each component of JSS3 is as follows;

TOKI-SORA: HPC System	
SORA: Suercomputer for earth Observation, Rockets, and Aeronautics	
PRIMEHPC FX1000	
Total nodes	5760 (15 racks)
Peck Performace	19.4 PFLOPS
Total Memory	180TiB (32GiB/node)

TOKI-RURI: General System	
RURI: all-RoUnd Role Infrastructure	
Peck Performace	1.24 PFLOPS
Total Memory	104 TiB
ST	PRIMERGY RX2540 M5 x 375 nodes (192 GiB/node, Quadro x 1)
GP	PRIMERGY CX2570 M5 x 32 nodes (384 GiB/node, Tesla V100 x 4)
XM	PRIMERGY RX2540 M5 x 2 nodes (DCPMM 6.0 TiB/node, Quadro x 1)
LM	PRIMERGY RX2540 M5 x 7 nodes (DCPMM1.5 TiB/node, Quadro x 1)

TOKI-FS: File System	
File System	FEFS
All-Flash NVMe Storage	10 PB
Hard Disk Drive Storage	40 PB

Computational resources used in the calculations of Chapter 4 in this study are as follows;

CPU: A64FX(Armv8.2-A +SVE)

Core: 48 Node: 80 Memory : 28G

Step size: 0.5 ns/step

Elapsed time= 2.9751E-01 [s/step]

1 case is about 40 hours.

Computational resources used in the calculations of Chapter 5 in this study are as follows;

Node: 100 Memory : 28G

Step size: 0.5 ns/step

Elapsed time for a single time step = 4.9751E-01 [s/step]

1 case is about 131 hours.

B.2 Detailed reaction model

Species:

CH4	O2	H2O	CO2	H	O	OH	HO2
H2	CO	H2O2	HCO	CH2O	CH3	CH	CH2
CH3O	C	C2H	C2H2	C2H3	C2H4	C2H5	C2H6
HCCO	CH2CO	C2H3O	CH2(S)	C3H6	aC3H5	N2	

Reactions:

H + O2 = O + OH	8.30E+13	0.000	14413.00
O + H2 = H + OH	5.00E+04	2.670	6290.00
H2 + OH = H + H2O	2.16E+08	1.510	3430.00
2OH = O + H2O	3.57E+04	2.40	-2110.00
2H + M = H2 + M	1.00E+18	-1.000	0.00
CH4/2.0/ H2O/0.0/ CO2/0.0/ H2/0.0/ C2H6/3.0/			
2H + H2O = H2 + H2O	6.00E+19	-1.250	0.00
H + OH + M = H2O + M	2.20E+22	-2.000	0.00
CH4/2.0/ H2O/3.65/ H2/0.73/ C2H6/3.0/			
O + H + M = OH + M	5.00E+17	-1.000	0.00
H2/2.0/ H2O/6.0/ CH4/2.0/ CO/1.5/ CO2/2.0/ C2H6/3.0/			
O2 + H + M = HO2 + M	2.80E+18	-0.860	0.00
O2/0.0/ N2/0.0/ H2O/0.0/ CO2/1.5/ CO/0.75/ C2H6/1.5/			
2O2 + H = O2 + HO2	3.00E+20	-1.720	0.00
O2 + H + H2O = H2O + HO2	1.65E+19	-0.760	0.00
O2 + H + N2 = N2 + HO2	2.60E+19	-1.240	0.00

2OH(+M) = H2O2(+M)	7.40E+13	-0.370	0.00
LOW / 2.300E+18 -0.900 -1700.00/			
TROE / 0.7346 94.00 1756.00 5182.00 /			
H2/2.0/ H2O/6.0/ CH4/2.0/ CO/1.5/ CO2/2.0/ C2H6/3.0/			
HO2 + H = O + H2O	3.97E+12	0.000	671.00
HO2 + H = H2 + O2	2.80E+13	0.000	1068.00
HO2 + H = 2OH	1.34E+14	0.000	635.00
HO2 + O = O2 + OH	2.00E+13	0.000	0.00
HO2 + OH = O2 + H2O	4.64E+13	0.000	-500.00
2HO2 = O2 + H2O2	1.30E+11	0.000	-1630.00
DUPLICATE			
2HO2 = O2 + H2O2	4.20E+14	0.000	12000.00
DUPLICATE			
H2O2 + H = H2 + HO2	1.21E+07	2.000	5200.00
H2O2 + H = H2O + OH	1.00E+13	0.000	3600.00
H2O2 + O = OH + HO2	9.63E+06	2.000	4000.00
H2O2 + OH = H2O + HO2	1.75E+12	0.000	320.00
DUPLICATE			
H2O2 + OH = H2O + HO2	5.80E+14	0.000	9560.00
DUPLICATE			
CO + O + M = CO2 +M	6.02E+14	0.000	3000.00
CH4/2.0/ O2/6.0/ H2O/6.0/ CO2/3.5/ H2/2.0/ CO/1.5/ C		2H6/3.0	/
CO + OH = H + CO2	4.76E+07	1.230	0 70.00
CO + O2 = O + CO2	2.50E+12	0.000	47800.00
CO + HO2 = CO2 + OH	1.50E+14	0.000	23600.00

C + O2 = O + CO	5.80E+13	0.000	576.00
CH + H = H2 +C	1.10E+14	0.000	0.00
CH + O = H + CO	5.70E+13	0.000	0.00
CH + OH = H + HCO	3.00E+13	0.000	0.00
CH + H2 = H + CH2	1.11E+08	1.790	0 1670.00
CH + H2O = H + CH2O	5.71E+12	0.000	-755.00
CH + O2 = O + HCO	3.30E+13	0.000	0.00
CH + CO2 = CO + HCO	3.40E+12	0.000	690.00
HCO + H = H2 + CO	7.34E+13	0.000	0.00
HCO + O = OH + CO	3.00E+13	0.000	0.00
HCO + O = H + CO2	3.00E+13	0.000	0.00
HCO + OH = H2O + CO	5.00E+13	0.000	0.00
HCO + M = H + CO +M	1.87E+17	-1.000	17000.00
CH4/2.0/ H2O/18.0/ CO2/2.0/ H2/2.0/ CO/1.5/ C2H6/3.0		/	
HCO + O2 = HO2 + CO	7.60E+12	0.000	400.00
CH2 + H(+M) = CH3(+M)	2.50E+16	-0.800	0.00
LOW / 3.200E+27 -3.140 1230.00/			
TROE / 0.6800 78.00 1995.00 5590.00/			
H2/2.0/ H2O/6.0/ CH4/2.0/ CO/1.5/ CO2/2.0/ C2H6/3.0/			
CH2 + O = H + HCO	8.00E+13	0.000	0.00
CH2 + OH = H + CH2O	2.00E+13	0.000	0.00
CH2 + OH = H2O + CH	1.13E+07	2.000	3000.00
CH2 + O2 = OH + HCO	1.32E+13	0.000	1500.00
CH2 + CO(+M) = CH2CO(+M)	8.10E+11	0.500	4510.00
LOW / 2.690E+33 -5.110 7095.00/			
TROE / 0.5907 275.00 1226.00 5185.00/			

H2/2.0/ H2O/6.0/ CH4/2.0/ CO/1.5/ CO2/2.0/ C2H6/3.0/			
2CH2 = H2 + C2H2	3.20E+13	0.000	0.00
CH2(S) + N2 = N2 + CH2	1.50E+01	3 0.	000 600.00
CH2(S) + OH = H + CH2O	3.00E+01	3 0.	000 0.00
CH2(S) + H2 = H + CH3	7.00E+01	3 0.	000 0.00
CH2(S) + O2 = H + OH + CO	2.80E+01	3 0.	000 0.00
CH2(S) + O2 = H2O + CO	1.20E+01	3 0.	000 0.00
CH2(S) + H2O = H2O + CH2	3.00E+01	3 0.	000 0.00
CH2(S) + CO = CO + CH2	9.00E+01	2 0.	000 0.00
CH2(S) + CO2 = CO + CH2O	1.40E+01	3 0.	000 0.00
CH2O + H(+M) = CH3O(+M)	5.40E+11	0.450	260.00
LOW / 2.200E+30 -4.800 5560.00/			
TROE/ 0.7580 94.00 1555.00 4200.00 /			
H2/2.0/ H2O/6.0/ CH4/2.0/ CO/1.5/ CO2/2.0/ C2H6/3.0/			
CH2O + H = H2 + HCO	2.30E+10	1.100	3275.00
CH2O + O = OH + HCO	3.90E+13	0.000	3540.00
CH2O + OH = H2O + HCO	3.43E+09	1.180	-447.00
CH2O + CH = H + CH2CO	9.46E+13	0.000	-515.00
CH3 + H(+M) = CH4(+M)	1.27E+16	-0.630	383.00
LOW / 2.477E+33 -4.760 2440.00/			
TROE/ 0.7830 74.00 2941.00 6964.00 /			
H2/2.0/ H2O/6.0/ CH4/2.0/ CO/1.5/ CO2/2.0/ C2H6/3.0/			
CH3 + O = H + CH2O	8.43E+13	0.000	0.00
CH3 + OH = H2O + CH2	5.60E+07	1.600	5420.00

CH3 + OH = H2O + CH2(S)	2.50E+13	0.000	0.00
CH3 + O2 = O + CH3O	3.08E+13	0.000	28800.00
CH3 + O2 = OH + CH2O	3.60E+10	0.000	8940.00
CH3 + HO2= OH + CH3O	1.34E+13	0.000	0.00
CH3 + CH = H + C2H3	3.00E+13	0.000	0.00
CH3 + HCO = CH4 + CO	2.65E+13	0.000	0.00
CH3 + CH2O = CH4 + HCO	3.32E+03	2.810	5860.00
CH3 + CH2 = H + C2H4	4.00E+13	0.000	0.00
2CH3(+M) = C2H6(+M)	2.12E+16	-0.970	620.00
LOW / 1.770E+50 -9.670 6220.00/			
TROE/ 0.5325 151.00 1038.00 4970.00 /			
H2/2.0/ H2O/6.0/ CH4/2.0/ CO/1.5/ CO2/2.0/ C2H6/3.0/			
2CH3 = H + C2H5	4.99E+12	0.100	10600.00
CH3O + O2 = HO2 + CH2O	4.28E-13	7.600	-3530.00
CH4 + H = H2 + CH3	6.60E+08	1.600	10840.00
CH4 + O = OH + CH3	1.02E+09	1.500	8600.00
CH4 + OH = H2O + CH3	1.00E+08	1.600	3120.00
CH4 + CH = H + C2H4	6.00E+13	0.000	0.00
C2H + O2 = CO + HCO	5.00E+13	0.000	1500.00
HCCO + H = CO + CH2(S)	1.00E+14	0.000	0.00
HCCO + O = H + 2CO	1.00E+14	0.000	0.00
HCCO + O2 = OH + 2CO	1.60E+12	0.000	854.00
HCCO + CH2 = CO + C2H3	3.00E+13	0.000	0.00
C2H2 + H(+M) = C2H3(+M)	5.60E+12	0.000	2400.00
LOW / 3.800E+40 -7.270 7220.00/			
TROE/ 0.7507 98.50 1302.00 4167.00 /			

H2/2.0/ H2O/6.0/ CH4/2.0/ CO/1.5/ CO2/2.0/ C2H6/3.0/			
C2H2 + O = H + HCCO	1.02E+07	2.000	1900.00
C2H2 + O = CO + CH2	1.02E+07	2.000	1900.00
C2H2 + OH = H + CH2CO	2.18E-04	4.500	-1000.00
C2H2 + OH = H2O + C2H	3.37E+07	2.000	14000.00
CH2CO + H = CO + CH3	1.50E+09	1.430	2690.00
CH2CO + OH = HCO + CH2O	1.00E+13	0.000	0.00
C2H3 + H(+M) = C2H4(+M)	6.08E+12	0.270	280.00
LOW / 1.400E+30 -3.860 3320.00/			
TROE/ 0.7820 207.50 2663.00 6095.00 /			
H2/2.0/ H2O/6.0/ CH4/2.0/ CO/1.5/ CO2/2.0/ C2H6/3.0/			
C2H3 + H = H2 + C2H2	6.00E+13	0.000	0.00
C2H3 + O = H + CH2CO	6.00E+13	0.000	0.00
C2H3 + OH = H2O + C2H2	5.00E+12	0.000	0.00
C2H3 + O2 = O + C2H3O	1.24E+13	-0.120	1696.00
C2H3 + O2 = HCO + CH2O	8.60E+21	-2.970	3320.00
C2H4 + H(+M) = C2H5(+M)	1.08E+12	0.450	1820.00
LOW / 1.200E+42 -7.620 6970.00/			
TROE/ 0.9753 210.00 984.00 4374.00 /			
H2/2.0/ H2O/6.0/ CH4/2.0/ CO/1.5/ CO2/2.0/ C2H6/3.0/			
C2H4 + H = H2 + C2H3	1.33E+06	2.530	12240.00
C2H4 + O = HCO + CH3	1.92E+07	1.830	220.00
C2H4 + OH = H2O + C2H3	1.80E+06	2.000	2500.00
C2H4 + CH3 = CH4 + C2H3	2.27E+05	2.000	9200.00
C2H5 + O = CH3 + CH2O	1.32E+14	0.000	0.00
C2H6 + H = H2 + C2H5	1.15E+08	1.900	7530.00

C2H6 + OH = H2O + C2H5	3.54E+06	2.120	870.00
C2H3O = CO + CH3	7.80E+41	-9.150	46900.00
CH2CO + H(+M) = C2H3O(+M)	3.30E+14	-0.060	8500.00
LOW / 3.800E+41 -7.640 11900.00/			
TROE/ 0.3370 1707.00 3200.00 4131.00 /			
CH4/2.0/ H2O/6.0/ CO2/2.0/ H2/2.0/ CO/1.5/ C2H2/3.0/		C2H4/3	.0/ C2H6/3.0/
C2H3O + H = H2 + CH2CO	3.00E+13	0.000	0.00
C2H3O + O = HCO + CH2O	1.00E+14	0.000	0.00
CH3 + HCCO = CO + C2H4	5.00E+13	0.000	0.00
C2H3 + HCO = CO + C2H4	9.00E+13	0.000	0.00
C3H6 + H = CH3 + C2H4	1.60E+22	-2.390	11180.00
C3H6 + H = H2 + aC3H5	1.70E+05	2.500	2490.00
C3H6 + O = H + CH3 + CH2CO	1.20E+08	1.650	327.00
C3H6 + O = HCO + C2H5	3.50E+07	1.650	-972.00
C3H6 + OH = H2O + aC3H5	3.10E+06	2.000	-298.00
aC3H5 + H(+M) = C3H6(+M)	2.00E+14	0.000	0.00
LOW / 1.330E+60 -12.000 5967.80/			
TROE / 0.020 1096.6 1096.6 6859.5 /			
H2/2.0/ H2O/6.0/ CH4/2.0/ CO/1.5/ CO2/2.0/ C2H6/3.0/			
C2H3 + CH3(+M) = C3H6(+M)	2.50E+13	0.000	0.00
LOW / 4.270E+58 -11.940 9769.80/			
TROE / 0.175 1340.6 60000.0 10139.8 /			
H2/2/ H2O/6/ CH4/2/ CO/1.5/ CO2/2/ C2H6/3/ C2H2/3.00		/ C2H4/	3.00/
C2H3 + CH3 = H + aC3H5	1.50E+24	-2.830	18618.00
CH3 + HO2 = CH4 + O2	1.00E+12	0.000	0.00
C2H3 + O2 = HO2 + C2H2	1.00E+11	0.000	0.00

C2H3O + O2 = HO2 + CH2CO	1.40E+11	0.000	0.00
C2H4 + O2 = HO2 + C2H3	4.22E+13	0.000	60800.00
CH3 + H2O2 = CH4 + HO2	2.45E+04	2.470	5180.00
CH2O + HO2 = HCO + H2O2	1.00E+12	0.000	8000.00
CH2O + O2 = HO2 + HCO	1.00E+14	0.000	40000.00

B.3 Thermodynamic

THERMO ALL

300.000 1000.000 5000.000

GRI-Mech Version 3.0 Thermodynamics released 7/30/99

NASA Polynomial format for CHEMKIN-II

O L 1/90O 1 G 200.000 3500.000 1000.000	1
2.56942078E+00-8.59741137E-05 4.19484589E-08-1.00177799E-11 1.22833691E-15	2
2.92175791E+04 4.78433864E+00 3.16826710E+00-3.27931884E-03 6.64306396E-06	3
-6.12806624E-09 2.11265971E-12 2.91222592E+04 2.05193346E+00	4
O2 TPIS89O 2 G 200.000 3500.000 1000.000	1
3.28253784E+00 1.48308754E-03-7.57966669E-07 2.09470555E-10-2.16717794E-14	2
-1.08845772E+03 5.45323129E+00 3.78245636E+00-2.99673416E-03 9.84730201E-06	3
-9.68129509E-09 3.24372837E-12-1.06394356E+03 3.65767573E+00	4
H L 7/88H 1 G 200.000 3500.000 1000.000	1
2.50000001E+00-2.30842973E-11 1.61561948E-14-4.73515235E-18 4.98197357E-22	2
2.54736599E+04-4.46682914E-01 2.50000000E+00 7.05332819E-13-1.99591964E-15	3
2.30081632E-18-9.27732332E-22 2.54736599E+04-4.46682853E-01	4
H2 TPIS78H 2 G 200.000 3500.000 1000.000	1
3.33727920E+00-4.94024731E-05 4.99456778E-07-1.79566394E-10 2.00255376E-14	2

-9.50158922E+02-3.20502331E+00 2.34433112E+00 7.98052075E-03-1.94781510E-05 3
2.01572094E-08-7.37611761E-12-9.17935173E+02 6.83010238E-01 4
OH RUS 78O 1H 1 G 200.000 3500.000 1000.000 1
3.09288767E+00 5.48429716E-04 1.26505228E-07-8.79461556E-11 1.17412376E-14 2
3.85865700E+03 4.47669610E+00 3.99201543E+00-2.40131752E-03 4.61793841E-06 3
-3.88113333E-09 1.36411470E-12 3.61508056E+03-1.03925458E-01 4
H2O L 8/89H 2O 1 G 200.000 3500.000 1000.000 1
3.03399249E+00 2.17691804E-03-1.64072518E-07-9.70419870E-11 1.68200992E-14 2
-3.00042971E+04 4.96677010E+00 4.19864056E+00-2.03643410E-03 6.52040211E-06 3
-5.48797062E-09 1.77197817E-12-3.02937267E+04-8.49032208E-01 4
HO2 L 5/89H 1O 2 G 200.000 3500.000 1000.000 1
4.01721090E+00 2.23982013E-03-6.33658150E-07 1.14246370E-10-1.07908535E-14 2
1.11856713E+02 3.78510215E+00 4.30179801E+00-4.74912051E-03 2.11582891E-05 3
-2.42763894E-08 9.29225124E-12 2.94808040E+02 3.71666245E+00 4
H2O2 L 7/88H 2O 2 G 200.000 3500.000 1000.000 1
4.16500285E+00 4.90831694E-03-1.90139225E-06 3.71185986E-10-2.87908305E-14 2
-1.78617877E+04 2.91615662E+00 4.27611269E+00-5.42822417E-04 1.67335701E-05 3
-2.15770813E-08 8.62454363E-12-1.77025821E+04 3.43505074E+00 4
C L11/88C 1 G 200.000 3500.000 1000.000 1
2.49266888E+00 4.79889284E-05-7.24335020E-08 3.74291029E-11-4.87277893E-15 2
8.54512953E+04 4.80150373E+00 2.55423955E+00-3.21537724E-04 7.33792245E-07 3
-7.32234889E-10 2.66521446E-13 8.54438832E+04 4.53130848E+00 4
CH TPIS79C 1H 1 G 200.000 3500.000 1000.000 1
2.87846473E+00 9.70913681E-04 1.44445655E-07-1.30687849E-10 1.76079383E-14 2
7.10124364E+04 5.48497999E+00 3.48981665E+00 3.23835541E-04-1.68899065E-06 3
3.16217327E-09-1.40609067E-12 7.07972934E+04 2.08401108E+00 4

```
CH2 L S/93C 1H 2 G 200.000 3500.000 1000.000                                    1
2.87410113E+00 3.65639292E-03-1.40894597E-06 2.60179549E-10-1.87727567E-14      2
4.62636040E+04 6.17119324E+00 3.76267867E+00 9.68872143E-04 2.79489841E-06      3
-3.85091153E-09 1.68741719E-12 4.60040401E+04 1.56253185E+00                    4
CH2(S) L S/93C 1H 2 G 200.000 3500.000 1000.000                                 1
2.29203842E+00 4.65588637E-03-2.01191947E-06 4.17906000E-10-3.39716365E-14      2
5.09259997E+04 8.62650169E+00 4.19860411E+00-2.36661419E-03 8.23296220E-06      3
-6.68815981E-09 1.94314737E-12 5.04968163E+04-7.69118967E-01                    4
CH3 L11/89C 1H 3 G 200.000 3500.000 1000.000                                    1
2.28571772E+00 7.23990037E-03-2.98714348E-06 5.95684644E-10-4.67154394E-14      2
1.67755843E+04 8.48007179E+00 3.67359040E+00 2.01095175E-03 5.73021856E-06      3
-6.87117425E-09 2.54385734E-12 1.64449988E+04 1.60456433E+00                    4
CH4 L 8/88C 1H 4 G 200.000 3500.000 1000.000                                    1
7.48514950E-02 1.33909467E-02-5.73285809E-06 1.22292535E-09-1.01815230E-13      2
-9.46834459E+03 1.84373180E+01 5.14987613E+00-1.36709788E-02 4.91800599E-05     3
-4.84743026E-08 1.66693956E-11-1.02466476E+04-4.64130376E+00                    4
CO TPIS79C 1O 1 G 200.000 3500.000 1000.000                                     1
2.71518561E+00 2.06252743E-03-9.98825771E-07 2.30053008E-10-2.03647716E-14      2
-1.41518724E+04 7.81868772E+00 3.57953347E+00-6.10353680E-04 1.01681433E-06     3
9.07005884E-10-9.04424499E-13-1.43440860E+04 3.50840928E+00                     4
CO2 L 7/88C 1O 2 G 200.000 3500.000 1000.000                                    1
3.85746029E+00 4.41437026E-03-2.21481404E-06 5.23490188E-10-4.72084164E-14      2
-4.87591660E+04 2.27163806E+00 2.35677352E+00 8.98459677E-03-7.12356269E-06     3
2.45919022E-09-1.43699548E-13-4.83719697E+04 9.90105222E+00                     4
HCO L12/89H 1C 1O 1 G 200.000 3500.000 1000.000                                 1
2.77217438E+00 4.95695526E-03-2.48445613E-06 5.89161778E-10-5.33508711E-14      2
```

4.01191815E+03 9.79834492E+00 4.22118584E+00-3.24392532E-03 1.37799446E-05 3
-1.33144093E-08 4.33768865E-12 3.83956496E+03 3.39437243E+00 4
CH2O L 8/88H 2C 1O 1 G 200.000 3500.000 1000.000 1
1.76069008E+00 9.20000082E-03-4.42258813E-06 1.00641212E-09-8.83855640E-14 2
-1.39958323E+04 1.36563230E+01 4.79372315E+00-9.90833369E-03 3.73220008E-05 3
-3.79285261E-08 1.31772652E-11-1.43089567E+04 6.02812900E-01 4
CH2OH GUNL93C 1H 3O 1 G 200.000 3500.000 1000.000 1
3.69266569E+00 8.64576797E-03-3.75101120E-06 7.87234636E-10-6.48554201E-14 2
-3.24250627E+03 5.81043215E+00 3.86388918E+00 5.59672304E-03 5.93271791E-06 3
-1.04532012E-08 4.36967278E-12-3.19391367E+03 5.47302243E+00 4
CH3O 121686C 1H 3O 1 G 300.00 3000.00 1000.000 1
0.03770799E+02 0.07871497E-01-0.02656384E-04 0.03944431E-08-0.02112616E-12 2
0.12783252E+03 0.02929575E+02 0.02106204E+02 0.07216595E-01 0.05338472E-04 3
-0.07377636E-07 0.02075610E-10 0.09786011E+04 0.13152177E+02 4
CH3OH L 8/88C 1H 4O 1 G 200.000 3500.000 1000.000 1
1.78970791E+00 1.40938292E-02-6.36500835E-06 1.38171085E-09-1.17060220E-13 2
-2.53748747E+04 1.45023623E+01 5.71539582E+00-1.52309129E-02 6.52441155E-05 3
-7.10806889E-08 2.61352698E-11-2.56427656E+04-1.50409823E+00 4
C2H L 1/91C 2H 1 G 200.000 3500.000 1000.000 1
3.16780652E+00 4.75221902E-03-1.83787077E-06 3.04190252E-10-1.77232770E-14 2
6.71210650E+04 6.63589475E+00 2.88965733E+00 1.34099611E-02-2.84769501E-05 3
2.94791045E-08-1.09331511E-11 6.68393932E+04 6.22296438E+00 4
C2H2 L 1/91C 2H 2 G 200.000 3500.000 1000.000 1
4.14756964E+00 5.96166664E-03-2.37294852E-06 4.67412171E-10-3.61235213E-14 2
2.59359992E+04-1.23028121E+00 8.08681094E-01 2.33615629E-02-3.55171815E-05 3
2.80152437E-08-8.50072974E-12 2.64289807E+04 1.39397051E+01 4

```
C2H3 L 2/92C 2H 3 G 200.000 3500.000 1000.000                    1
3.01672400E+00 1.03302292E-02-4.68082349E-06 1.01763288E-09-8.62607041E-14  2
3.46128739E+04 7.78732378E+00 3.21246645E+00 1.51479162E-03 2.59209412E-05  3
-3.57657847E-08 1.47150873E-11 3.48598468E+04 8.51054025E+00               4
C2H4 L 1/91C 2H 4 G 200.000 3500.000 1000.000                    1
2.03611116E+00 1.46454151E-02-6.71077915E-06 1.47222923E-09-1.25706061E-13  2
4.93988614E+03 1.03053693E+01 3.95920148E+00-7.57052247E-03 5.70990292E-05  3
-6.91588753E-08 2.69884373E-11 5.08977593E+03 4.09733096E+00               4
C2H5 L12/92C 2H 5 G 200.000 3500.000 1000.000                    1
1.95465642E+00 1.73972722E-02-7.98206668E-06 1.75217689E-09-1.49641576E-13  2
1.28575200E+04 1.34624343E+01 4.30646568E+00-4.18658892E-03 4.97142807E-05  3
-5.99126606E-08 2.30509004E-11 1.28416265E+04 4.70720924E+00               4
C2H6 L 8/88C 2H 6 G 200.000 3500.000 1000.000                    1
1.07188150E+00 2.16852677E-02-1.00256067E-05 2.21412001E-09-1.90002890E-13  2
-1.14263932E+04 1.51156107E+01 4.29142492E+00-5.50154270E-03 5.99438288E-05  3
-7.08466285E-08 2.68685771E-11-1.15222055E+04 2.66682316E+00               4
CH2CO L 5/90C 2H 2O 1 G 200.000 3500.000 1000.000                1
4.51129732E+00 9.00359745E-03-4.16939635E-06 9.23345882E-10-7.94838201E-14  2
-7.55105311E+03 6.32247205E-01 2.13583630E+00 1.81188721E-02-1.73947474E-05  3
9.34397568E-09-2.01457615E-12-7.04291804E+03 1.22156480E+01               4
HCCO SRIC91H 1C 2O 1 G 300.00 4000.00 1000.000                   1
0.56282058E+01 0.40853401E-02-0.15934547E-05 0.28626052E-09-0.19407832E-13  2
0.19327215E+05-0.39302595E+01 0.22517214E+01 0.17655021E-01-0.23729101E-04  3
0.17275759E-07-0.50664811E-11 0.20059449E+05 0.12490417E+02               4
HCCOH SRI91C 2O 1H 2 G 300.000 5000.000 1000.000                 1
0.59238291E+01 0.67923600E-02-0.25658564E-05 0.44987841E-09-0.29940101E-13  2
```

0.72646260E+04-0.76017742E+01 0.12423733E+01 0.31072201E-01-0.50866864E-04 3
0.43137131E-07-0.14014594E-10 0.80316143E+04 0.13874319E+02 4
H2CN 41687H 2C 1N 1 G 300.00 4000.000 1000.000 1
0.52097030E+01 0.29692911E-02-0.28555891E-06-0.16355500E-09 0.30432589E-13 2
0.27677109E+05-0.44444780E+01 0.28516610E+01 0.56952331E-02 0.10711400E-05 3
-0.16226120E-08-0.23511081E-12 0.28637820E+05 0.89927511E+01 4
HCN GRI/98H 1C 1N 1 G 200.000 6000.000 1000.000 1
0.38022392E+01 0.31464228E-02-0.10632185E-05 0.16619757E-09-0.97997570E-14 2
0.14407292E+05 0.15754601E+01 0.22589886E+01 0.10051170E-01-0.13351763E-04 3
0.10092349E-07-0.30089028E-11 0.14712633E+05 0.89164419E+01 4
HNO And93 H 1N 1O 1 G 200.000 6000.000 1000.000 1
0.29792509E+01 0.34944059E-02-0.78549778E-06 0.57479594E-10-0.19335916E-15 2
0.11750582E+05 0.86063728E+01 0.45334916E+01-0.56696171E-02 0.18473207E-04 3
-0.17137094E-07 0.55454573E-11 0.11548297E+05 0.17498417E+01 4
N L 6/88N 1 G 200.000 6000.000 1000.000 1
0.24159429E+01 0.17489065E-03-0.11902369E-06 0.30226245E-10-0.20360982E-14 2
0.56133773E+05 0.46496096E+01 0.25000000E+01 0.00000000E+00 0.00000000E+00 3
0.00000000E+00 0.00000000E+00 0.56104637E+05 0.41939087E+01 4
NNH T07/93N 2H 1 G 200.000 6000.000 1000.000 1
0.37667544E+01 0.28915082E-02-0.10416620E-05 0.16842594E-09-0.10091896E-13 2
0.28650697E+05 0.44705067E+01 0.43446927E+01-0.48497072E-02 0.20059459E-04 3
-0.21726464E-07 0.79469539E-11 0.28791973E+05 0.29779410E+01 4
N2O L 7/88N 2O 1 G 200.000 6000.000 1000.000 1
0.48230729E+01 0.26270251E-02-0.95850874E-06 0.16000712E-09-0.97752303E-14 2
0.80734048E+04-0.22017207E+01 0.22571502E+01 0.11304728E-01-0.13671319E-04 3
0.96819806E-08-0.29307182E-11 0.87417744E+04 0.10757992E+02 4

```
NH And94 N 1H 1 G 200.000 6000.000 1000.000                                     1
0.27836928E+01 0.13298430E-02-0.42478047E-06 0.78348501E-10-0.55044470E-14      2
0.42120848E+05 0.57407799E+01 0.34929085E+01 0.31179198E-03-0.14890484E-05      3
0.24816442E-08-0.10356967E-11 0.41880629E+05 0.18483278E+01                     4
NH2 And89 N 1H 2 G 200.000 6000.000 1000.000                                    1
0.28347421E+01 0.32073082E-02-0.93390804E-06 0.13702953E-09-0.79206144E-14      2
0.22171957E+05 0.65204163E+01 0.42040029E+01-0.21061385E-02 0.71068348E-05      3
-0.56115197E-08 0.16440717E-11 0.21885910E+05-0.14184248E+00                    4
NH3 J 6/77N 1H 3 G 200.000 6000.000 1000.000                                    1
0.26344521E+01 0.56662560E-02-0.17278676E-05 0.23867161E-09-0.12578786E-13      2
-0.65446958E+04 0.65662928E+01 0.42860274E+01-0.46605230E-02 0.21718513E-04     3
-0.22808887E-07 0.82638046E-11-0.67417285E+04-0.62537277E+00                    4
NO RUS 78N 1O 1 G 200.000 6000.000 1000.000                                     1
0.32606056E+01 0.11911043E-02-0.42917048E-06 0.69457669E-10-0.40336099E-14      2
0.99209746E+04 0.63693027E+01 0.42184763E+01-0.46389760E-02 0.11041022E-04      3
-0.93361354E-08 0.28035770E-11 0.98446230E+04 0.22808464E+01                    4
NO2 L 7/88N 1O 2 G 200.000 6000.000 1000.000                                    1
0.48847542E+01 0.21723956E-02-0.82806906E-06 0.15747510E-09-0.10510895E-13      2
0.23164983E+04-0.11741695E+00 0.39440312E+01-0.15854290E-02 0.16657812E-04      3
-0.20475426E-07 0.78350564E-11 0.28966179E+04 0.63119917E+01                    4
HCNO BDEA94H 1N 1C 1O 1G 300.000 5000.000 1382.000                              1
6.59860456E+00 3.02778626E-03-1.07704346E-06 1.71666528E-10-1.01439391E-14      2
1.79661339E+04-1.03306599E+01 2.64727989E+00 1.27505342E-02-1.04794236E-05      3
4.41432836E-09-7.57521466E-13 1.92990252E+04 1.07332972E+01                     4
HOCN BDEA94H 1N 1C 1O 1G 300.000 5000.000 1368.000                              1
5.89784885E+00 3.16789393E-03-1.11801064E-06 1.77243144E-10-1.04339177E-14      2
```

-3.70653331E+03-6.18167825E+00 3.78604952E+00 6.88667922E-03-3.21487864E-06 3
5.17195767E-10 1.19360788E-14-2.82698400E+03 5.63292162E+00 4
HNCO BDEA94H 1N 1C 1O 1G 300.000 5000.000 1478.000 1
6.22395134E+00 3.17864004E-03-1.09378755E-06 1.70735163E-10-9.95021955E-15 2
-1.66599344E+04-8.38224741E+00 3.63096317E+00 7.30282357E-03-2.28050003E-06 3
-6.61271298E-10 3.62235752E-13-1.55873636E+04 6.19457727E+00 4
NCO EA 93 N 1C 1O 1 G 200.000 6000.000 1000.000 1
0.51521845E+01 0.23051761E-02-0.88033153E-06 0.14789098E-09-0.90977996E-14 2
0.14004123E+05-0.25442660E+01 0.28269308E+01 0.88051688E-02-0.83866134E-05 3
0.48016964E-08-0.13313595E-11 0.14682477E+05 0.95504646E+01 4
CN HBH92 C 1N 1 G 200.000 6000.000 1000.000 1
0.37459805E+01 0.43450775E-04 0.29705984E-06-0.68651806E-10 0.44134173E-14 2
0.51536188E+05 0.27867601E+01 0.36129351E+01-0.95551327E-03 0.21442977E-05 3
-0.31516323E-09-0.46430356E-12 0.51708340E+05 0.39804995E+01 4
HCNN SRI/94C 1N 2H 1 G 300.000 5000.000 1000.000 1
0.58946362E+01 0.39895959E-02-0.15982380E-05 0.29249395E-09-0.20094686E-13 2
0.53452941E+05-0.51030502E+01 0.25243194E+01 0.15960619E-01-0.18816354E-04 3
0.12125540E-07-0.32357378E-11 0.54261984E+05 0.11675870E+02 4
N2 121286N 2 G 300.000 5000.000 1000.000 1
0.02926640E+02 0.14879768E-02-0.05684760E-05 0.10097038E-09-0.06753351E-13 2
-0.09227977E+04 0.05980528E+02 0.03298677E+02 0.14082404E-02-0.03963222E-04 3
0.05641515E-07-0.02444854E-10-0.10208999E+04 0.03950372E+02 4
AR 120186AR 1 G 300.000 5000.000 1000.000 1
0.02500000E+02 0.00000000E+00 0.00000000E+00 0.00000000E+00 0.00000000E+00 2
-0.07453750E+04 0.04366000E+02 0.02500000E+02 0.00000000E+00 0.00000000E+00 3
0.00000000E+00 0.00000000E+00-0.07453750E+04 0.04366000E+02 4

```
C3H8 L 4/85C 3H 8 G 300.000 5000.000 1000.000                                    1
0.75341368E+01 0.18872239E-01-0.62718491E-05 0.91475649E-09-0.47838069E-13       2
-0.16467516E+05-0.17892349E+02 0.93355381E+00 0.26424579E-01 0.61059727E-05      3
-0.21977499E-07 0.95149253E-11-0.13958520E+05 0.19201691E+02                     4
C3H7 L 9/84C 3H 7 G 300.000 5000.000 1000.000                                    1
0.77026987E+01 0.16044203E-01-0.52833220E-05 0.76298590E-09-0.39392284E-13       2
0.82984336E+04-0.15480180E+02 0.10515518E+01 0.25991980E-01 0.23800540E-05      3
-0.19609569E-07 0.93732470E-11 0.10631863E+05 0.21122559E+02                     4
CH3CHO L 8/88C 2H 4O 1 G 200.000 6000.000 1000.000                               1
0.54041108E+01 0.11723059E-01-0.42263137E-05 0.68372451E-09-0.40984863E-13       2
-0.22593122E+05-0.34807917E+01 0.47294595E+01-0.31932858E-02 0.47534921E-04      3
-0.57458611E-07 0.21931112E-10-0.21572878E+05 0.41030159E+01                     4
CH2CHO SAND86O 1H 3C 2 G 300.000 5000.000 1000.000                               1
0.05975670E+02 0.08130591E-01-0.02743624E-04 0.04070304E-08-0.02176017E-12       2
0.04903218E+04-0.05045251E+02 0.03409062E+02 0.10738574E-01 0.01891492E-04      3
-0.07158583E-07 0.02867385E-10 0.15214766E+04 0.09558290E+02                     4
C2H3O A 1/05C 2H 3O 1 0G 200.000 6000.000 1000.                                  1
5.60158035E+00 9.17613962E-03-3.28028902E-06 5.27903888E-10-3.15362241E-14       2
1.71446252E+04-5.47228512E+00 3.58349017E+00-6.02275805E-03 6.32426867E-05      3
-8.18540707E-08 3.30444505E-11 1.85681353E+04 9.59725926E+00 1.97814471E+04      4
C3H6 120186C 3H 6 G 0300.00 5000.00 1000.00                                      1
0.06732257E+02 0.01490834E+00-0.04949899E-04 0.07212022E-08-0.03766204E-12       2
-0.09235703E+04-0.01331335E+03 0.01493307E+02 0.02092518E+00 0.04486794E-04      3
-0.01668912E-06 0.07158146E-10 0.01074826E+05 0.01614534E+03                     4
aC3H5 PD5/98C 3H 5 0 0G 300.000 3000.000                                         1
0.65007877E+01 0.14324731E-01-0.56781632E-05 0.11080801E-08-0.90363887E-13       2
```

0.17482449E+05-0.11243050E+02 0.13631835E+01 0.19813821E-01 0.12497060E-04 3
-0.33355555E-07 0.15846571E-10 0.19245629E+05 0.17173214E+02 4

B.4 Transport properties

TRANFT: Transport property fitting, CHEMKIN-II Version 3.0, November 1990 DOUBLE PRECISION

OUTPUT FROM THE TRANSPORT PROPERTY FITTING PACKAGE

CKLIB: Chemical Kinetics Library CHEMKIN-II Version 4.9, April 1994 DOUBLE PRECISION

DATA HAS BEEN FIT OVER THE RANGE: TLOW= 300.00, THIGH= 3500.00

TRANSPORT PARAMETERS FROM DATA BASE:

C	0	71.400	3.298	0.000	0.000	0.000
C2H	1	209.000	4.100	0.000	0.000	2.500
C2H2	1	209.000	4.100	0.000	0.000	2.500
C2H3	2	209.000	4.100	0.000	0.000	1.000
C2H4	2	280.800	3.971	0.000	0.000	1.500
C2H5	2	252.300	4.302	0.000	0.000	1.500
C2H6	2	252.300	4.302	0.000	0.000	1.500
C3H7	2	266.800	4.982	0.000	0.000	1.000
C3H8	2	266.800	4.982	0.000	0.000	1.000
CH	1	80.000	2.750	0.000	0.000	0.000
CH2	1	144.000	3.800	0.000	0.000	0.000
CH2(S)	1	144.000	3.800	0.000	0.000	0.000

CH2CO	2	436.000	3.970	0.000	0.000	2.000
CH2O	2	498.000	3.590	0.000	0.000	2.000
CH2OH	2	417.000	3.690	1.700	0.000	2.000
CH3	1	144.000	3.800	0.000	0.000	0.000
CH3CHO	2	436.000	3.970	0.000	0.000	2.000
CH2CHO	2	436.000	3.970	0.000	0.000	2.000
CH3O	2	417.000	3.690	1.700	0.000	2.000
CH3OH	2	481.800	3.626	0.000	0.000	1.000
CH4	2	141.400	3.746	0.000	2.600	13.000
CO	1	98.100	3.650	0.000	1.950	1.800
CO2	1	244.000	3.763	0.000	2.650	2.100
H	0	145.000	2.050	0.000	0.000	0.000
H2	1	38.000	2.920	0.000	0.790	280.000
H2O	2	572.400	2.605	1.844	0.000	4.000
H2O2	2	107.400	3.458	0.000	0.000	3.800
HCCO	2	150.000	2.500	0.000	0.000	1.000
HCCOH	2	436.000	3.970	0.000	0.000	2.000
HCO	2	498.000	3.590	0.000	0.000	0.000
HO2	2	107.400	3.458	0.000	0.000	1.000
N2	1	97.530	3.621	0.000	1.760	4.000
O	0	80.000	2.750	0.000	0.000	0.000
O2	1	107.400	3.458	0.000	1.600	3.800
OH	1	80.000	2.750	0.000	0.000	0.000

Coefficients for species viscosities:

MAXIMUM FITTING ERROR = 2.655E-03

VISCOSITY:
CH4
-2.00E+01 3.569547095E+00-3.874927848E-01 1.71E-02
O2
-1.72E+01 2.678085480E+00-2.721588436E-01 1.21E-02
H2O
-11.9353064 4.214153204E-01-2.414501571E-02
CO2
-2.40E+01 5.130428118E+00-5.724287559E-01 2.44E-02
H
-2.04E+01 3.652696513E+00-3.980310504E-01 1.76E-02
O
-1.51E+01 1.929020467E+00-1.738651327E-01 7.84E-03
OH
-1.51E+01 1.929020467E+00-1.738651327E-01 7.84E-03
HO2
-1.71E+01 2.678085480E+00-2.721588436E-01 1.21E-02
H2
-1.38E+01 1.003492097E+00-5.016056447E-02 2.33E-03
CO
-1.66E+01 2.400968097E+00-2.357707584E-01 1.05E-02
H2O2
-1.71E+01 2.678085480E+00-2.721588436E-01 1.21E-02
HCO
-1.99E+01 2.703808873E+00-1.672351428E-01 3.21E-03
CH2O

-1.99E+01 2.703808873E+00-1.672351428E-01 3.21E-03
CH3
-2.02E+01 3.630413753E+00-3.952264472E-01 1.75E-02
CH
-1.52E+01 1.929020467E+00-1.738651327E-01 7.84E-03
CH2
-2.03E+01 3.630413753E+00-3.952264472E-01 1.75E-02
CH3O
-2.00E+01 2.861642804E+00-2.024742066E-01 5.36E-03
C
-1.50E+01 1.706338106E+00-1.443624417E-01 6.54E-03
C2H
-2.34E+01 4.790352428E+00-5.364561449E-01 2.32E-02
C2H2
-2.33E+01 4.790352428E+00-5.364561449E-01 2.32E-02
C2H3
-2.33E+01 4.790352428E+00-5.364561449E-01 2.32E-02
C2H4
-2.50E+01 5.332794624E+00-5.890462937E-01 2.47E-02
C2H5
-2.46E+01 5.183143327E+00-5.771880519E-01 2.45E-02
C2H6
-2.46E+01 5.183143327E+00-5.771880519E-01 2.45E-02
HCCO
-1.92E+01 3.751327914E+00-4.102639728E-01 1.81E-02
CH2CO

-2.23E+01 3.866549995E+00-3.419575514E-01 1.17E-02
C2H3O
-2.23E+01 3.866549995E+00-3.419575514E-01 1.17E-02
CH2(S)
-2.03E+01 3.630413753E+00-3.952264472E-01 1.75E-02
C3H6
-2.51E+01 5.297301601E+00-5.883844716E-01 2.49E-02
aC3H5
-2.51E+01 5.297301601E+00-5.883844716E-01 2.49E-02
N2
-1.66E+01 2.388160006E+00-2.341198015E-01 1.05E-02

Coefficients for species conductivities

MAXIMUM FITTING ERROR = 9.016E-03

Conductivity:
CH4
1.330607416E+01-4.960303524E+00 1.032815702E+00-5.633620403E-02
O2
-1.936689669E+00 2.890449953E+00-2.709545074E-01
H2O
2.336646642E+01-8.966300547E+00 1.528897704E+00-7.590501248E-02
CO2
-1.135084001E+01 5.875696541E+00-5.678002336E-01
H
-8.555006658E-01 3.652696513E+00-3.980310504E-01
O

1.684973637E+00 1.929020467E+00-1.738651327E-01
OH
1.416254156E+01-3.244769088E+00 5.336784136E-01-2.328204177E-02
HO2
-1.130100152E+00 2.340049375E+00-1.632022890E-01
H2
9.236015216E+00-4.675196838E-01 1.156852091E-01-2.596474270E-03
CO
1.187758894E+01-3.155034812E+00 6.020824539E-01-3.032877929E-02
H2O2
8.827615600E-01 1.315508803E+00 1.9166
HCO
6.296078589E+00-2.225326983E+00 6.369235051E-01-3.808498965E-02
CH2O
5.384244205E+00-2.389223307E+00 7.390003185E-01-4.581464985E-02
CH3
1.399185251E+01-4.641943977E+00 9.076545000E-01-4.772457046E-02
CH
2.080511443E+01-6.240167559E+00 9.821714977E-01-4.502673965E-02
CH2
1.291655734E+01-3.737175320E+00 7.158107200E-01-3.638458173E-02
CH3O
-6.138155716E+00 2.471261592E+00 6.4770
C
2.041508440E+00 1.706338106E+00-1.443624417E-01
C2H

1.336279456E+01-4.326339766E+00 8.368163029E-01-4.380382750E-02
C2H2
-7.691138301E+00 4.564180531E+00-4.040789811E-01
C2H3
-9.095587607E+00 4.544308964E+00-3.175883449E-01
C2H4
-1.460905899E+01 6.359840483E+00-5.034674197E-01
C2H5
-8.942057024E+00 4.021654855E+00-1.835761761E-01-1.963075713E-03
C2H6
-1.098257705E+01 4.703148026E+00-2.518079208E-01
HCCO
-5.965855110E+00 4.394171147E+00-3.976649700E-01
CH2CO
-8.329497458E+00 3.971078777E+00-2.213342734E-01
C2H3O
-2.469760391E+01 1.040468567E+01-1.058757107E+00
CH2(S)
1.893673079E+01-6.509742809E+00 1.132877447E+00-5.695912349E-02
C3H6
-1.704646643E+01 7.356867279E+00-6.525161805E-01
aC3H5
-2.141391655E+01 9.406178748E+00-9.659387429E-01
N2
1.293059349E+01-3.528637463E+00 6.456212270E-01-3.194596392E-02

Coefficients for species diffusion coefficients

MAXIMUM FITTING ERROR = 3.707E-03

Diffusion:

CH4 CH4

-1.760279612E+01 4.320034358E+00-3.477957927E-01 1.515060688E-02

O2 CH4

-1.696131608E+01 4.074165937E+00-3.182573739E-01 1.396610989E-02

O2 O2

-1.605076774E+01 3.688226235E+00-2.690947042E-01 1.187504153E-02

H2O CH4

-2.052801076E+01 5.190796435E+00-4.197132671E-01 1.661888903E-02

H2O O2

-2.029802374E+01 5.167995093E+00-4.260628490E-01 1.725356479E-02

H2O H2O

-1.180206766E+01 8.886062886E-01 2.461982152E-01 -1.607191687E-02

CO2 CH4

-1.920917401E+01 4.764710227E+00-3.942400993E-01 1.668921487E-02

CO2 O2

-1.868514283E+01 4.565512563E+00-3.754539076E-01 1.617305905E-02

CO2 H2O

-1.924810083E+01 4.356703427E+00-2.835789752E-01 9.646896833E-03

CO2 CO2

-2.074682878E+01 5.125916904E+00-4.300041647E-01 1.780190312E-02

H CH4
-1.790236108E+01 5.054239010E+00-4.413160055E-01 1.910839802E-02
H O2
-1.761107473E+01 5.048252384E+00-4.490716599E-01 1.981330549E-02
H H2O
-1.651314932E+01 4.220700983E+00-2.825946969E-01 1.018064676E-02
H CO2
-1.725033893E+01 4.566918362E+00-3.509187796E-01 1.402682861E-02
H H
-1.519084022E+01 4.384303709E+00-3.557546141E-01 1.548012947E-02

O CH4
-1.556218014E+01 3.683629037E+00-2.686556473E-01 1.186253354E-02
O O2
-1.511165822E+01 3.515444701E+00-2.491203680E-01 1.111627671E-02
O H2O
-1.906508684E+01 4.989055713E+00-4.192832737E-01 1.761870766E-02
O CO2
-1.793673259E+01 4.489873138E+00-3.697552089E-01 1.609251729E-02
O H
-1.531287558E+01 4.270888005E+00-3.482328329E-01 1.545097305E-02
O O
-1.356849264E+01 3.062183244E+00-1.889702775E-01 8.454195135E-03

OH CH4

-1.556533030E+01 3.678661496E+00-2.679777607E-01 1.183177254E-02
OH O2
-1.509621640E+01 3.500308160E+00-2.470165008E-01 1.101912706E-02
OH H2O
-1.908171116E+01 4.989633580E+00-4.194071514E-01 1.762633022E-02
OH CO2
-1.792453425E+01 4.476324205E+00-3.680187025E-01 1.601858519E-02
OH H
-1.533072459E+01 4.277567665E+00-3.491406936E-01 1.549202609E-02
OH O
-1.358468451E+01 3.062679111E+00-1.890396577E-01 8.457418012E-03
OH OH
-1.359904042E+01 3.062183244E+00-1.889702775E-01 8.454195135E-03

HO2 CH4
-1.698005836E+01 4.079754122E+00-3.190091041E-01 1.399974884E-02
HO2 O2
-1.605887774E+01 3.688399523E+00-2.691183052E-01 1.187611033E-02
HO2 H2O
-1.969227647E+01 4.975026876E+00-4.062735871E-01 1.660123780E-02
HO2 CO2
-1.868972761E+01 4.564003287E+00-3.752914424E-01 1.616757044E-02
HO2 H
-1.762110952E+01 5.052178473E+00-4.495998311E-01 1.983694951E-02
HO2 O
-1.513525217E+01 3.523301396E+00-2.502123503E-01 1.116669951E-02

HO2 OH
-1.511947081E+01 3.507930921E+00-2.480760212E-01 1.106805265E-02
HO2 HO2
-1.606627488E+01 3.688226235E+00-2.690947042E-01 1.187504153E-02

H2 CH4
-1.353826022E+01 3.227360673E+00-2.134256737E-01 9.644706316E-03
H2 O2
-1.270709388E+01 2.929626523E+00-1.739680837E-01 7.901250164E-03
H2 H2O
-1.818504723E+01 5.043649643E+00-4.377097453E-01 1.887656413E-02
H2 CO2
-1.564739656E+01 4.025827522E+00-3.181198250E-01 1.422137872E-02
H2 H
-1.201912295E+01 3.033147089E+00-1.860162057E-01 8.361686291E-03
H2 O
-1.093372904E+01 2.306135807E+00-8.736463554E-02 3.897545153E-03
H2 OH
-1.093673502E+01 2.306120328E+00-8.736274609E-02 3.897467312E-03
H2 HO2
-1.271125832E+01 2.931054698E+00-1.741690061E-01 7.910636748E-03
H2 H2
-1.031824434E+01 2.192406860E+00-7.538951284E-02 3.511183915E-03

CO CH4
-1.654504015E+01 3.902989298E+00-2.959724763E-01 1.299730149E-02

CO O2
-1.582244531E+01 3.599212287E+00-2.581899063E-01 1.143096775E-02
CO H2O
-2.031237936E+01 5.186324400E+00-4.313754455E-01 1.759978341E-02
CO CO2
-1.853079415E+01 4.516961186E+00-3.708426164E-01 1.604367644E-02
CO H
-1.719132402E+01 4.859366081E+00-4.240579015E-01 1.870695312E-02
CO O
-1.478200095E+01 3.371097855E+00-2.298575526E-01 1.025849790E-02
CO OH
-1.476986417E+01 3.357756474E+00-2.280054505E-01 1.017307353E-02
CO HO2
-1.583284728E+01 3.600570645E+00-2.583774171E-01 1.143956872E-02
CO H2
-1.268298232E+01 2.903434293E+00-1.707676302E-01 7.771157268E-03
CO CO
-1.551400805E+01 3.472779360E+00-2.416434309E-01 1.070800928E-02

H2O2 CH4
-1.699844022E+01 4.085299205E+00-3.197550391E-01 1.403312881E-02
H2O2 O2
-1.606742344E+01 3.688898129E+00-2.691862126E-01 1.187918561E-02
H2O2 H2O
-1.967562585E+01 4.964899372E+00-4.047376014E-01 1.652519649E-02
H2O2 CO2

-1.869430896E+01 4.562621216E+00-3.751419312E-01 1.616247951E-02
H2O2 H
-1.763070446E+01 5.055935364E+00-4.501052540E-01 1.985957570E-02
H2O2 O
-1.515825478E+01 3.531014869E+00-2.512844003E-01 1.121620107E-02
H2O2 OH
-1.514220600E+01 3.515444701E+00-2.491203680E-01 1.111627671E-02
H2O2 HO2
-1.607413051E+01 3.688389256E+00-2.691169069E-01 1.187604701E-02
H2O2 H2
-1.271520206E+01 2.932408989E+00-1.743595317E-01 7.919537539E-03
H2O2 CO
-1.584365217E+01 3.602237408E+00-2.586074419E-01 1.145011749E-02
H2O2 H2O2
-1.608131552E+01 3.688226235E+00-2.690947042E-01 1.187504153E-02

HCO CH4
-2.048734314E+01 5.132891364E+00-4.243041989E-01 1.728907041E-02
HCO O2
-2.031658605E+01 5.113617471E+00-4.319297136E-01 1.802807477E-02
HCO H2O
-1.757312689E+01 3.511207417E+00-1.497970247E-01 2.966601580E-03
HCO CO2
-2.103479641E+01 5.058658986E+00-3.955870918E-01 1.531362269E-02
HCO H
-1.540645380E+01 3.572428706E+00-1.878765897E-01 5.591995709E-03

HCO O
-1.915075164E+01 4.868836274E+00-4.046206779E-01 1.701121293E-02
HCO OH
-1.918204232E+01 4.875613604E+00-4.058259105E-01 1.707793067E-02
HCO HO2
-2.032174130E+01 5.112658897E+00-4.317898712E-01 1.802138536E-02
HCO H2
-1.746998686E+01 4.670553786E+00-3.931784730E-01 1.709977467E-02
HCO CO
-2.009021799E+01 5.037635616E+00-4.241198697E-01 1.777021744E-02
HCO H2O2
-2.032585541E+01 5.111362936E+00-4.315973859E-01 1.801202832E-02
HCO HCO
-1.885553633E+01 3.923354037E+00-2.115868580E-01 5.939300452E-03

CH2O CH4
-2.047278723E+01 5.123416927E+00-4.228709864E-01 1.721821288E-02
CH2O O2
-2.032689881E+01 5.114224091E+00-4.320140229E-01 1.803192490E-02
CH2O H2O
-1.757470890E+01 3.509439624E+00-1.496107047E-01 2.961995182E-03
CH2O CO2
-2.106202604E+01 5.066197445E+00-3.966841980E-01 1.536584789E-02
CH2O H
-1.539084361E+01 3.565008160E+00-1.867583089E-01 5.536895739E-03
CH2O O

-1.914986288E+01 4.864897408E+00-4.039216934E-01 1.697257048E-02
CH2O OH
-1.918176588E+01 4.871870986E+00-4.051599172E-01 1.704104851E-02
CH2O HO2
-2.033308645E+01 5.113692762E+00-4.319404969E-01 1.802858184E-02
CH2O H2
-1.747771381E+01 4.673156937E+00-3.935105496E-01 1.711384774E-02
CH2O CO
-2.009778393E+01 5.037182908E+00-4.240364358E-01 1.776547635E-02
CH2O H2O2
-2.033819161E+01 5.112806455E+00-4.318116028E-01 1.802243384E-02
CH2O HCO
-1.886381419E+01 3.923281500E+00-2.115780404E-01 5.938985274E-03
CH2O CH2O
-1.887260920E+01 3.923354037E+00-2.115868580E-01 5.939300452E-03

CH3 CH4
-1.766458834E+01 4.343240121E+00-3.506765555E-01 1.527022788E-02
CH3 O2
-1.707094400E+01 4.119808690E+00-3.242841480E-01 1.423183078E-02
CH3 H2O
-2.042453456E+01 5.222435483E+00-4.324987297E-01 1.751958000E-02
CH3 CO2
-1.923135415E+01 4.771649902E+00-3.944963417E-01 1.667281076E-02
CH3 H
-1.801636401E+01 5.090086349E+00-4.457548702E-01 1.929139676E-02

```
CH3                 O
-1.561687140E+01    3.703886270E+00-2.712409598E-01    1.197280364E-02
CH3                 OH
-1.562210644E+01    3.699988722E+00-2.707080833E-01    1.194857827E-02
CH3                 HO2
-1.709002711E+01    4.125626066E+00-3.250667199E-01    1.426685069E-02
CH3                 H2
-1.358416799E+01    3.239853678E+00-2.150511937E-01    9.715282318E-03
CH3                 CO
-1.661214441E+01    3.930380705E+00-2.994308130E-01    1.314285351E-02
CH3                 H2O2
-1.710868108E+01    4.131368460E+00-3.258392062E-01    1.430141955E-02
CH3                 HCO
-2.046646778E+01    5.118754490E+00-4.214662210E-01    1.712476246E-02
CH3                 CH2O
-2.045023975E+01    5.108642883E+00-4.199389693E-01    1.704934461E-02
CH3                 CH3
-1.772990211E+01    4.367696733E+00-3.537273902E-01    1.539753038E-02

CH                  CH4
-1.557193598E+01    3.710292275E+00-2.722899898E-01    1.202726367E-02
CH                  O2
-1.516682404E+01    3.569091351E+00-2.565760617E-01    1.146053026E-02
CH                  H2O
-1.898988104E+01    4.979356554E+00-4.176235448E-01    1.752883173E-02
CH                  CO2
```

-1.797274762E+01 4.534579042E+00-3.754820605E-01 1.633621958E-02
CH H
-1.524698812E+01 4.246332650E+00-3.448954990E-01 1.530006418E-02
CH O
-1.352726344E+01 3.067763123E+00-1.897509881E-01 8.490460772E-03
CH OH
-1.354937095E+01 3.071481255E+00-1.902711998E-01 8.514625376E-03
CH HO2
-1.519066891E+01 3.577342664E+00-2.577227064E-01 1.151347129E-02
CH H2
-1.092231090E+01 2.306202928E+00-8.737280936E-02 3.897883069E-03
CH CO
-1.482896592E+01 3.420001629E+00-2.366459270E-01 1.057157644E-02
CH H2O2
-1.521373009E+01 3.585356976E+00-2.588363903E-01 1.156488973E-02
CH HCO
-1.903795445E+01 4.843813725E+00-4.001933607E-01 1.676691158E-02
CH CH2O
-1.903547062E+01 4.839450197E+00-3.994238332E-01 1.672453708E-02
CH CH3
-1.562066235E+01 3.727389397E+00-2.744484271E-01 1.211835622E-02
CH CH
-1.346542655E+01 3.062183244E+00-1.889702775E-01 8.454195135E-03

CH2 CH4
-1.765053055E+01 4.344870429E+00-3.508848705E-01 1.527906464E-02

CH2 O2
-1.707915129E+01 4.132968305E+00-3.260544226E-01 1.431105055E-02
CH2 H2O
-2.040913387E+01 5.224092154E+00-4.327352339E-01 1.753063744E-02
CH2 CO2
-1.920159447E+01 4.768582927E+00-3.938474246E-01 1.663348229E-02
CH2 H
-1.798723961E+01 5.079563954E+00-4.444136859E-01 1.923461015E-02
CH2 O
-1.558834476E+01 3.699567569E+00-2.706504419E-01 1.194595507E-02
CH2 OH
-1.559686028E+01 3.697253935E+00-2.703332304E-01 1.193149436E-02
CH2 HO2
-1.709852890E+01 4.139000763E+00-3.268659281E-01 1.434736576E-02
CH2 H2
-1.355982380E+01 3.231190003E+00-2.138418525E-01 9.659202107E-03
CH2 CO
-1.661775187E+01 3.942048792E+00-3.009974379E-01 1.321282808E-02
CH2 H2O2
-1.711740123E+01 4.144923053E+00-3.276626105E-01 1.438301773E-02
CH2 HCO
-2.039806611E+01 5.097935506E+00-4.183219307E-01 1.696950199E-02
CH2 CH2O
-2.038050275E+01 5.087332841E+00-4.167208822E-01 1.689045699E-02
CH2 CH3
-1.771390718E+01 4.368346040E+00-3.538103602E-01 1.540105015E-02

CH2 CH
-1.558104549E+01 3.717715492E+00-2.731288057E-01 1.205849837E-02
CH2 CH2
-1.769520494E+01 4.367696733E+00-3.537273902E-01 1.539753038E-02

CH3O CH4
-2.034324060E+01 5.089570993E+00-4.211901835E-01 1.724914065E-02
CH3O O2
-2.016015400E+01 5.063573879E+00-4.281524946E-01 1.797184378E-02
CH3O H2O
-1.619570588E+01 2.843144426E+00-5.102877842E-02 -1.708651859E-03
CH3O CO2
-2.111192919E+01 5.114999670E+00-4.073072062E-01 1.598591458E-02
CH3O H
-1.561126529E+01 3.698147585E+00-2.103085359E-01 6.792229447E-03
CH3O O
-1.878354675E+01 4.745967814E+00-3.924367984E-01 1.663657656E-02
CH3O OH
-1.880408513E+01 4.747893975E+00-3.929509375E-01 1.667069852E-02
CH3O HO2
-1.994316498E+01 4.989293155E+00-4.200959405E-01 1.768642895E-02
CH3O H2
-1.797856302E+01 4.905027232E+00-4.293092642E-01 1.891306308E-02
CH3O CO
-2.003302717E+01 5.028627767E+00-4.259385728E-01 1.797007881E-02
CH3O H2O2

-1.994945671E+01 4.988909576E+00-4.200448105E-01 1.768418608E-02
CH3O HCO
-1.981646415E+01 4.378886014E+00-2.813828651E-01 9.370857064E-03
CH3O CH2O
-1.982650548E+01 4.379424310E+00-2.814553225E-01 9.373961876E-03
CH3O CH3
-2.012689711E+01 5.018250687E+00-4.131419578E-01 1.694648548E-02
CH3O CH
-1.870999936E+01 4.738675824E+00-3.905506800E-01 1.651275231E-02
CH3O CH2
-2.006425983E+01 4.999968754E+00-4.103333006E-01 1.680584964E-02
CH3O CH3O
-1.906234023E+01 4.049274338E+00-2.359744963E-01 7.307409617E-03

C CH4
-1.530099940E+01 3.556646808E+00-2.527121104E-01 1.119536389E-02
C O2
-1.480660875E+01 3.371230339E+00-2.300786606E-01 1.027673169E-02
C H2O
-1.896641520E+01 4.932215783E+00-4.145718316E-01 1.752185885E-02
C CO2
-1.780941243E+01 4.440463877E+00-3.655222820E-01 1.600112071E-02
C H
-1.560174045E+01 4.330819826E+00-3.589812183E-01 1.604703557E-02
C O
-1.340380735E+01 2.956613030E+00-1.751304776E-01 7.848747231E-03

C OH
-1.342267506E+01 2.959201877E+00-1.754927801E-01 7.865575406E-03
C HO2
-1.482503960E+01 3.377291292E+00-2.309197414E-01 1.031551090E-02
C H2
-1.081044916E+01 2.188985248E+00-7.096779397E-02 3.131620171E-03
C CO
-1.451843785E+01 3.244177530E+00-2.131833276E-01 9.527346573E-03
C H2O2
-1.484282413E+01 3.383168884E+00-2.317353520E-01 1.035311496E-02
C HCO
-1.895961054E+01 4.791447036E+00-3.969915100E-01 1.677812218E-02
C CH2O
-1.896275418E+01 4.789831930E+00-3.966410673E-01 1.675663174E-02
C CH3
-1.536331842E+01 3.579934822E+00-2.557556206E-01 1.132821094E-02
C CH
-1.335132581E+01 2.954156796E+00-1.747854712E-01 7.832680219E-03
C CH2
-1.532763210E+01 3.571505864E+00-2.545912443E-01 1.127476104E-02
C CH3O
-1.867823213E+01 4.704906125E+00-3.897246316E-01 1.662675194E-02
C C
-1.328347053E+01 2.871652184E+00-1.641230215E-01 7.373125843E-03

C2H CH4

-1.887960604E+01 4.679549323E+00-3.880188595E-01 1.662435905E-02
C2H O2
-1.816374469E+01 4.404536855E+00-3.569510943E-01 1.547161834E-02
C2H H2O
-2.027560548E+01 4.923007396E+00-3.762752739E-01 1.440491310E-02
C2H CO2
-2.036670213E+01 5.042703447E+00-4.228385471E-01 1.763444009E-02
C2H H
-1.774160236E+01 4.779665970E+00-3.856862623E-01 1.583473875E-02
C2H O
-1.728281068E+01 4.249573180E+00-3.404509297E-01 1.490328466E-02
C2H OH
-1.726463364E+01 4.234772784E+00-3.384929826E-01 1.481712577E-02
C2H HO2
-1.817177784E+01 4.404988271E+00-3.570004186E-01 1.547332877E-02
C2H H2
-1.527558021E+01 3.862568375E+00-2.980847922E-01 1.340591756E-02
C2H CO
-1.800841153E+01 4.351918453E+00-3.517359557E-01 1.531341565E-02
C2H H2O2
-1.817987706E+01 4.405583600E+00-3.570671924E-01 1.547573620E-02
C2H HCO
-2.111948667E+01 5.171724548E+00-4.171064950E-01 1.650847358E-02
C2H CH2O
-2.112276163E+01 5.169663451E+00-4.168000974E-01 1.649355408E-02
C2H CH3

-1.893404492E+01 4.699654384E+00-3.902379476E-01 1.670404907E-02
C2H CH
-1.735339352E+01 4.304532074E+00-3.477170689E-01 1.522284514E-02
C2H CH2
-1.891736743E+01 4.700703077E+00-3.902103646E-01 1.669544777E-02
C2H CH3O
-2.111130191E+01 5.217490561E+00-4.300185152E-01 1.734091644E-02
C2H C
-1.700831681E+01 4.130720010E+00-3.260469047E-01 1.432172721E-02
C2H C2H
-2.006338845E+01 4.983892108E+00-4.201560754E-01 1.772039037E-02

C2H2 CH4
-1.889022694E+01 4.680202649E+00-3.880193510E-01 1.662056462E-02
C2H2 O2
-1.817374225E+01 4.404207492E+00-3.569177911E-01 1.547060649E-02
C2H2 H2O
-2.024505470E+01 4.905826285E+00-3.737700294E-01 1.428532529E-02
C2H2 CO2
-2.039137658E+01 5.048553979E+00-4.237558075E-01 1.768107412E-02
C2H2 H
-1.774507013E+01 4.780158032E+00-3.856585610E-01 1.582941933E-02
C2H2 O
-1.731508937E+01 4.259551244E+00-3.417705997E-01 1.496134239E-02
C2H2 OH
-1.729594002E+01 4.244243958E+00-3.397459979E-01 1.487226739E-02

C2H2 HO2
-1.818134947E+01 4.404442853E+00-3.569411430E-01 1.547129030E-02
C2H2 H2
-1.528922800E+01 3.867757812E+00-2.988050349E-01 1.343914016E-02
C2H2 CO
-1.801975419E+01 4.352349917E+00-3.517961505E-01 1.531619809E-02
C2H2 H2O2
-1.818904897E+01 4.404833852E+00-3.569833530E-01 1.547272671E-02
C2H2 HCO
-2.113317209E+01 5.173173016E+00-4.173231771E-01 1.651908982E-02
C2H2 CH2O
-2.113855169E+01 5.171979206E+00-4.171444496E-01 1.651032642E-02
C2H2 CH3
-1.894432714E+01 4.700245508E+00-3.902230508E-01 1.669925809E-02
C2H2 CH
-1.738771412E+01 4.315707390E+00-3.491939113E-01 1.528776897E-02
C2H2 CH2
-1.892750112E+01 4.701317927E+00-3.901918390E-01 1.669019746E-02
C2H2 CH3O
-2.112928959E+01 5.220747314E+00-4.305056001E-01 1.736475837E-02
C2H2 C
-1.704125329E+01 4.141670585E+00-3.275233419E-01 1.438794373E-02
C2H2 C2H
-2.007277686E+01 4.983696755E+00-4.201240508E-01 1.771870857E-02
C2H2 C2H2
-2.008312862E+01 4.983892108E+00-4.201560754E-01 1.772039037E-02

C2H3 CH4
-1.890039038E+01 4.680851712E+00-3.880182918E-01 1.661665863E-02
C2H3 O2
-1.818388827E+01 4.404156641E+00-3.569177273E-01 1.547089684E-02
C2H3 H2O
-2.021382111E+01 4.888557347E+00-3.712517682E-01 1.416510584E-02
C2H3 CO2
-2.041425100E+01 5.053851124E+00-4.245864064E-01 1.772330650E-02
C2H3 H
-1.774834115E+01 4.780625519E+00-3.856326215E-01 1.582439877E-02
C2H3 O
-1.734665274E+01 4.269425445E+00-3.430763058E-01 1.501877625E-02
C2H3 OH
-1.732666861E+01 4.253672109E+00-3.409930719E-01 1.492713698E-02
C2H3 HO2
-1.819107108E+01 4.404178438E+00-3.569154082E-01 1.547056603E-02
C2H3 H2
-1.530202288E+01 3.872628555E+00-2.994810208E-01 1.347032033E-02
C2H3 CO
-1.803148054E+01 4.353156379E+00-3.519040153E-01 1.532099172E-02
C2H3 H2O2
-1.819836993E+01 4.404366586E+00-3.569332334E-01 1.547103859E-02
C2H3 HCO
-2.114400868E+01 5.173605730E+00-4.173901990E-01 1.652248306E-02
C2H3 CH2O

-2.115144328E+01 5.173259682E+00-4.173362707E-01 1.651973750E-02
C2H3 CH3
-1.895414261E+01 4.700827748E+00-3.902067422E-01 1.669439498E-02
C2H3 CH
-1.742089559E+01 4.326589594E+00-3.506318450E-01 1.535097532E-02
C2H3 CH2
-1.893715775E+01 4.701919281E+00-3.901721750E-01 1.668492635E-02
C2H3 CH3O
-2.114445973E+01 5.222997629E+00-4.308429547E-01 1.738130784E-02
C2H3 C
-1.707305049E+01 4.152315609E+00-3.289584457E-01 1.445230116E-02
C2H3 C2H
-2.008090149E+01 4.983141078E+00-4.200329582E-01 1.771392477E-02
C2H3 C2H2
-2.009217799E+01 4.983711308E+00-4.201264365E-01 1.771883386E-02
C2H3 C2H3
-2.010211894E+01 4.983892108E+00-4.201560754E-01 1.772039037E-02

C2H4 CH4
-1.957015267E+01 4.890648271E+00-4.088561759E-01 1.725719228E-02
C2H4 O2
-1.901929199E+01 4.693838538E+00-3.900998243E-01 1.672630578E-02
C2H4 H2O
-1.988687644E+01 4.655343638E+00-3.287192758E-01 1.186460817E-02
C2H4 CO2
-2.089328545E+01 5.166932936E+00-4.306293067E-01 1.764268928E-02

C2H4 H
-1.694496836E+01 4.353288926E+00-3.147438649E-01 1.210200561E-02
C2H4 O
-1.800091226E+01 4.493069787E+00-3.678447876E-01 1.591446526E-02
C2H4 OH
-1.799417424E+01 4.483235037E+00-3.666454498E-01 1.586622503E-02
C2H4 HO2
-1.902570604E+01 4.693486076E+00-3.900469793E-01 1.672371418E-02
C2H4 H2
-1.646041212E+01 4.329098350E+00-3.588538948E-01 1.604603202E-02
C2H4 CO
-1.879104016E+01 4.613167296E+00-3.811821576E-01 1.640354070E-02
C2H4 H2O2
-1.903192246E+01 4.693160941E+00-3.899937226E-01 1.672092546E-02
C2H4 HCO
-2.090931786E+01 4.972992363E+00-3.786878754E-01 1.435801062E-02
C2H4 CH2O
-2.091773466E+01 4.973022810E+00-3.786902861E-01 1.435801974E-02
C2H4 CH3
-1.960184464E+01 4.900344295E+00-4.094942297E-01 1.725871082E-02
C2H4 CH
-1.802581953E+01 4.528205567E+00-3.721202547E-01 1.608600341E-02
C2H4 CH2
-1.956675215E+01 4.893592131E+00-4.083221850E-01 1.719479408E-02
C2H4 CH3O
-2.114546485E+01 5.122843677E+00-4.061100429E-01 1.585324791E-02

C2H4 C
-1.790605723E+01 4.454149418E+00-3.650605005E-01 1.588911588E-02
C2H4 C2H
-2.061603851E+01 5.123766054E+00-4.301686788E-01 1.782697218E-02
C2H4 C2H2
-2.062922277E+01 5.125114251E+00-4.303775213E-01 1.783749957E-02
C2H4 C2H3
-2.064027594E+01 5.125732997E+00-4.304742300E-01 1.784241024E-02
C2H4 C2H4
-2.117733187E+01 5.262507951E+00-4.398579387E-01 1.792490029E-02

C2H5 CH4
-1.938495806E+01 4.803648773E+00-3.995401500E-01 1.693218793E-02
C2H5 O2
-1.881741176E+01 4.595519883E+00-3.791053735E-01 1.632232602E-02
C2H5 H2O
-2.010032140E+01 4.740601578E+00-3.442892742E-01 1.271236185E-02
C2H5 CO2
-2.075863214E+01 5.108420639E+00-4.262855997E-01 1.758282828E-02
C2H5 H
-1.738385397E+01 4.515892014E+00-3.391851731E-01 1.329274563E-02
C2H5 O
-1.802433028E+01 4.483643636E+00-3.688147269E-01 1.604824242E-02
C2H5 OH
-1.800542375E+01 4.468501600E+00-3.668688442E-01 1.596517323E-02
C2H5 HO2

-1.882326159E+01	4.594958140E+00-3.790361067E-01	1.631950926E-02
C2H5	H2	
-1.615268360E+01	4.174123268E+00-3.383478022E-01	1.513994628E-02
C2H5	CO	
-1.864571887E+01	4.539069573E+00-3.735011269E-01	1.615133624E-02
C2H5	H2O2	
-1.882911370E+01	4.594509543E+00-3.789782949E-01	1.631703998E-02
C2H5	HCO	
-2.110605825E+01	5.056381084E+00-3.941306839E-01	1.520383351E-02
C2H5	CH2O	
-2.111906380E+01	5.058376683E+00-3.944189400E-01	1.521744944E-02
C2H5	CH3	
-1.943924633E+01	4.823353713E+00-4.015869504E-01	1.699926053E-02
C2H5	CH	
-1.809136110E+01	4.537199055E+00-3.756915059E-01	1.634157224E-02
C2H5	CH2	
-1.941108589E+01	4.819575184E+00-4.008185299E-01	1.695353171E-02
C2H5	CH3O	
-2.123091556E+01	5.158617106E+00-4.148427731E-01	1.638778267E-02
C2H5	C	
-1.792077885E+01	4.443304672E+00-3.657000664E-01	1.600228602E-02
C2H5	C2H	
-2.057807212E+01	5.105516635E+00-4.311356556E-01	1.800318515E-02
C2H5	C2H2	
-2.059391653E+01	5.108071198E+00-4.315351765E-01	1.802346473E-02
C2H5	C2H3	

-2.060779448E+01 5.109965054E+00-4.318316184E-01 1.803852200E-02
C2H5 C2H4
-2.108190131E+01 5.219098644E+00-4.371169228E-01 1.791477372E-02
C2H5 C2H5
-2.091185704E+01 5.148563251E+00-4.310566855E-01 1.777361168E-02

C2H6 CH4
-1.938900212E+01 4.802048888E+00-3.992039550E-01 1.691186905E-02
C2H6 O2
-1.882824633E+01 4.596254559E+00-3.791929174E-01 1.632574162E-02
C2H6 H2O
-2.007380408E+01 4.726139041E+00-3.422099496E-01 1.261483910E-02
C2H6 CO2
-2.077841456E+01 5.112883063E+00-4.269669326E-01 1.761675963E-02
C2H6 H
-1.738223245E+01 4.514296668E+00-3.388647369E-01 1.327381057E-02
C2H6 O
-1.805221251E+01 4.492276861E+00-3.699238201E-01 1.609557416E-02
C2H6 OH
-1.803293259E+01 4.476896093E+00-3.679477111E-01 1.601123416E-02
C2H6 HO2
-1.883388858E+01 4.595581220E+00-3.791127931E-01 1.632262093E-02
C2H6 H2
-1.616515914E+01 4.178912439E+00-3.390065276E-01 1.517007386E-02
C2H6 CO
-1.865835381E+01 4.540734594E+00-3.737078382E-01 1.615981856E-02

C2H6 H2O2
-1.883954157E+01 4.595025150E+00-3.790445174E-01 1.631985829E-02
C2H6 HCO
-2.110835144E+01 5.053669031E+00-3.937380840E-01 1.518524469E-02
C2H6 CH2O
-2.112312643E+01 5.056384561E+00-3.941311868E-01 1.520385730E-02
C2H6 CH3
-1.944255809E+01 4.821519115E+00-4.012136003E-01 1.697703470E-02
C2H6 CH
-1.811958246E+01 4.546262957E+00-3.768546568E-01 1.639115705E-02
C2H6 CH2
-1.941401238E+01 4.817659358E+00-4.004296568E-01 1.693041201E-02
C2H6 CH3O
-2.123706054E+01 5.157471244E+00-4.146759099E-01 1.637982472E-02
C2H6 C
-1.794868955E+01 4.452593229E+00-3.669286888E-01 1.605634583E-02
C2H6 C2H
-2.058029128E+01 5.102838459E+00-4.307170153E-01 1.798194351E-02
C2H6 C2H2
-2.059736527E+01 5.105899868E+00-4.311955757E-01 1.800622606E-02
C2H6 C2H3
-2.061244564E+01 5.108290466E+00-4.315694834E-01 1.802520671E-02
C2H6 C2H4
-2.108551138E+01 5.216947739E+00-4.367929394E-01 1.789881582E-02
C2H6 C2H5
-2.091966642E+01 5.148265410E+00-4.310113356E-01 1.777135773E-02

C2H6 C2H6
-2.092890471E+01 5.148563251E+00-4.310566855E-01 1.777361168E-02

HCCO CH4
-1.775785970E+01 4.446006792E+00-3.635785554E-01 1.580978106E-02
HCCO O2
-1.687140239E+01 4.075866019E+00-3.175538933E-01 1.389705877E-02
HCCO H2O
-1.993850917E+01 5.098661975E+00-4.129847878E-01 1.653577163E-02
HCCO CO2
-1.934675859E+01 4.844114216E+00-4.050650409E-01 1.718560391E-02
HCCO H
-1.695212450E+01 4.856354911E+00-4.155356134E-01 1.799468824E-02
HCCO O
-1.575708077E+01 3.859037540E+00-2.920670470E-01 1.290448854E-02
HCCO OH
-1.574882499E+01 3.846524848E+00-2.903597991E-01 1.282703187E-02
HCCO HO2
-1.687995291E+01 4.075813861E+00-3.175454692E-01 1.389662615E-02
HCCO H2
-1.309374639E+01 3.192065207E+00-2.080520240E-01 9.377333020E-03
HCCO CO
-1.658529844E+01 3.962482415E+00-3.034257508E-01 1.330923058E-02
HCCO H2O2
-1.688882143E+01 4.076040759E+00-3.175738229E-01 1.389780553E-02
HCCO HCO

-2.062895845E+01 5.231226529E+00-4.370161878E-01 1.784653117E-02
HCCO CH2O
-2.063989715E+01 5.231646654E+00-4.370734005E-01 1.784908134E-02
HCCO CH3
-1.782505593E+01 4.472547643E+00-3.668212245E-01 1.594177157E-02
HCCO CH
-1.578342462E+01 3.901748761E+00-2.978933744E-01 1.316877999E-02
HCCO CH2
-1.781814295E+01 4.479875585E+00-3.677555119E-01 1.598130788E-02
HCCO CH3O
-2.025197625E+01 5.111048794E+00-4.261817146E-01 1.756074634E-02
HCCO C
-1.559790303E+01 3.773945299E+00-2.821503359E-01 1.252380660E-02
HCCO C2H
-1.891360867E+01 4.728415981E+00-3.935827863E-01 1.683442959E-02
HCCO C2H2
-1.892575951E+01 4.728498392E+00-3.936074427E-01 1.683612939E-02
HCCO C2H3
-1.893741382E+01 4.728592897E+00-3.936268651E-01 1.683729519E-02
HCCO C2H4
-1.961481355E+01 4.942830658E+00-4.152108200E-01 1.752037256E-02
HCCO C2H5
-1.945124176E+01 4.857426088E+00-4.062318140E-01 1.721511045E-02
HCCO C2H6
-1.946052410E+01 4.857001524E+00-4.061492631E-01 1.721031229E-02
HCCO HCCO

-1.753044761E+01 4.405875605E+00-3.571389214E-01 1.548048343E-02

CH2CO CH4
-2.008186832E+01 4.928938499E+00-3.987532267E-01 1.620684452E-02
CH2CO O2
-2.009809903E+01 4.977640936E+00-4.165324966E-01 1.744636268E-02
CH2CO H2O
-1.836390873E+01 3.824968257E+00-1.992930245E-01 5.478620993E-03
CH2CO CO2
-2.140521789E+01 5.181864969E+00-4.179644579E-01 1.653088436E-02
CH2CO H
-1.510630635E+01 3.409062164E+00-1.659099387E-01 4.585477758E-03
CH2CO O
-1.900239965E+01 4.757005792E+00-3.907889443E-01 1.643021710E-02
CH2CO OH
-1.902751170E+01 4.760375255E+00-3.915553595E-01 1.647815983E-02
CH2CO HO2
-2.011350754E+01 4.980977783E+00-4.170735087E-01 1.747456081E-02
CH2CO H2
-1.769071790E+01 4.739683718E+00-4.053727260E-01 1.776341245E-02
CH2CO CO
-1.996446099E+01 4.943052505E+00-4.143584158E-01 1.744553394E-02
CH2CO H2O2
-2.012780861E+01 4.983955132E+00-4.175570791E-01 1.749979741E-02
CH2CO HCO
-1.972933692E+01 4.264735969E+00-2.639984265E-01 8.526031650E-03

CH2CO CH2O
-1.974668988E+01 4.267777070E+00-2.644051801E-01 8.543272840E-03
CH2CO CH3
-2.004561269E+01 4.909857875E+00-3.952298637E-01 1.601056276E-02
CH2CO CH
-1.891456138E+01 4.745550644E+00-3.882046776E-01 1.626913060E-02
CH2CO CH2
-1.997314299E+01 4.888137393E+00-3.919152248E-01 1.584555122E-02
CH2CO CH3O
-2.039592553E+01 4.595574296E+00-3.164277625E-01 1.115467065E-02
CH2CO C
-1.894979842E+01 4.748231990E+00-3.930776881E-01 1.667236979E-02
CH2CO C2H
-2.106258777E+01 5.117956796E+00-4.136127658E-01 1.648626376E-02
CH2CO C2H2
-2.109959559E+01 5.129131223E+00-4.152732472E-01 1.656708052E-02
CH2CO C2H3
-2.113362674E+01 5.139251046E+00-4.167772128E-01 1.664028886E-02
CH2CO C2H4
-2.115552038E+01 5.049404420E+00-3.939336395E-01 1.522306606E-02
CH2CO C2H5
-2.129367289E+01 5.109797247E+00-4.062920938E-01 1.593136189E-02
CH2CO C2H6
-2.131778323E+01 5.116105803E+00-4.072198384E-01 1.597604188E-02
CH2CO HCCO
-2.042383831E+01 5.091195540E+00-4.210915234E-01 1.723544732E-02

CH2CO CH2CO
-2.047887295E+01 4.549053308E+00-3.083703998E-01 1.072672905E-02

C2H3O CH4
-2.006943349E+01 4.921628262E+00-3.976357302E-01 1.615114252E-02
C2H3O O2
-2.009773101E+01 4.974913979E+00-4.160909506E-01 1.742337120E-02
C2H3O H2O
-1.836101494E+01 3.822489374E+00-1.989974495E-01 5.468475375E-03
C2H3O CO2
-2.141050645E+01 5.181527124E+00-4.179134915E-01 1.652836941E-02
C2H3O H
-1.509682111E+01 3.404528853E+00-1.652192693E-01 4.551149069E-03
C2H3O O
-1.900438537E+01 4.755691052E+00-3.904907747E-01 1.641158878E-02
C2H3O OH
-1.902967527E+01 4.759072759E+00-3.912586902E-01 1.645959101E-02
C2H3O HO2
-2.011364277E+01 4.978452464E+00-4.166639933E-01 1.745321341E-02
C2H3O H2
-1.769632128E+01 4.741723421E+00-4.056410349E-01 1.777515792E-02
C2H3O CO
-1.996456807E+01 4.940640748E+00-4.139538305E-01 1.742394991E-02
C2H3O H2O2
-2.012844470E+01 4.981631479E+00-4.171796034E-01 1.748009477E-02
C2H3O HCO

-1.972877230E+01	4.262506092E+00	-2.637001414E-01 8.513386039E-03
C2H3O	CH2O	
-1.974656333E+01	4.265688719E+00	-2.641258652E-01 8.531433825E-03
C2H3O	CH3	
-2.003274039E+01	4.902428749E+00	-3.940961078E-01 1.595411952E-02
C2H3O	CH	
-1.891604063E+01	4.744244072E+00	-3.879116332E-01 1.625091064E-02
C2H3O	CH2	
-1.996021783E+01	4.880757055E+00	-3.907890304E-01 1.578948989E-02
C2H3O	CH3O	
-2.039403671E+01	4.592611884E+00	-3.160121252E-01 1.113579099E-02
C2H3O	C	
-1.895462474E+01	4.748609683E+00	-3.930482364E-01 1.666754827E-02
C2H3O	C2H	
-2.105147250E+01	5.110950767E+00	-4.125717892E-01 1.643560330E-02
C2H3O	C2H2	
-2.108942462E+01	5.122501602E+00	-4.142880841E-01 1.651913080E-02
C2H3O	C2H3	
-2.112442966E+01	5.133012638E+00	-4.158500626E-01 1.659515693E-02
C2H3O	C2H4	
-2.114783521E+01	5.043896450E+00	-3.931295527E-01 1.518466042E-02
C2H3O	C2H5	
-2.128790052E+01	5.105064227E+00	-4.055961585E-01 1.589785119E-02
C2H3O	C2H6	
-2.131303269E+01	5.111785368E+00	-4.065844497E-01 1.594544071E-02
C2H3O	HCCO	

-2.041743105E+01 5.085509215E+00-4.202237207E-01 1.719222310E-02
C2H3O CH2CO
-2.048455456E+01 4.548964860E+00-3.083581033E-01 1.072617762E-02
C2H3O C2H3O
-2.049072037E+01 4.549053308E+00-3.083703998E-01 1.072672905E-02

CH2(S) CH4
-1.765053055E+01 4.344870429E+00-3.508848705E-01 1.527906464E-02
CH2(S) O2
-1.707915129E+01 4.132968305E+00-3.260544226E-01 1.431105055E-02
CH2(S) H2O
-2.040913387E+01 5.224092154E+00-4.327352339E-01 1.753063744E-02
CH2(S) CO2
-1.920159447E+01 4.768582927E+00-3.938474246E-01 1.663348229E-02
CH2(S) H
-1.798723961E+01 5.079563954E+00-4.444136859E-01 1.923461015E-02
CH2(S) O
-1.558834476E+01 3.699567569E+00-2.706504419E-01 1.194595507E-02
CH2(S) OH
-1.559686028E+01 3.697253935E+00-2.703332304E-01 1.193149436E-02
CH2(S) HO2
-1.709852890E+01 4.139000763E+00-3.268659281E-01 1.434736576E-02
CH2(S) H2
-1.355982380E+01 3.231190003E+00-2.138418525E-01 9.659202107E-03
CH2(S) CO
-1.661775187E+01 3.942048792E+00-3.009974379E-01 1.321282808E-02

CH2(S)	H2O2	
-1.711740123E+01	4.144923053E+00	-3.276626105E-01 1.438301773E-02
CH2(S)	HCO	
-2.039806611E+01	5.097935506E+00	-4.183219307E-01 1.696950199E-02
CH2(S)	CH2O	
-2.038050275E+01	5.087332841E+00	-4.167208822E-01 1.689045699E-02
CH2(S)	CH3	
-1.771390718E+01	4.368346040E+00	-3.538103602E-01 1.540105015E-02
CH2(S)	CH	
-1.558104549E+01	3.717715492E+00	-2.731288057E-01 1.205849837E-02
CH2(S)	CH2	
-1.769520494E+01	4.367696733E+00	-3.537273902E-01 1.539753038E-02
CH2(S)	CH3O	
-2.006425983E+01	4.999968754E+00	-4.103333006E-01 1.680584964E-02
CH2(S)	C	
-1.532763210E+01	3.571505864E+00	-2.545912443E-01 1.127476104E-02
CH2(S)	C2H	
-1.891736743E+01	4.700703077E+00	-3.902103646E-01 1.669544777E-02
CH2(S)	C2H2	
-1.892750112E+01	4.701317927E+00	-3.901918390E-01 1.669019746E-02
CH2(S)	C2H3	
-1.893715775E+01	4.701919281E+00	-3.901721750E-01 1.668492635E-02
CH2(S)	C2H4	
-1.956675215E+01	4.893592131E+00	-4.083221850E-01 1.719479408E-02
CH2(S)	C2H5	
-1.941108589E+01	4.819575184E+00	-4.008185299E-01 1.695353171E-02

CH2(S) C2H6
-1.941401238E+01 4.817659358E+00-4.004296568E-01 1.693041201E-02
CH2(S) HCCO
-1.781814295E+01 4.479875585E+00-3.677555119E-01 1.598130788E-02
CH2(S) CH2CO
-1.997314299E+01 4.888137393E+00-3.919152248E-01 1.584555122E-02
CH2(S) C2H3O
-1.996021783E+01 4.880757055E+00-3.907890304E-01 1.578948989E-02
CH2(S) CH2(S)
-1.769520494E+01 4.367696733E+00-3.537273902E-01 1.539753038E-02

C3H6 CH4
-1.962070916E+01 4.778265725E+00-3.921341326E-01 1.643424991E-02
C3H6 O2
-1.935527282E+01 4.694011644E+00-3.905451837E-01 1.675930382E-02
C3H6 H2O
-1.964847822E+01 4.414193676E+00-2.959202673E-01 1.040179140E-02
C3H6 CO2
-2.115481074E+01 5.144828035E+00-4.294841894E-01 1.766059570E-02
C3H6 H
-1.686939037E+01 4.139657099E+00-2.772482471E-01 1.004123878E-02
C3H6 O
-1.893701838E+01 4.740892950E+00-4.014433101E-01 1.742525084E-02
C3H6 OH
-1.890811840E+01 4.720900410E+00-3.988818351E-01 1.731624662E-02
C3H6 HO2

-1.935794430E+01	4.691989108E+00-3.903437327E-01	1.675339156E-02
C3H6	H2	
-1.725181921E+01	4.549937945E+00-3.897682487E-01	1.748127033E-02
C3H6	CO	
-1.905408499E+01	4.586524709E+00-3.776967787E-01	1.624775789E-02
C3H6	H2O2	
-1.936066168E+01	4.690102468E+00-3.901549633E-01	1.674780138E-02
C3H6	HCO	
-2.105354419E+01	4.902923934E+00-3.701091590E-01	1.400529417E-02
C3H6	CH2O	
-2.108920264E+01	4.914232430E+00-3.717475746E-01	1.408290820E-02
C3H6	CH3	
-1.964477873E+01	4.786148557E+00-3.924516693E-01	1.641793615E-02
C3H6	CH	
-1.902843904E+01	4.806987414E+00-4.099079585E-01	1.778532651E-02
C3H6	CH2	
-1.960451231E+01	4.777904055E+00-3.909921946E-01	1.633743404E-02
C3H6	CH3O	
-2.122956760E+01	5.026477131E+00-3.937316197E-01	1.531665407E-02
C3H6	C	
-1.847140925E+01	4.559174916E+00-3.788126512E-01	1.648457958E-02
C3H6	C2H	
-2.068173533E+01	5.021720539E+00-4.160542096E-01	1.717111645E-02
C3H6	C2H2	
-2.071500066E+01	5.031658716E+00-4.175948408E-01	1.724881067E-02
C3H6	C2H3	

-2.074598893E+01 5.040822082E+00-4.190154328E-01 1.732045450E-02
C3H6 C2H4
-2.121525315E+01 5.147763729E+00-4.243389184E-01 1.721854672E-02
C3H6 C2H5
-2.118198364E+01 5.138675100E+00-4.271024680E-01 1.749434513E-02
C3H6 C2H6
-2.120925363E+01 5.146634823E+00-4.283076558E-01 1.755394825E-02
C3H6 HCCO
-1.983536973E+01 4.870285313E+00-4.049039437E-01 1.702862730E-02
C3H6 CH2CO
-2.161341553E+01 5.115833758E+00-4.053150824E-01 1.582339535E-02
C3H6 C2H3O
-2.162413755E+01 5.117976064E+00-4.056272203E-01 1.583827907E-02
C3H6 CH2(S)
-1.960451231E+01 4.777904055E+00-3.909921946E-01 1.633743404E-02
C3H6 C3H6
-2.166177490E+01 5.223496727E+00-4.375914661E-01 1.793164915E-02

aC3H5 CH4
-1.962211026E+01 4.781035236E+00-3.926296825E-01 1.646175617E-02
aC3H5 O2
-1.934522796E+01 4.692423989E+00-3.903871239E-01 1.675466946E-02
aC3H5 H2O
-1.967508206E+01 4.427420816E+00-2.978131411E-01 1.049003577E-02
aC3H5 CO2
-2.115302691E+01 5.146888898E+00-4.297974187E-01 1.767614058E-02

aC3H5	H	
-1.687272694E+01	4.141741024E+00	-2.776191872E-01 1.006175693E-02
aC3H5	O	
-1.891350269E+01	4.732971440E+00	-4.004284565E-01 1.738206602E-02
aC3H5	OH	
-1.888437129E+01	4.712945753E+00	-3.978625237E-01 1.727286352E-02
aC3H5	HO2	
-1.934800207E+01	4.690462631E+00	-3.901910688E-01 1.674887464E-02
aC3H5	H2	
-1.724212799E+01	4.546100112E+00	-3.892401588E-01 1.745710673E-02
aC3H5	CO	
-1.904355283E+01	4.584573755E+00	-3.774897278E-01 1.624092029E-02
aC3H5	H2O2	
-1.935082547E+01	4.688637526E+00	-3.900077408E-01 1.674340378E-02
aC3H5	HCO	
-2.106687984E+01	4.911008454E+00	-3.712804859E-01 1.406078219E-02
aC3H5	CH2O	
-2.110156424E+01	4.921930876E+00	-3.728628782E-01 1.413573789E-02
aC3H5	CH3	
-1.964663015E+01	4.789039128E+00	-3.929635530E-01 1.644617744E-02
aC3H5	CH	
-1.900616167E+01	4.799368807E+00	-4.089325076E-01 1.774384224E-02
aC3H5	CH2	
-1.960649986E+01	4.780777817E+00	-3.915008335E-01 1.636548655E-02
aC3H5	CH3O	
-2.124221557E+01	5.034426751E+00	-3.948967020E-01 1.537257287E-02

aC3H5 C
-1.845444730E+01 4.553569920E+00-3.780949828E-01 1.645405221E-02
aC3H5 C2H
-2.069016418E+01 5.027871474E+00-4.170077276E-01 1.721920207E-02
aC3H5 C2H2
-2.072277847E+01 5.037555028E+00-4.185089344E-01 1.729491021E-02
aC3H5 C2H3
-2.075309668E+01 5.046453175E+00-4.198884572E-01 1.736448487E-02
aC3H5 C2H4
-2.122698428E+01 5.155356958E+00-4.254790077E-01 1.727453676E-02
aC3H5 C2H5
-2.118937511E+01 5.144384955E+00-4.279670008E-01 1.753710095E-02
aC3H5 C2H6
-2.121578606E+01 5.151994778E+00-4.291192154E-01 1.759408451E-02
aC3H5 HCCO
-1.983442626E+01 4.873124579E+00-4.054007663E-01 1.705585005E-02
aC3H5 CH2CO
-2.161225362E+01 5.118021497E+00-4.056338375E-01 1.583859447E-02
aC3H5 C2H3O
-2.162207869E+01 5.119796448E+00-4.058922336E-01 1.585090458E-02
aC3H5 CH2(S)
-1.960649986E+01 4.780777817E+00-3.915008335E-01 1.636548655E-02
aC3H5 C3H6
-2.165530688E+01 5.223326758E+00-4.375658299E-01 1.793038479E-02
aC3H5 aC3H5
-2.164965266E+01 5.223496727E+00-4.375914661E-01 1.793164915E-02

N2 CH4
-1.651845374E+01 3.896131715E+00-2.951168666E-01 1.296169193E-02
N2 O2
-1.578874095E+01 3.589258796E+00-2.568719643E-01 1.137272205E-02
N2 H2O
-2.024335679E+01 5.167072961E+00-4.292633012E-01 1.752044622E-02
N2 CO2
-1.850244299E+01 4.509545428E+00-3.699248652E-01 1.600568321E-02
N2 H
-1.711566827E+01 4.833263531E+00-4.205906575E-01 1.855344619E-02
N2 O
-1.474821144E+01 3.361316902E+00-2.285473221E-01 1.019994586E-02
N2 OH
-1.473662675E+01 3.348209961E+00-2.267279585E-01 1.011604019E-02
N2 HO2
-1.579929388E+01 3.590680573E+00-2.570682099E-01 1.138172294E-02
N2 H2
-1.266067773E+01 2.898081865E+00-1.700462638E-01 7.738735187E-03
N2 CO
-1.549018247E+01 3.466861175E+00-2.408858507E-01 1.067562976E-02
N2 H2O2
-1.581023929E+01 3.592406376E+00-2.573063628E-01 1.139264371E-02
N2 HCO
-2.006577405E+01 5.032537823E+00-4.235927840E-01 1.775280320E-02
N2 CH2O

-2.007324022E+01 5.032034577E+00-4.235011165E-01 1.774763201E-02
N2 CH3
-1.658229727E+01 3.922183618E+00-2.983957397E-01 1.309926016E-02
N2 CH
-1.479326525E+01 3.409409136E+00-2.352223389E-01 1.050776445E-02
N2 CH2
-1.658740390E+01 3.933645118E+00-2.999342570E-01 1.316796277E-02
N2 CH3O
-2.000089661E+01 5.021793256E+00-4.253483834E-01 1.795667901E-02
N2 C
-1.449022760E+01 3.236454458E+00-2.121629081E-01 9.482396910E-03
N2 C2H
-1.797950219E+01 4.344097733E+00-3.507607394E-01 1.527274280E-02
N2 C2H2
-1.799100666E+01 4.344592660E+00-3.508290643E-01 1.527587122E-02
N2 C2H3
-1.800288730E+01 4.345459709E+00-3.509446981E-01 1.528099582E-02
N2 C2H4
-1.876345332E+01 4.606235359E+00-3.803642103E-01 1.637150165E-02
N2 C2H5
-1.861866098E+01 4.532059806E+00-3.726515936E-01 1.611699608E-02
N2 C2H6
-1.863141846E+01 4.533771818E+00-3.728641549E-01 1.612571963E-02
N2 HCCO
-1.654368925E+01 3.949970896E+00-3.017787782E-01 1.323684171E-02
N2 CH2CO

-1.994081967E+01	4.937900787E+00	-4.137960641E-01 1.742540531E-02
N2	C2H3O	
-1.994095172E+01	4.935495600E+00	-4.133918304E-01 1.740381460E-02
N2	CH2(S)	
-1.658740390E+01	3.933645118E+00	-2.999342570E-01 1.316796277E-02
N2	C3H6	
-1.903198246E+01	4.581304178E+00	-3.770866373E-01 1.622404271E-02
N2	aC3H5	
-1.902137076E+01	4.579323053E+00	-3.768759020E-01 1.621705616E-02
N2	N2	
-1.546613221E+01	3.460860427E+00	-2.401167225E-01 1.064271712E-02